LONQUIST & CO. LLC

PETROLEUM ENGINEERS | ENERGY ADVISORS

AUSTIN · HOUSTON · CALGARY · REGINA
DENVER · COLLEGE STATION · BATON ROUGE · WICHITA

Fall 2022 InSAR Survey of Ground Displacement and Subsidence Monitoring Report

Sulphur Mines Salt Dome

ANNUAL SURVEY

Prepared for:

Eagle US 2, LLC

Prepared by:

Lonquist & Co., LLC
12912 Hill Country Blvd. / Suite F-200
Austin, TX 78738

Louisiana Firm License Number EF-5937

April 2023

Fall 2022 InSAR Survey of Ground Displacement and Subsidence Monitoring Report

Sulphur Mines Salt Dome

ANNUAL SURVEY

CERTIFIED BY:
Lonquist & Co., LLC
Louisiana Registration No. EF5937

Teresa H. Rougon, P.G.
Principal Geologist
Louisiana License No. 330

Nathaniel L. Byars, P.E.
Principal Engineer
Louisiana License No. 40697

Executive Summary

Lonquist and Co., LLC ("Lonquist") was contracted by the three (3) operators at the Sulphur Mines Salt Dome to prepare a subsidence monitoring plan that utilizes InSAR (Interferometric Synthetic Aperture Radar) data to detect ground displacement. TRE Altamira ("TREA") was contracted by Lonquist to collect, process, and analyze the data across the dome and surrounding area. Upon completion of the InSAR subsidence analysis by TREA, Lonquist is providing the Louisiana Department of Natural Resources ("LA DNR"), Injection Mining Division ("IMD"), with a detailed review of the reported data and a supplementary evaluation of the subsidence trends that have been observed over the dome.

Statewide Order 29-M-3 and Statewide Order 29-M (Rev. 3), require that both brine mining operators and hydrocarbon storage operators conduct subsidence monitoring surveys on an annual basis during the same period. Monitoring at Sulphur Mines is carried out in the fall of each year. The analysis performed by TREA serves as the Fall 2022 subsidence survey for of the dome.

The evaluation discussed herein details ground displacement measurements as captured by two satellites over the time spans of October 2016 - December 2022 and June 2022 - December 2022, respectively. True vertical displacement and east-west displacement were identified via triangulation of the two satellite datasets during the June 2022 - December 2022 timeframe when data was collected from both satellites.

The methodology of subsidence evaluation follows guidance provided by the IMD in 2019 for estimation of subsidence rate trends and apparent rate changes for survey monuments over the dome. The charts provided within this report illustrate the historical ground displacement and subsidence trends within areas of interest (AOIs) in lieu of survey monument locations. The contour maps generated from this data depict the spatial distribution and present condition of vertical and east-west ground displacement across the dome.

<u>No anomalous subsidence trends or regions have been identified in the Fall 2022 survey.</u> This indicates that rates of cavern closure and other factors of influence are continuing to act in a consistent manner at this time.

As the first annual survey preformed with InSAR data, this report is also intended to provide evaluation and clarification of the following: 1) Introduction of InSAR technology and resulting modifications to subsidence evaluation methodology over the dome, 2) Comparison of current subsidence rates indicated by InSAR to past rates calculated from historical level surveys, 3) Review of the 6-year InSAR dataset to confirm historical rate consistency, and 4) Identification of data gaps over caverns or past monitoring locations in the level surveys.

Table of Contents

APPENDICES

Acronyms and Abbreviations

1-D	1-Dimensional - Line of Site
2-D	2-Dimensional – Vertical and East-West
AOI	Area of Interest
IMD	Injection and Mining Division
InSAR	Interferometric Synthetic Aperture Radar
LA DNR	Louisiana Department of Natural Resources
LOS	Line of Sight
SNT	Sentinel 1 Satellite
SPR	Strategic Petroleum Reserve
TREA	TRE-Altamira
TSX	TerraSAR-X Satellite
TSX/PAZ	TerraSAR-X and PAZ Satellite Constellation

1.0 Background

Salt caverns are created through a process called solution mining. This is achieved by drilling into a salt formation and circulating water into the drilled hole to dissolve the salt. This process forms a brine-filled cavern within the salt structure. Salt caverns can then be used to store various fluids such as natural gas and refined hydrocarbon products. Salt domes have been known to experience deformation due to gradual closure of the mined spaces within the salt formation or other geological processes related to the salt and overlying caprock. The gradual closure of cavern space is formally known as salt creep and stops only when the cavern has reached a geostatic equilibrium with the surrounding rock. Factors such as cavern depth, ground temperature, salt properties, regional stresses, overburden density, operating pressures, and the geometry of and proximity to neighboring caverns affect the magnitude of salt creep.

Due to salt creep, the overburden rock structure begins to move downward towards the caverns. This can be seen on the surface as subsidence (or ground displacement) vertically and to a lesser extent horizontally toward the center of the subsidence basin. Consequently, it is anticipated that surface subsidence will transpire over all solution-mined caverns in domal and bedded salt to varying extents. The vertical displacement rate over a solution-mined cavern generally ranges from less than ¼ inch annually to several inches per year. Pursuant to the provisions of Statewide Order 29-M (LAC 43: XVII. Subpart 3) and Statewide Order 29-M-3 (LAC 43: XVII. Subpart 5), subsidence must be measured annually over all solution-mining and storage caverns.

1.1 Monitoring History

Subsidence monitoring over salt caverns allows operators and regulators to prepare for and respond to potential stability issues in a proactive manner. Monitoring of surface elevations has been undertaken for a number of years by individual companies operating on the Sulphur Mines Salt Dome. The data provided to Lonquist & Co., LLC ("Lonquist") indicates level surveying for subsidence monitoring purposes was initiated in 1993 by Eagle US 2, LLC ("Eagle") (formerly PPG Ind., Inc. – Ind. Chem. Div.) and was generally conducted on a two-year basis. These elevation surveys were conducted internally by a PPG staff surveyor. In addition to the surveys being performed by Eagle/PPG, surveys were also conducted by American Surveyors, LLC, on behalf of Liberty Gas Storage, LLC ("Liberty") and Boardwalk Louisiana Midstream, LLC ("Boardwalk").

In 2015, an agreement was reached between all three (3) operators to conduct a coordinated precision level survey across the Sulphur Mines Salt Dome utilizing a common set of benchmarks and monuments. Hydro Consultants, Inc. ("Hydro Consultants"), a professional land surveying company, was subcontracted by Lonquist to conduct the survey. A survey plan was created and a set of benchmarks and monitoring stations were selected to be surveyed. Level surveys were performed in accordance with this plan through the Fall 2021 survey. Following that survey, the decision was made to transition to InSAR subsidence monitoring for the next annual survey in Fall 2022.

Since the coordinated monitoring effort began in 2015, continual and relatively consistent ground displacement has been observed. The greatest subsidence rates have been identified over the central portion of the dome with a gradual tapering toward the dome flank.

1.2 Sulfur Extraction

Although the current monitoring program is affiliated with cavern operations on the dome, the primary source of subsidence has been attributed to past sulfur extraction from the overlying caprock. Between 1902 and 1924 the caprock was heavily drilled and molten sulfur was mined through wellbores resulting in a total production of 10.5 million US tons of sulfur. This tonnage equates to 28 million barrels or 3,600 acre-feet of extracted volume. Over the approximately 75 acres of caprock extent, an average 48-foot thickness of sulfur is estimated to have been removed. By the time mining was completed in the late 1920's, the collapse of voids left by the sulfur extraction had resulted in subsidence in excess of 20 feet. This led to the creation of a lake extending across the mined area, surrounding the present-day salt cavern locations.

Subsidence continued at lesser rates over the following century and large sections of the lake were backfilled to support infrastructure and well pads. Dredging of the surrounding area to provide fill material is what led to the creation of the large lakes that surround the site. A study performed in 1965 comparing data from wells drilled before and after the sulfur mining operations, resulted in the development of a caprock collapse map identifying changes in caprock thickness below ground. Large collapses up to 163 feet were identified in some places, but most values ranged between 25 and 50 feet across the mined area.

In a 1980 study commissioned by the Strategic Petroleum Reserve ("SPR"), subsidence was estimated from level survey data to be occurring at an average rate of about 1.2 inches/year above the existing SPR cavern locations (PPG Nos. 2, 4, 5, 6, and 7). The study noted that this rate of subsidence had been occurring for some time and was likely to continue into the foreseeable future. These subsidence rates agree with current survey data, indicating that the trend has remained consistent to present day. The study concluded that subsidence over the dome was the result of the following factors: 1) Continual closure of caprock voids from the past sulfur mining, 2) Consolidation of soils used to fill subsided regions, and 3) Natural dissolution of evaporite layers and collapse of preexisting voids from groundwater flow within the caprock.[1] Although not acknowledged as a factor in the report, creep closure in the Sulphur Mines salt caverns may have been contributing in some degree to the rates of observed subsidence.

1.3 Eagle US 2, LLC

Eagle US 2, LLC operates only Class III Solution-Mining caverns which are regulated by SWO 29-M-3. The statutory compliance requirements found therein mandate that Eagle perform an annual survey as part of the ongoing monitoring program established at the dome. The InSAR survey and this supplementary evaluation report are being submitted to fulfill the annual monitoring effort for the Fall of 2022.

2.0 Fall 2022 InSAR Survey

For the 2022 subsidence evaluation, the decision was made to employ an alternative survey method known as Interferometric Synthetic Aperture Radar, or "InSAR". This method of data collection relies on satellite-based ground displacement readings calculated from radar imagery. Compared to traditional level surveys, data resolution is improved both spatially and temporally, allowing for the analysis of thousands of ground locations on regular, multi-day intervals. InSAR is a high-accuracy, remote sensing technology that effectively provides an updated level survey of a target area with each successive pass of an orbiting satellite. Spatial density of the measurement points varies, but in areas of non-vegetated ground cover, a substantial number of ground targets can surveyed on a regular basis.

TRE-Altamira ("TREA"), a global leader in InSAR ground displacement monitoring, was contracted by Lonquist to collect, process, and analyze ground displacement data over the Sulphur Mines site. TREA utilizes an advanced, proprietary form of InSAR data processing that tracks ground movement by analyzing a stack of radar images collected over time. This technology, termed "SqueeSAR®", provides a collection of spatially distributed measurement points that each contain a time series of ground deformation measurements reported to a 0.1 mm (0.004 inch) scale. Measurement accuracy is on par with traditional rod and level surveys in terms of error range with vertical displacement rate precision being estimated at ±0.02 in/yr. The analysis report prepared by TREA has been provided for reference as Appendix E. The report contains a general description of

[1] **Whiting, G H. 1980.** "Strategic Petroleum Reserve (SPR) geological site characterization report, Sulphur Mines Salt Dome: Section I, Section II, and Section III". United States.

subsidence related observations over the analysis area as well as a detailed description of the InSAR monitoring system and data processing method.

2.1 Data Properties

Imagery collected via satellites over successive orbital passes is used to identify and define measurement points on the ground. Objects or ground features providing a stable reflection of radar energy such as buildings, roads, and infrastructure produce the highest quality of measurement points. Measurement points can be generated in some areas with vegetation, but data quality is affected by changing ground characteristics over time, leading to data gaps in areas with dense vegetation, farming or wetlands. In the absence of stable reflectors, additional datapoints can sometimes be generated in areas with lower but homogenous signal return by averaging groups of readings into a single measurement point.

InSAR uses phase and amplitude in the radar signal images to measure the distance between the satellite sensor and the measurement points on the ground. The data generated from the InSAR technique results in a time series of displacement values at each measurement point. These displacement values are reported in relation to the original distance measured for each point in the dataset.

When a measurement point on the ground moves, whether that be vertically or laterally, the phase value detected by the sensor on the satellite is impacted due to a change in the distance between the sensor and ground target. Displacement values generated in this way are referred to as 1-D Line-of-sight ("LOS") measurements, referring to the line-of-sight of the satellite to the ground target. Data collected in this manner is understood to convey a movement distance that is not purely vertical. This distinction only affects the assignment of a precise direction to the movement identified. As the primary component of the observed displacement is often vertical, InSAR analyses based on 1-D data are regularly used to identify and monitor the consistency of movement trends related to ground subsidence.

If precise delineation of vertical movement is required, datasets from a pair of satellite orbits can be utilized to calculate the vertical component of ground displacement via triangulation. Data generated from a pair of 1-D LOS datasets processed in this manner are referred to as 2-D measurements. These datasets identify vertical and horizontal ground displacement. Due to the orbital direction of the satellites, radar images are always captured from an eastern or western direction relative to the target area. Therefore, horizontal ground movement identified via InSAR is defined as east-west displacement. The north-south component of ground movement is unknown in 2-D datasets, and cannot be identified via InSAR due to the viewing direction of the satellites.

Analysis of an InSAR dataset allows for the identification of displacement velocity in inches/year and acceleration in inches/year^2. Measurement precision is affected by the satellite sensor resolution and the timeframe of the dataset. Average accuracy ranges for individual measurements can vary between ±0.20 inches for a low-resolution satellite and ±0.03 inches for a high-resolution satellite. With time, velocity trends can be measured with high accuracy yielding standard deviations in the range of ±0.01 inches/year.

2.2 Reference Point

The InSAR survey method relies on the selection of a local reference point from among the measured ground targets. The reference point is represented as static in order to produce calculations of relative movement at all other measurement points. In this way the reference point is similar to the off-dome, deep-rod benchmark monuments used in past level surveys at the site. However, unlike benchmark monuments, the reference point is chosen more for its motion behavior and radar properties than its location and construction. The reference point used for the evaluation of each dataset must exhibit high-quality signal return and not be affected by fluctuating ground movement within the time period evaluated.

Movement, if present at the reference point, is confirmed to be linear and assumed to be representative of broad regional displacement that extends beyond analysis area. Once this movement is zeroed out at the reference point, regional movement is assumed to be excluded from the displacement rates calculated at other measurement points. This is similar to historical ground surveys that relied on relative measurements from benchmark monuments. Ideally, the reference point will not change between surveys, but future non-linear movement or increased signal noise may require selection of a new location.

As discussed in the following sections, two InSAR datasets were collected from a pair of satellites which were used to triangulate vertical and east-west 2-D data. The reference points for each dataset are located near to each other, 1.68 miles to the southeast of the approximate dome center. The off-dome benchmark used in past surveys was located at a similar distance from the site at 1.79 miles to the south-southwest of the dome center.

2.3 Satellite Data Sources

Two satellite datasets were used in the InSAR analysis which were acquired from satellites on both ascending and descending orbits. An ascending orbit denotes the satellite's longitudinal course from south to north as it passes over the site, while a descending orbit implies the satellite is moving from north to south.

The first dataset was captured from a Sentinel 1 ("SNT") low-resolution satellite on an ascending orbit. The dataset timeframe covers a 6-year period from October 4, 2016 to December 20, 2022 with a 12-day image capture frequency. Data from this satellite was originally processed and evaluated in May 2022. Given the availability of a multi-year data span from the SNT satellite, the objective at that time was to compare subsidence trends identified via InSAR to the historical level surveys, and to establish historical baseline trends for future InSAR surveys. That evaluation led to the following conclusions: 1) Trends were identified as matching historical level surveys in the degree of consistency of linear ground movement observed, 2) Horizontal ground displacement was evident necessitating the use of a second satellite in future surveys to triangulate the vertical and lateral components, and 3) Due to data gaps in vegetated and marshy areas, the second dataset would need to come from a high-resolution satellite to maximize the spatial density of data point capture.

For the Fall 2022 survey, the second dataset was gathered via a TerraSAR-X ("TSX") high-resolution satellite on a descending orbit with an 11-day revisit frequency. The dataset timeframe covers a 6-month period from June 16, 2022 to December 20, 2022. High-resolution commercial satellites must be tasked for these purposes so historical data preceding the selection of the satellite for monitoring is not available.

Table 1 below provides additional information on the satellite data parameters. Figure 1 depicts the data capture timeline and a diagram of the orbital paths in relation to the Sulphur Mines site.

Table 1 – Satellite Data Parameters, Data Timeline, and Orbit Visualization

Analysis Characteristics	Sentinel-1 (SNT)	TerraSAR-X (TSX)
Satellite Properties		
Band (Wavelength)	C-band (2.20 in)	X-band (1.22 in)
Track	T136	T29
Pixel resolution	65 x 16 ft	3 x 3 ft
Revisit frequency	12 days	11 days
Orbit (LOS Angle, θ)	Ascending (42.52°)	Descending (17.18°)
Data Properties		
Period covered	10/04/2016 - 12/20/2022	06/16/2022 - 12/20/2022
No. of images processed	166	18
Reference Point location - *WGS 84*	Lat: 30.235768 Long: -93.392732	Lat: 30.235862 Long: -93.392611
No. of measurement points	25,761	28,635
Average point density	1,880 pts/mi^2	2,090 pts/mi^2
Average displacement rate standard deviation	± 0.01 in/yr	± 0.13 in/yr
Average time series measurement error bar	± 0.20 in	± 0.03 in

Figure 1 – Satellite Data Timeline, and Orbit Visualization

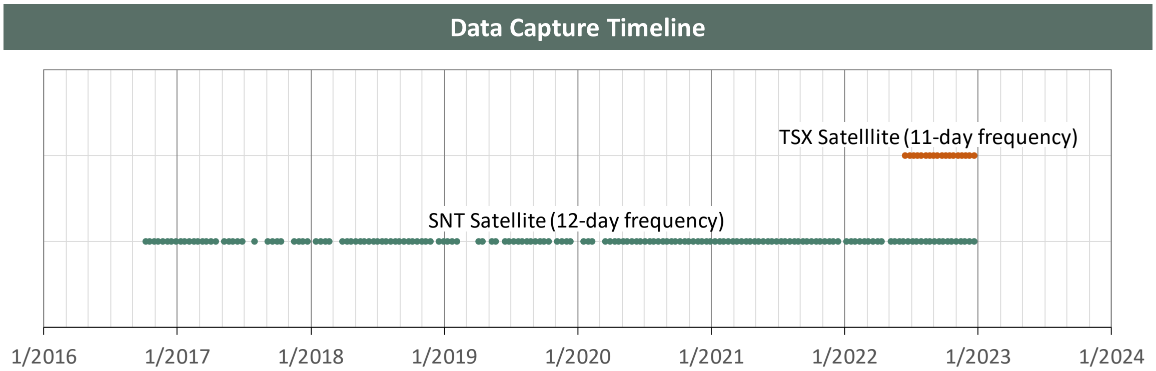

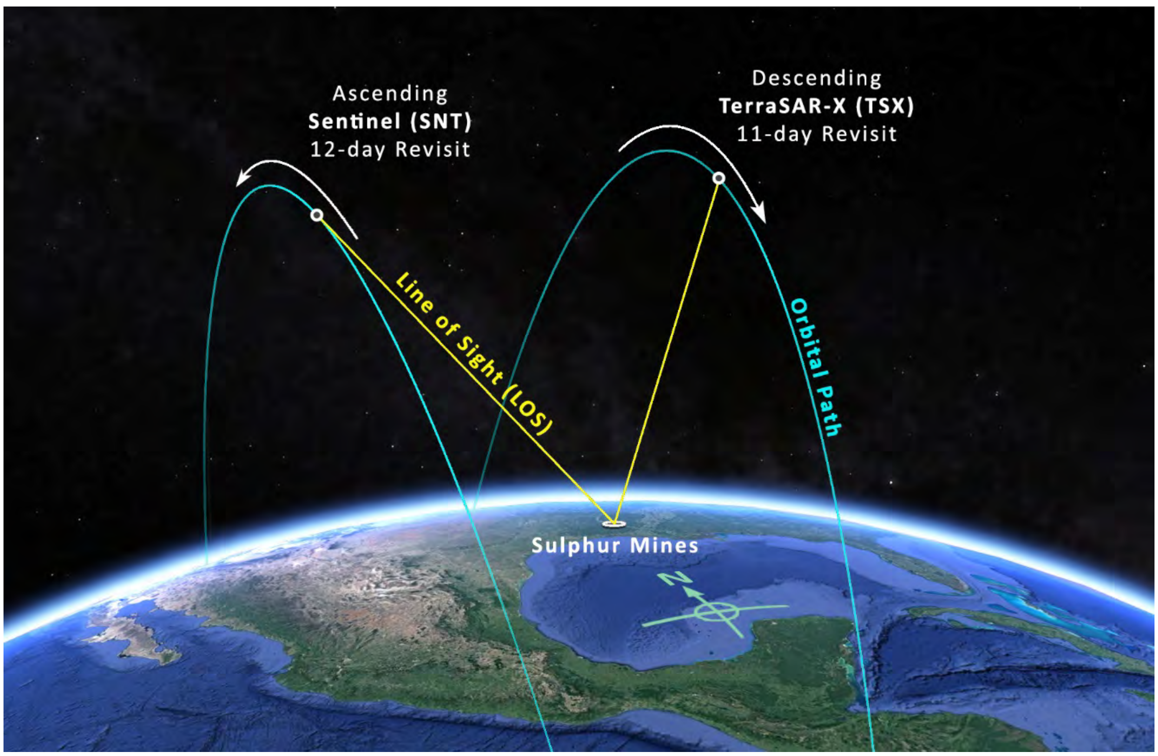

The 1-D LOS InSAR datasets generated from the two satellites each cover a 13.7-square mile area that extends roughly 1.85 miles out from the center of the Sulphur Mines Salt Dome. Figure 2 below depicts the measurement point locations, reference points, and data extent for the SNT and TSX datasets in relation to the dome structure contours. Areas of dense data capture are situated over roadways and infrastructure associated with dome operations and the city of Sulphur, Louisiana to the southeast. Areas showing farmland, forests, and water bodies can be seen to lack measurement data.

Figure 2 – SNT and TSX 1-D LOS Measurement Points

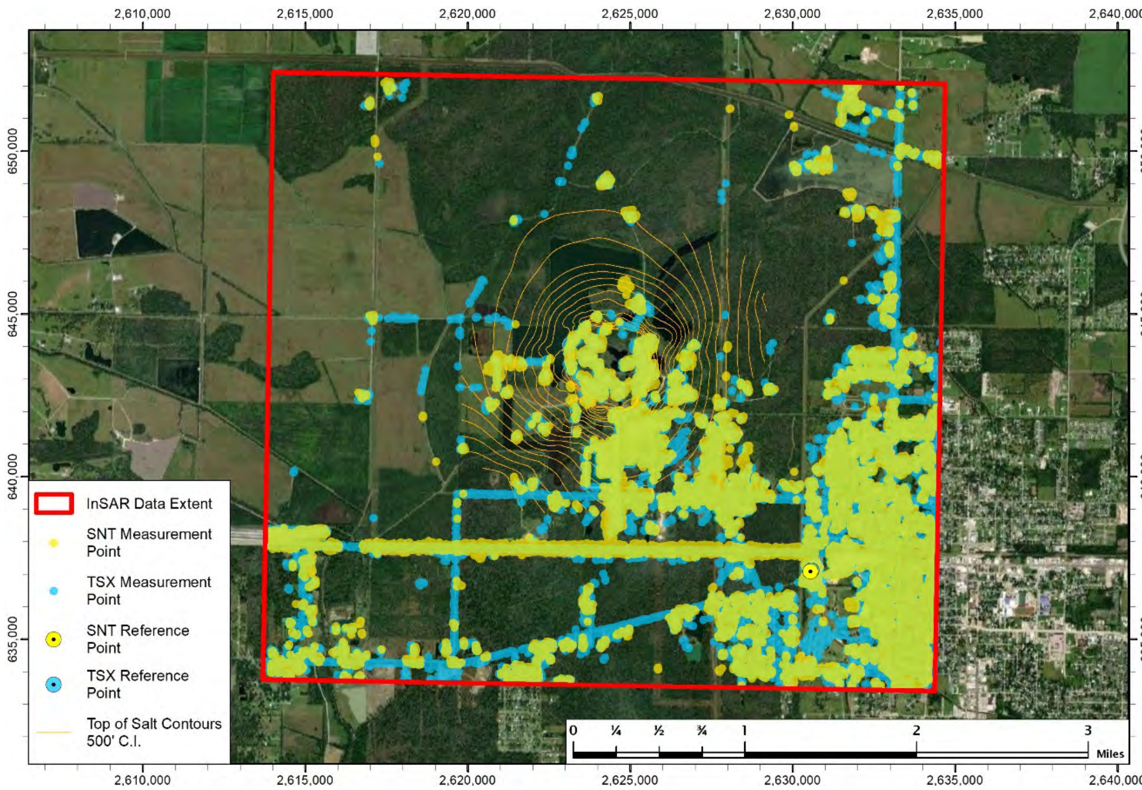

2.4 *Vertical and East-West Data*

In order to generate the 2-D dataset from the 1-D LOS data, a grid of cells measuring 82 x 82 feet was created across the 13.7 square mile data extent. For cells that contained at least one measurement point from each of ascending and descending 1-D datasets, a vertical and east-west displacement value was calculated by triangulation of the 1-D displacement values. If multiple 1-D measurement points from the same dataset were present within a particular cell, those values were averaged to produce a single 1-D displacement value prior to the calculation. The 2-D measurement points are located within the center of each cell for which the calculation was performed.

Two datasets were generated from this process, a vertical displacement and an east-west displacement dataset, with a time series of displacement values for each measurement point. The time series for these two datasets span the 6-month overlap of the data, June 16, 2022 to December 20, 2022. Interpolation of the data in time allows for a displacement value to be calculated for each date of data capture from either satellite. The resulting displacement time series display a higher frequency of displacement values than the source data. Figure 3 below provides additional information on the 2-D data parameters, calculated data timeline, and a diagram of the calculated displacement components in relation to the Sulphur Mines site.

Figure 3 – 2-D Data Parameters, Data Timeline, and Displacement Visualization

Analysis Characteristics	Vertical	East-West
Period covered	06/16/2022 - 12/20/2022	
No. of images processed	32	
Reference Point location - *WGS 84*	Lat: 30.235753 Long: -93.392842	
No. of measurement cells	3,536	
Cell size	82 x 82 ft	
Average displacement rate standard deviation	± 0.02 in	± 0.05 in

Calculated Data Timeline

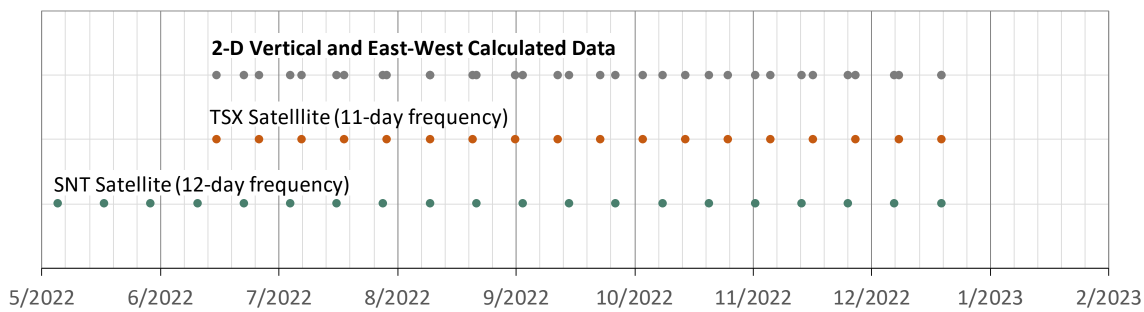

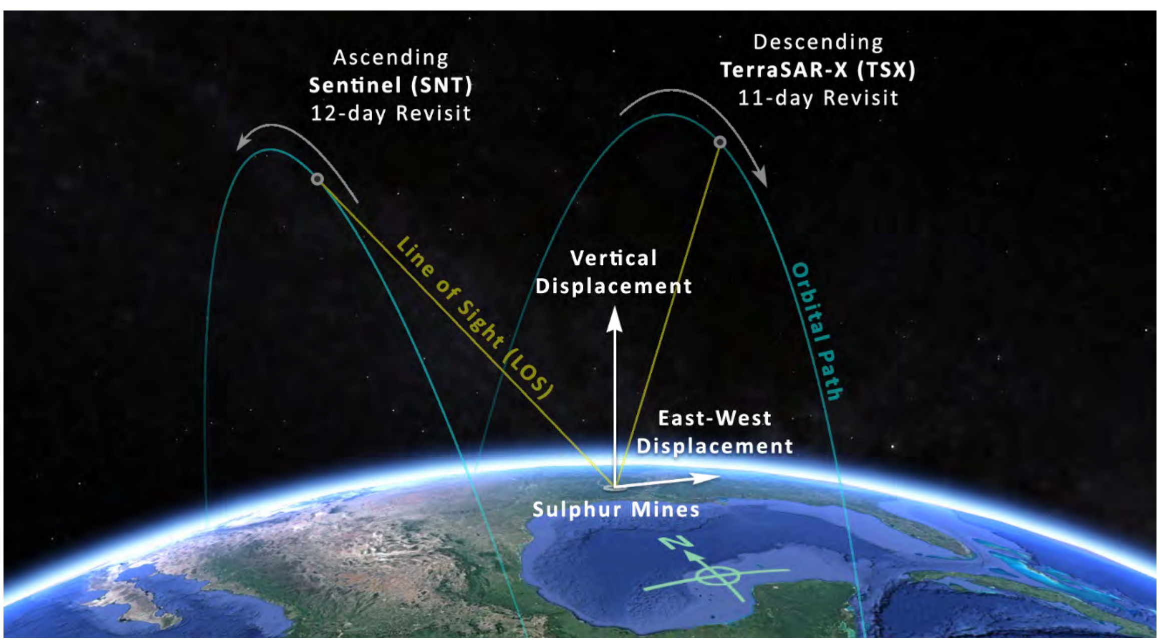

The vertical and east-west 2-D datasets generated from the 1D LOS data cover the same 13.7-square mile area. Figure 4 below depicts the grid cell positions with calculated measurement points in relation to the dome structure contours. Data coverage indicates areas where both SNT and TSX data were present within the data extent.

Figure 4 – 2-D Vertical and East-West Measurement Points

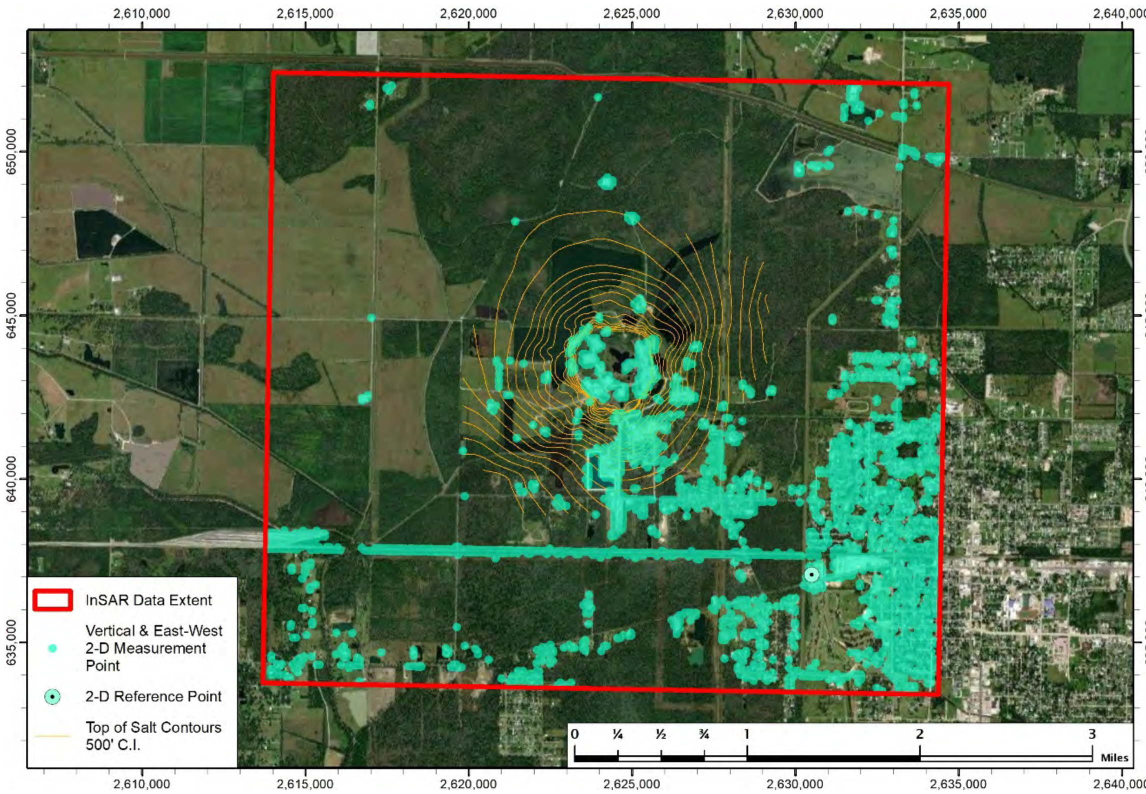

2.5 *Future Satellite Data Sources*

Future InSAR surveys will continue to utilize the historical dataset and 12-day revisit frequency of the ascending SNT satellite which captures data from the west of the site. However, in future surveys, the descending, high-resolution data captured from the east of the site will be provided by a separate satellite source than the current TSX satellite.

The descending data source will transition to a pair of high-resolution satellites that share the same orbit. These are another TSX satellite and the PAZ satellite, both with an 11-day revisit frequency. Their orbits are offset with the PAZ satellite passing over the site 4 days after the TSX satellite. This pair is referred to as the TSX/PAZ satellite constellation. The reason for the transition to the TSX/PAZ constellation is the increased data frequency that will result from a 4 and 7-day revisit period. Data capture for the TSX/PAZ constellation began on January 24, 2023 and will be maintained going forward for use in future surveys. Data capture from the current TSX satellite will be terminated in May 2023, providing ample overlap in the two high-resolution datasets to facilitate analysis efforts.

3.0 Areas of Interest

Past level surveys were performed on a set of thirty-six (36) physical monuments located on cavern wellheads, abandoned cavern well caps, and additional monuments positioned over and around the dome. Of this total, there were two (2) off-dome benchmark deep-rod monuments, twelve (12) additional rod monuments, and twenty-two (22) wells. Fifteen (15) of the wells are owned by Eagle, five (5) wells by Boardwalk, and two (2) by Liberty.

This system was designed to provide comprehensive monitoring for any areas that may be subject to subsidence as a result of current or past cavern operations. Survey measurements of these monument elevations were used to show time series charts of the elevation changes and movement trends as well as contour maps of the interpolated subsidence velocity and acceleration across the dome.

Similarly, the displacement values associated with each measurement point in an InSAR dataset can be used to generate contour maps of displacement velocity and acceleration, indicating the spatial distribution of subsidence magnitudes. Velocity and acceleration rates are determined via trend analysis of the displacement time series for each individual measurement point. In total, 3,536 calculated measurement points are available in the 2-D dataset for generation of contour maps. Roughly 300 of the points are located in close proximity to the dome top and cavern locations.

Given this number of measurement locations, a data reduction method must be considered to visually convey and evaluate trend consistency in displacement time series charts. This can be achieved by the grouping of measurement points to generate time series of the averaged displacement values for each group. Averaging of the displacement data within point groups also allows for the reduction of scatter (noise) in the plotted displacement values associated with individual measurement accuracy.

3.1 AOI Boundary Definition

In an effort to maintain a similar mode of reporting and analysis to past surveys, Areas of Interest (AOIs) defining the point groups were drawn to encompass the coverage achieved in prior monitoring. The following methodology was developed to standardize the creation of the AOI boundaries for grouping of the 2-D measurement point data:

- The 82 x 82-ft grid cell boundaries used to calculate the 2-D data were mapped to utilize the grid in drawing the AOIs.

- All digital cavern sonar files historically modeled by Lonquist at Sulphur Mines were overlaid and used to trace the "historical" maximum areal extent of each cavern in the dome.

- In place of the monuments previously surveyed above active and abandoned caverns, AOI boundaries were drawn to encompass each grid cell intersected by the historical sonar extent for each cavern. To cover a sufficient area above smaller caverns, a minimum 9-cell square (246 x 246 ft) was defined with the centroid of the cavern's areal extent falling within the center cell. Cavern AOIs are named according to the cavern location they monitor.

- In place of the monuments previously surveyed at additional positions around the dome, a minimum 9-cell square was again used with the historical monument position falling within the center cell of the 9-cell grid. Monument AOIs are named according to the historical survey monument they contain.

- No AOIs were created for the two off-dome benchmarks used in past surveys as the need for benchmarks to derive relative elevation measures has been replaced by the reference points defined in the InSAR analysis method.

In total, nineteen (19) Cavern AOIs and eleven (11) Monument AOIs were created to evaluate displacement trend consistency for key areas around the dome. Certain measurement points are contained in overlapping regions of two AOIs. These points will be included in the averaged displacement values calculated for both AOIs. Two AOIs were found to lack 2-D measurement data - PPG No. 016 and SMS Monument No. 006. This resulted from a lack of overlap between SNT and TSX measurement locations within the grid cells of those AOIs. 1-D LOS data is present, however, allowing for confirmation of trend consistency. This is discussed further in Section 6.3 along with available measures that can be taken to ensure future 2-D data acquisition where needed across the dome.

Table 2 below provides a list of the AOI areas and 2-D measurement point counts. Figure 5 depicts the proposed AOI boundaries in relation to the historical maximum cavern extents and past level survey monuments.

Table 2 – InSAR Point Group Parameters

AOI Name	Area (Acres)	2-D Cell Count	2-D Point Count
Cavern AOIs			
Liberty Gas Storage No. 001	6.63	43	4
Liberty Gas Storage No. 002	5.55	36	9
PPG No. 002	7.09	46	23
PPG No. 004	4.01	26	16
PPG (Brine) No. 005	2.31	15	2
PPG No. 006	9.87	64	20
PPG No. 007	7.09	46	21
PPG No. 016	5.09	33	0
PPG No. 018	3.39	22	3
PPG No. 020	2.78	18	5
PPG No. 021	4.47	29	7
PPG Brine No. 022	2.47	16	4
Sulphur Mines Storage No. 001-A	1.85	12	5
Sulphur Mines Storage No. A-1	1.39	9	3
Sulphur Storage No. 001	1.39	9	7
Sulphur Storage No. 002	1.39	9	9
Sulphur Storage No. 003	1.39	9	3
Sulphur Storage No. 004	1.39	9	9
Sulphur Storage No. 005	1.39	9	7
Monument AOIs			
SMS Monument No. 001	1.39	9	5
SMS Monument No. 002	1.39	9	8
SMS Monument No. 003	1.39	9	5
SMS Monument No. 004	1.39	9	4
SMS Monument No. 005	1.39	9	2
SMS Monument No. 006	1.39	9	0
SMS Monument No. 007	1.39	9	2
SMS Monument No. 008	1.39	9	6
SMS No. 003	1.39	9	5
SMS No. 004	1.39	9	3
SMS No. 005	1.39	9	4

Figure 5 – InSAR Point Group AOI Boundaries

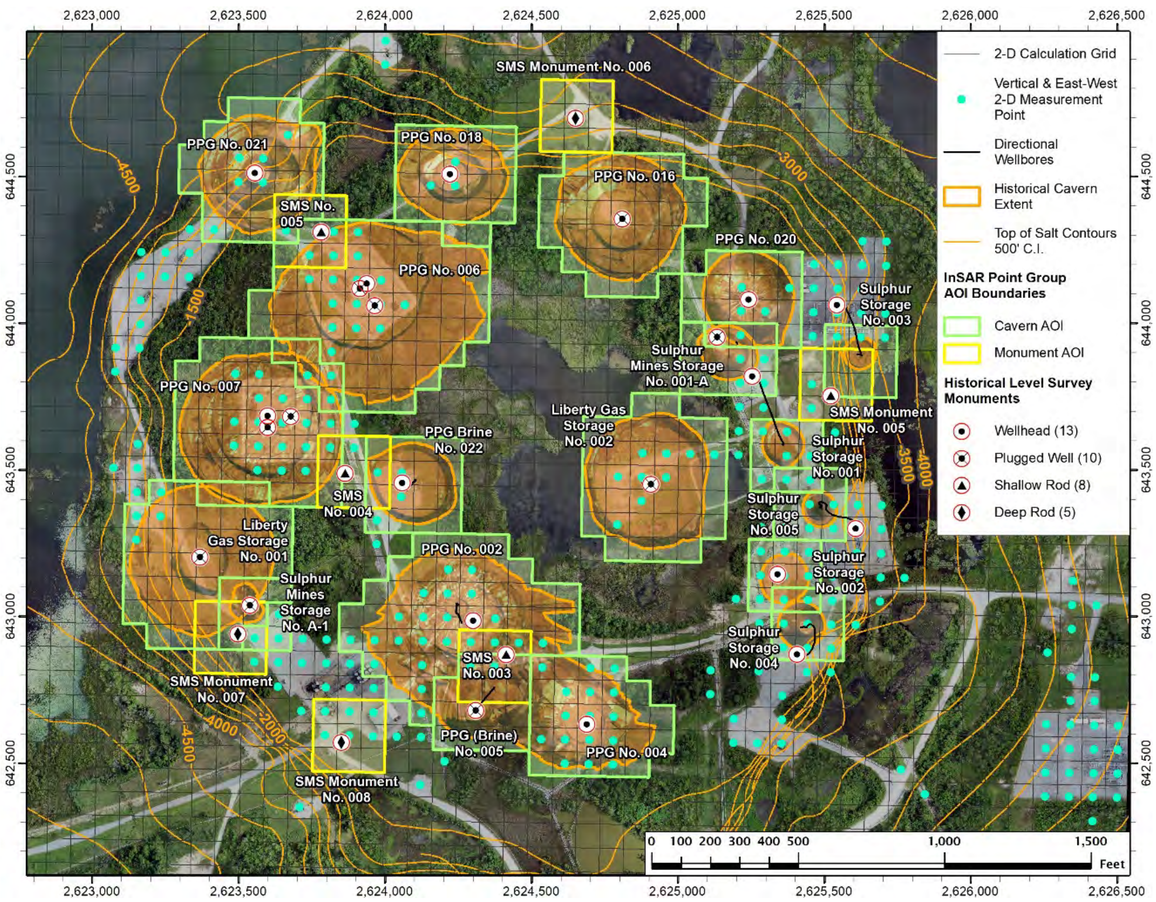

Four monument AOIs not shown above are located a few hundred feet further to the south over deeper portions of the dome. A larger format map has been included as Appendix A that more clearly delineates the boundaries of the proposed AOI regions in relation to the 2-D measurement point locations. The map also depicts the surface locations of cavern wells along with well names, serial numbers, and statuses.

4.0 Subsidence Rate Determination

Per guidance issued by the Injection and Mining Division of the LA DNR in 2019, a determination of the current rate of subsidence over each survey point is to be evaluated. This is considered the "velocity" of ground displacement at each monument. Additionally, the guidance requests that the rate at which this "velocity" is changing be determined if non-linear movement trends are identified. This rate of change is considered the "acceleration" of ground displacement at each monument. In place of monument elevations, the displacement values associated with each measurement point in the InSAR survey are used. The historical displacement data provides the basis for determining these ground movement rates through analysis of the long-term trends.

4.1 Selection of Trend Equation

Trend analysis data was generated by plotting average displacement values over time for the measurement point groups within the AOI regions. The use of non-linear trend equations was evaluated which could yield acceleration estimates in addition to velocity. However, due to the relatively short 6-month timeframe of the data in combination with the accuracy range of the measurements, calculated accelerations varied dramatically and were found to lack statistical significance.

Knowledge of the subsidence behavior over the site from past level surveys and evaluation of the 6-year SNT data provides evidence of nearly linear subsidence trends that contradict the acceleration values calculated for the 6-month 2-D data. The decision was made to calculate subsidence values using linear trend equations and to postpone evaluation of vertical and east-west acceleration across the site until longer-term datasets can be generated. For the time being, notable deviation from the calculated linear trends will be evident, if present, in the AOI time-series charts provided with this report, but the associated acceleration rates cannot be accurately estimated using the timeframe of the 2-D dataset.

Figure 6 below shows sample point groups from the SNT 1-D data that have been plotted to convey the discrepancy in accelerations identified using the 6-month timeframe. The charts provide examples of the acceleration rates, represented by the magnitude of curve in the trend lines, if a multi-year timeframe is used relative to a 6-month timeframe.

Figure 6 – Non-linear Trend Estimation for Multi-year vs. 6-Month Datasets

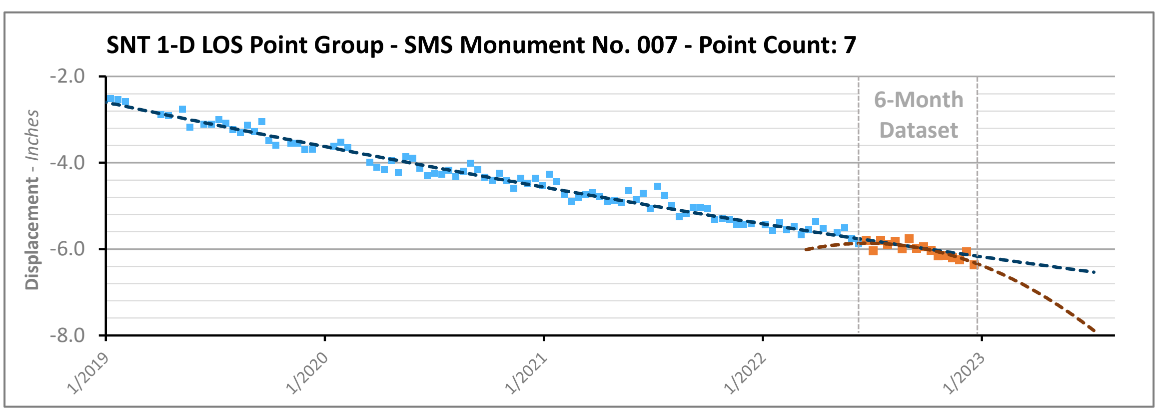

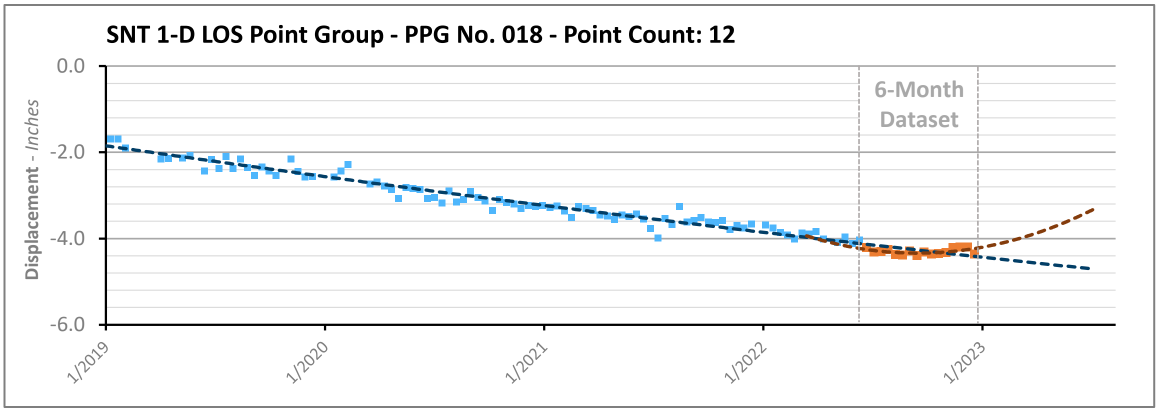

4.1 Linear Regression Analysis

To evaluate subsidence trends in the 2-D displacement data, a linear least squares regression analysis was performed to define trend variables for each AOI dataset. In least squares regression analysis, the sum of the squared difference between model-predicted and actual data is minimized by a computationally derived set of model variables. The model formula is shown below in Equation 1.

$$D(t) = \beta_0 + \beta_1 t \qquad \text{Equation 1}$$

where $D(t)$ is the predicted displacement at time (t), and β_0, and β_1, are fit parameters determined by the regression analysis performed on the historical dataset for each AOI.

Once this model has been defined, the predicted rate of displacement can be calculated by taking the derivative of the model equation with respect to time. The formula used to approximate the rate of displacement is provided below in Equation 2.

$$d/dt\ [D(t)] = \beta_1 \qquad \text{Equation 2}$$

where $d/dt\ [D(t)]$ is the predicted rate of displacement. This value represents the velocity of ground displacement estimated by the model for each AOI. Velocity is calculated irrespective of time (t) in linear regressions. In the vertical data, negative velocity values represent downward rates of ground displacement and positive values represent upward displacement. In the east-west data, negative values are associated with westward displacement rates, and positive values are eastward.

5.0 Data Analysis

5.1 Time Series Plots

Averaged displacement values for vertical and east-west movement were plotted for each AOI with respect to time. The resulting time series charts provide a visual depiction of the calculated trends and associated data. These plots are shown for reference in Appendix B. The modeled trends for each AOI are shown by the dashed lines that overlay the displacement measurements on each plot. No divergence was seen between the data and the linear trend lines that would imply material acceleration of displacement rates is occurring within any of the plotted AOI datasets.

AOIs with higher point counts were found to exhibit less scatter in the plotted data, indicating that the accuracy limitations in individual measurement point values were mitigated through data averaging. The properties of the 1-D SNT and TSX source data likely also play a role in the scatter depicted in the charts. The specific number and distribution of the 1-D measurement points and the quality of the radar targets within each AOI region will lead to variation in measurement precision for the averaged 2-D displacement data.

Overall, it was noted that scatter was greater in the east-west displacement data compared to the vertical data. This difference is supported by the standard deviation values provided for the vertical and east-west displacement rates reported by TREA. This may be generally indicative of the accuracy of vertical displacement relative to east-west displacement measurements in InSAR data.

The trend models generated for each AOI were used to identify the velocity of vertical and east-west displacement in inches/year. These calculated values are provided in Table 3 below.

5.2 Displacement Velocity Maps

The same process that was followed to generate trend equations for the AOI point groups was also performed on each individual measurement point in the 2-D dataset. The velocity values calculated for each point were used to generate contours to illustrate the spatial distribution of displacement velocities across the surveyed region. Vertical and east-west velocity contours are provided on maps in Appendices C and D, respectively, for reference.

Table 3 – InSAR Point Group Vertical and East-West Displacement Velocities

AOI Name	Vertical Displacement		East-West Displacement	
	Velocity *(Inches/Year)*	Direction	Velocity *(Inches/Year)*	Direction
Cavern AOIs				
Liberty Gas Storage No. 001	-0.92	Downward	0.08	Eastward
Liberty Gas Storage No. 002	-1.91	Downward	-1.10	Westward
PPG No. 002	-1.45	Downward	-0.06	Westward
PPG No. 004	-1.40	Downward	-0.28	Westward
PPG (Brine) No. 005	-1.71	Downward	0.30	Eastward
PPG No. 006	-1.21	Downward	-0.11	Westward
PPG No. 007	-1.29	Downward	0.15	Eastward
PPG No. 016	N/A	N/A	N/A	N/A
PPG No. 018	-0.91	Downward	-0.78	Westward
PPG No. 020	-1.28	Downward	-0.58	Westward
PPG No. 021	-0.95	Downward	0.04	Eastward
PPG Brine No. 022	-1.64	Downward	0.05	Eastward
Sulphur Mines Storage No. 001-A	-1.45	Downward	-0.79	Westward
Sulphur Mines Storage No. A-1	-0.96	Downward	0.18	Eastward
Sulphur Storage No. 001	-1.40	Downward	-0.81	Westward
Sulphur Storage No. 002	-1.42	Downward	-0.99	Westward
Sulphur Storage No. 003	-1.06	Downward	-0.94	Westward
Sulphur Storage No. 004	-1.21	Downward	-1.09	Westward
Sulphur Storage No. 005	-1.34	Downward	-0.99	Westward
Monument AOIs				
SMS Monument No. 001	-0.35	Downward	0.10	Eastward
SMS Monument No. 002	-0.59	Downward	-0.19	Westward
SMS Monument No. 003	-0.56	Downward	0.58	Eastward
SMS Monument No. 004	-0.69	Downward	-0.18	Westward
SMS Monument No. 005	-1.12	Downward	-0.58	Westward
SMS Monument No. 006	N/A	N/A	N/A	N/A
SMS Monument No. 007	-0.97	Downward	0.06	Eastward
SMS Monument No. 008	-1.07	Downward	-0.02	Westward
SMS No. 003	-1.62	Downward	0.01	Eastward
SMS No. 004	-1.48	Downward	0.14	Eastward
SMS No. 005	-0.99	Downward	0.03	Eastward

5.3 Observations

In general, the subsidence rate is greatest over the eastern-central portion of the dome with a gradual tapering toward the dome edges. Subsidence rates continue to slow at further distances from the dome, but the slowing trend is less uniform as evidenced to the south and southeast of the dome where data coverage is more densely present. The closest instance of zero subsidence is seen to the south-southeast at 0.83 miles from the approximate dome center.

The shape of the velocity contours generally agrees well with the Fall 2021 analysis of level survey data. Three main differences that were noted in the new data are: 1) A lesser rate of subsidence at PPG No. 006, which previously showed the second greatest subsidence rate of the monuments surveyed, 2) Higher rates of subsidence in the southern-central portion of the dome around PPG Brine No. 022 and the cavern gallery that includes caverns PPG No. 002, PPG No. 004 and PPG (Brine) No. 005, and 3) Higher rates of subsidence along the eastern flank of the dome and particularly at Sulphur Storage No. 002. Following analysis described in Sections 6.2 and 6.3, these observations are assumed to be related to differences in the survey methods and not indicative of changing subsidence trends.

The AOI point groups with the highest rates of subsidence were Liberty Gas Storage No. 002, PPG (Brine) No. 005 and PPG Brine No. 022, all located relatively centrally within the dome footprint. The maximum rate of subsidence was -1.91 inches/year for the Liberty Gas Storage No. 002 AOI in the eastern-central portion of the dome over the plugged and abandoned cavern of the same name. This agrees with prior level surveys, with the Liberty Storage No. 002 well cap identified as the fastest subsiding monument, at the same rate of -1.91 inches/year in the most recent Fall 2021 analysis. None of the AOI point groups exhibited upward movement in the calculated trends.

East-west displacement velocities were seen to generally indicate that lateral ground displacement is occurring toward the center of the dome. Lateral ground displacement can be expected to coincide with vertical displacement in this way. This is due to the imbalance of geomechanical stress within the sub-surface soils being directed inward toward the center of the subsidence basin. The phenomenon is akin to lateral soil creep that occurs over time on shallow slopes due to gravity. Although the dataset is limited to east-west displacement, it can be assumed that north-south movement is occurring in a similar fashion toward the dome center in accordance with the shape of the vertical subsidence basin. The counter-clockwise tilt in the east-west contour distribution may be partially explained by the viewing directions of the satellites not being precisely from the east and west, as was conveyed through correspondences with TREA.

On the eastern side of the dome, horizontal velocities are seen to be generally greater than velocities on the western side of the dome, suggesting that the eastern side of the dome may be more susceptible to horizontal movement. Additionally, it appears that horizontal displacement exhibits more spatial irregularity than vertical displacement across the analysis area. Similar magnitudes of east-west displacement observed within the dome footprint are observed sporadically across the full analysis area.

The AOI point groups with the highest rate of east-west displacement were Liberty Gas Storage No. 002 and Sulphur Storage No. 004 with westward displacement values of -1.10 and -1.09 inches/year, respectively. The AOI point groups PPG No. 018, Sulphur Mines Storage No. 001-A, and Sulphur Storage Nos. 001, 002, 003, and 005 all additionally exhibited notable westward displacement rates. The AOI point group with the highest rate of eastward displacement was SMS Monument No. 003 with a value of +0.58 inches/year. This AOI is positioned above the center of the cavern gallery that includes caverns PPG No. 002, PPG No. 004 and PPG (Brine) No. 005. It should be noted that knowledge of east-west movement is limited to this 6-month dataset and cannot be compared to a prior history to confirm consistency in the trends observed.

6.0 Supplementary Discussion

This was the first year that InSAR has been used to conduct the annual subsidence monitoring survey at the Sulphur Mines Salt Dome. A few additional areas of clarification regarding this transition are addressed in this section.

6.1 TRE-Altamira InSAR Analysis

Although similar results were ultimately obtained, it should be noted that the method of point grouping utilized in this analysis differs from the analysis performed by TREA which was based on circular 100-foot radius buffers drawn around the historical level survey monument locations. Subsidence rates and charts provided in the TREA analysis will show some differences as a result. Future analyses performed by TREA will utilize the same point groups developed for this analysis to better evaluate the ground areas located above the historical cavern footprints.

6.2 InSAR Comparison to Historical Analyses

As noted in Section 5.3, the vertical displacement rates identified in the InSAR analysis agree well with the trends established through past level surveys of the site. A few differences were observed as discussed in that section. These differences may be explained by the respective accuracy limitations of each dataset, namely the short timeframe of the current 6-month InSAR dataset and the lesser frequency and spatial density of the data in the level surveys. The overall agreement is encouraging in the validation it provides for each survey method. The following section summarizes additional evaluation that was performed to confirm multi-year trend consistency across the dome using the 6-year SNT dataset.

Agreement between the level surveys and InSAR survey is partly a consequence of the location of the control elevation used in each survey method. In past level surveys, the elevation of an off-dome benchmark monument was held constant for the purpose of calculating the relative elevations of the other monuments in the survey loops. In the InSAR analysis, a reference point is chosen from among the available measurement points for the same purpose. The vertical displacement at each measurement point relative to the displacement at other measurement points is known. Displacement over time is calculated for each point by assigning zero displacement to the reference point. The InSAR reference point and the off-dome level survey benchmark are located at similar distances from the dome, allowing for subsidence measurements to be made relative to a similar baseline in both survey methods.

Figure 7 below provides a comparison of the subsidence velocity contours generated following the Fall 2021 level survey and the Fall 2022 InSAR survey as well as the positions of the off-dome benchmark and the InSAR reference point.

Figure 7 – Comparison of 2021 and 2022 Subsidence Velocity Contours

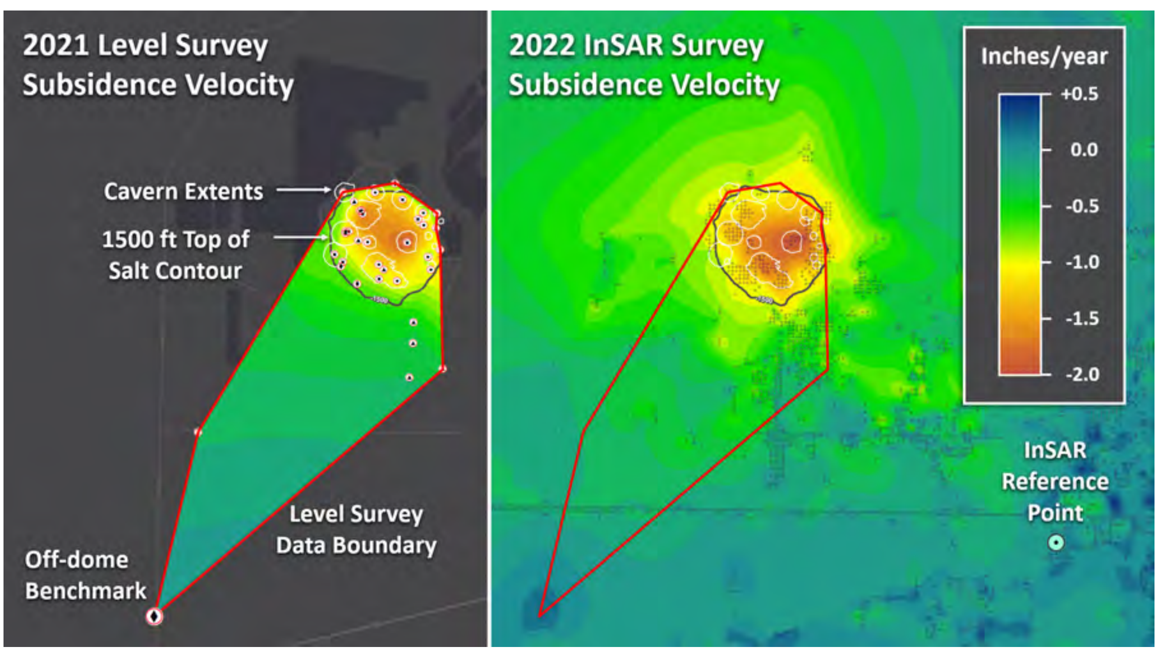

6.3 Sentinel 1 (SNT) 6-Year InSAR Dataset

A 5.5-year dataset from a Sentinel 1 (SNT) low-resolution satellite was originally processed and evaluated in May 2022. This analysis informed the decision to transition to InSAR surveys for subsequent annual subsidence monitoring over the dome. Subsidence trends were evaluated and compared to historical level survey results. The multi-year dataset showed highly-consistent and mostly linear displacement rates across the dome which supported the findings of prior level surveys.

Among the main findings of the review, was the influence of significant east-west ground movement on the 1-D LOS measurements gathered from the satellite's eastward and relatively shallow (42.5° from vertical) viewing direction. This was evident from lower-than-expected negative displacement rates on the eastern side of the dome. Westward ground movement (toward the satellite) on the eastern side of the dome was believed to be lowering the net negative displacement recorded from the satellite's vantage point. Additionally, the need to incorporate high-resolution satellite data in future surveys was identified in the review. This was due to the presence of data gaps over vegetated and marshy areas and areas subject to changing ground conditions.

The incorporation of a second satellite dataset from the east of the site confirmed the occurrence of lateral ground movement and allowed for accurate measurement of vertical and east-west displacement. Certain areas over the dome additionally benefitted from increased data density from the high-resolution TSX satellite.

The updated 6-year SNT dataset was evaluated again as part of this review. The primary objective was to confirm continuation of the trends identified in May 2022. Time series charts were generated for each of the AOI regions and reviewed for recent trend consistency. This was done to confirm that the subsidence trends identified using the 6-month 2-D data could be considered continuations of the historical trends within each AOI. Figure 8 below provides an example of a time series for an AOI region that was reviewed as part of the historical evaluation of the SNT 1-D LOS data.

No material deviations from the historical trends were observed during the 2022 timeframe that warranted further investigation. Overall, the subsidence rates identified through linear regression of the 6-month 2-D dataset are believed to agree with historical trends and to accurately represent ground displacement rates within the AOI regions.

Figure 8 – Sample SNT 1-D Displacement Time Series of AOI Region

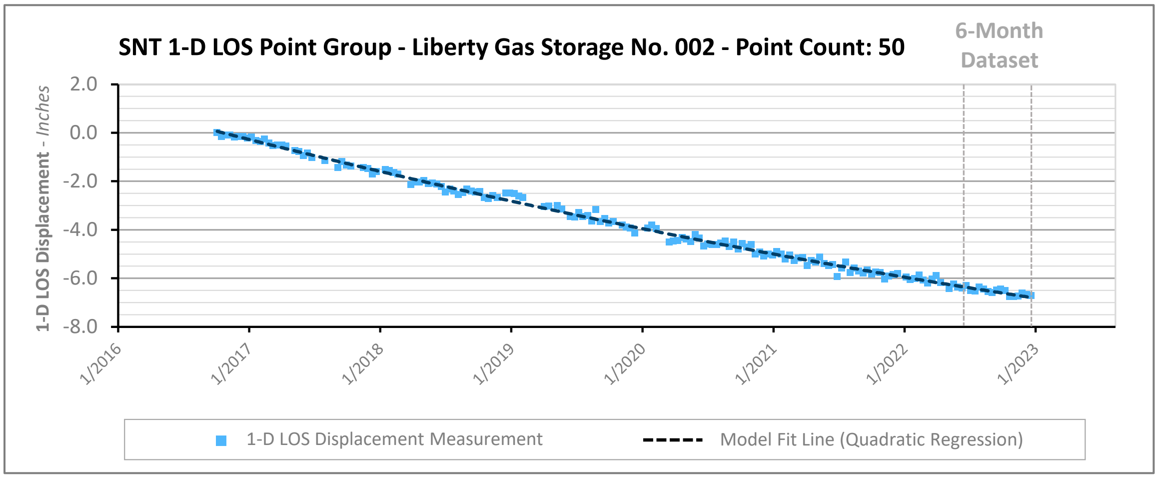

6.4 *Evaluation of Data Gaps*

Two AOI regions were not able to be evaluated for vertical and east-west displacement due to a lack of 2-D measurement data within their boundaries. These were PPG No. 016 and SMS Monument No. 006, which are adjacent AOIs in the northern portion of the dome. PPG No. 016 surrounds the areal extent of the plugged and abandoned cavern of the same name. SMS Monument No. 006 is a 9-cell square (246 x 246 ft) centered over a deep-rod monument of the same name. This monument was previously installed to monitor subsidence over the dome flank nearest to cavern PPG No. 016.

Calculated 2-D data was not available for these AOIs due to a lack of overlap between SNT and TSX measurement locations within their grid cells. 1-D LOS data is present within the AOI regions, however, allowing for an evaluation of trend consistency over the data timeframes. The PPG No. 016 AOI contained four (4) measurement points from the 6-month TSX dataset. The SMS Monument No. 006 AOI contained eight (8) measurement points from the TSX dataset and one (1) measurement point from the 6-year SNT dataset. The time series of the averaged 1-D displacement data are provided below in Figure 9 with trendlines overlaid.

Overall displacement rates can be seen to be consistent over the available data timeframes. Due to the presence of a single SNT measurement point in the SMS Monument No. 006 AOI, the associated chart displays a significant amount of data scatter. Trend consistency still appears to be generally present throughout the 2022 timeframe.

Figure 9 – 1-D Displacement Time Series of AOIs with No 2-D Data

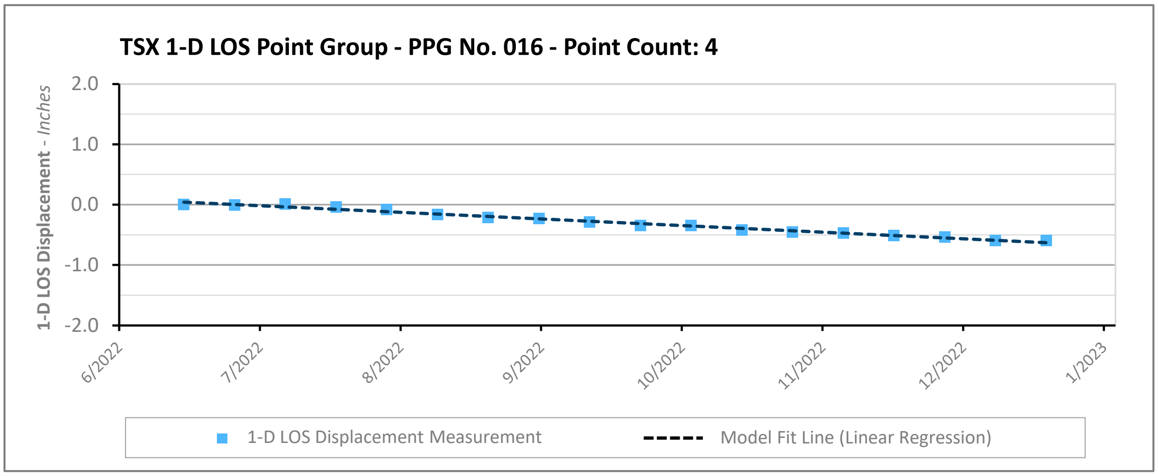

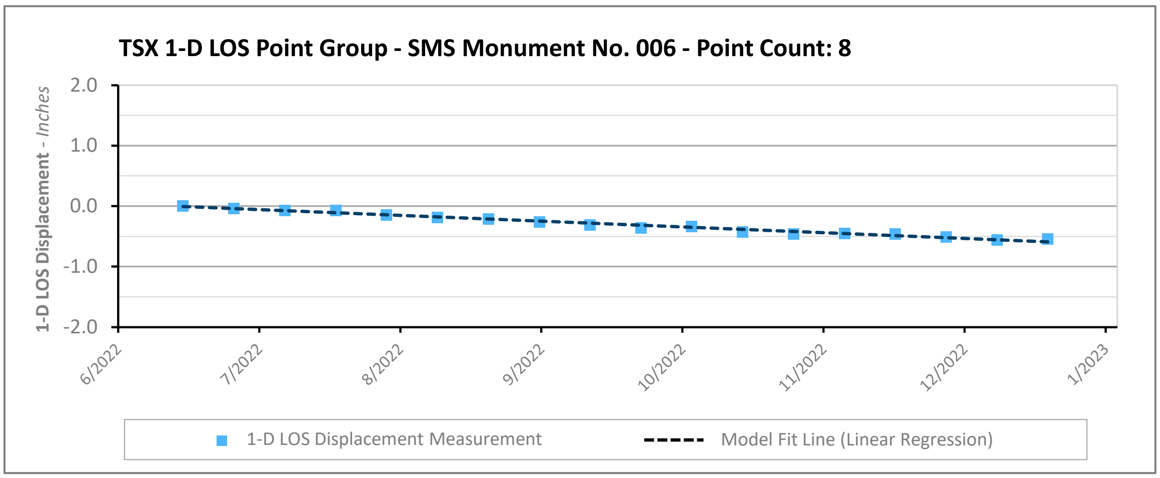

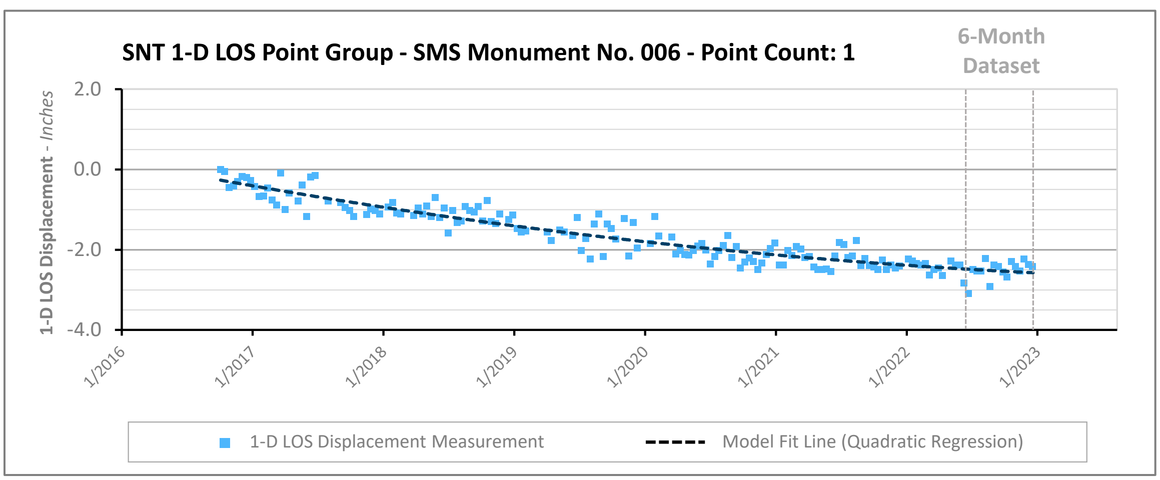

Due to the low availability of data in the PPG No. 016 and SMS Monument No. 006 AOIs, the installation of corner reflectors is recommended. Corner reflectors are metallic angular structures that can be erected at specific positions to ensure reliable data capture in future surveys. Corner reflectors provide a ground target with the highest amplitude of signal return in radar imagery.

6.5 Fall 2022 Trend Consistency

Based on the supplementary review of the 1-D LOS datasets and the evaluation of the calculated 2-D data, subsidence trends appear to be continuing as observed in the multi-year SNT data and as historically defined in past level surveys. This indicates that rates of cavern closure and other local factors of influence are continuing to act in a consistent manner at this time.

7.0 Conclusions

1. The first annual InSAR survey of the Sulphur Mines Salt Dome provided improved accuracy and definition of the subsidence basin geometry and lateral displacement occurring over the dome.

2. In general, the subsidence rate is greatest over the eastern-central portion of the dome with a gradual tapering toward the dome edges. At further distances from the dome, subsidence rates continue to slow but exhibit more variability in the mapped contours. The greatest subsidence rates were identified for the cavern AOIs Liberty Gas Storage No. 002, PPG (Brine) No. 005 and PPG Brine No. 022, with the maximum rate being -1.91 inches/year at Liberty Gas Storage No. 002.

3. East-west displacement velocities were seen to generally indicate that lateral ground displacement is occurring toward the center of the dome. The AOI point groups with the highest rate of east-west displacement were Liberty Gas Storage No. 002 and Sulphur Storage No. 004 with westward displacement values of -1.10 and -1.09 inches/year, respectively. The AOI point group with the highest rate of eastward displacement was SMS Monument No. 003 with a value of +0.58 inches/year.

4. Two AOI regions were not able to be evaluated for vertical and east-west displacement due to a lack of 2-D measurement data within their boundaries. An evaluation of the 1-D LOS data within the AOIs shows consistency of the subsidence trends over the available data timeframes. It is recommended that corner reflectors be installed in these areas to ensure reliable data capture in future surveys.

5. Subsidence rates identified in the InSAR analysis agree well with the trends established through past level surveys of the site. Based on the supplementary review of the 1-D LOS datasets and the evaluation of the calculated 2-D data, subsidence trends appear to be progressing as historically defined. This indicates that rates of cavern closure and other local factors of influence are continuing to act in a consistent manner at this time.

Appendix A – Map of 2-D InSAR Measurement Points and AOI Boundaries

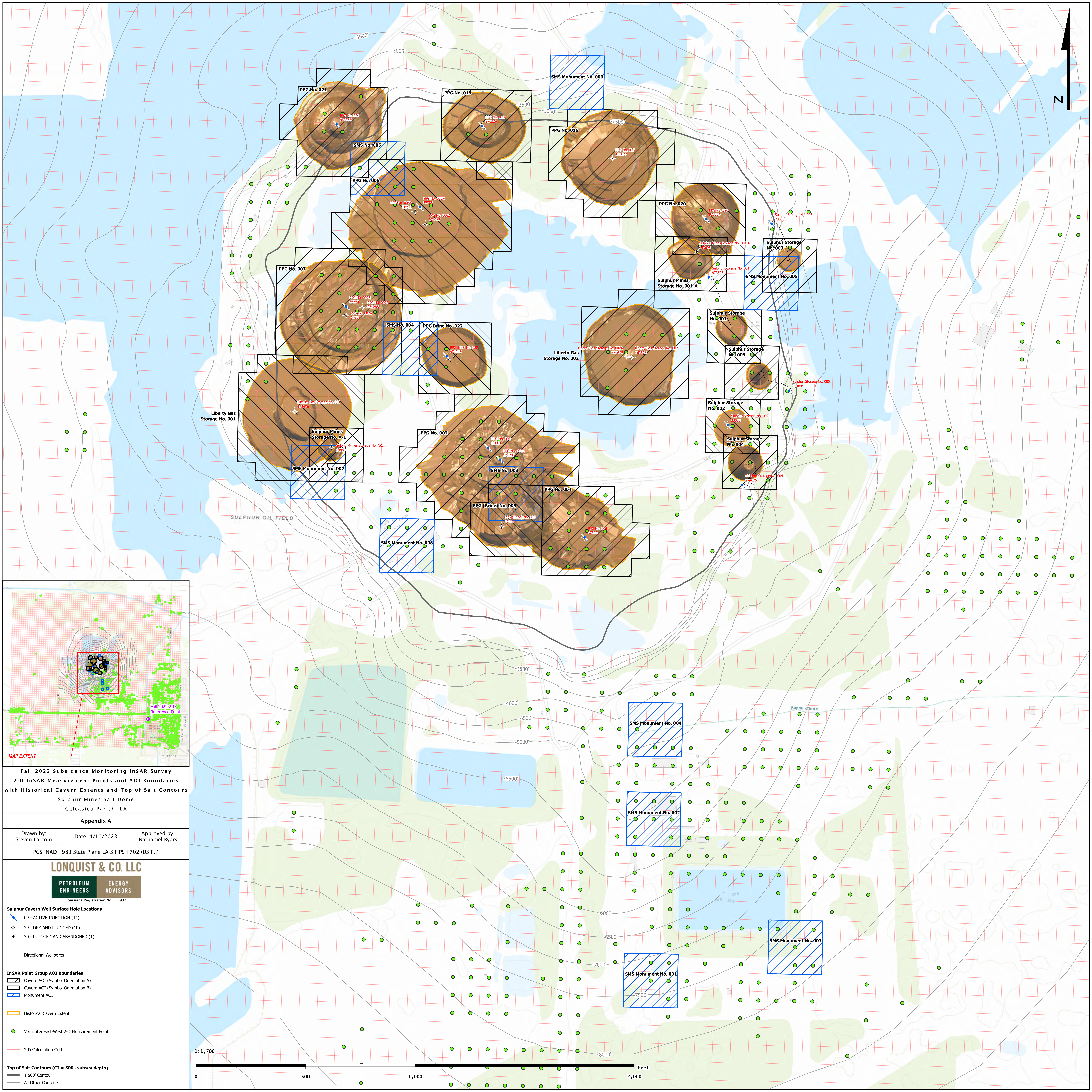

Fall 2022 Subsidence Monitoring InSAR Survey
2-D InSAR Measurement Points and AOI Boundaries
with Historical Cavern Extents and Top of Salt Contours
Sulphur Mines Salt Dome
Calcasieu Parish, LA

Appendix A

Drawn by: Steven Larcom	Date: 4/10/2023	Approved by: Nathaniel Byars

PCS: NAD 1983 State Plane LA-S FIPS 1702 (US Ft.)

LONQUIST & CO. LLC
PETROLEUM ENGINEERS | ENERGY ADVISORS
Louisiana Registration No. EF5937

Sulphur Cavern Well Surface Hole Locations
- 09 - ACTIVE INJECTION (14)
- 29 - DRY AND PLUGGED (10)
- 30 - PLUGGED AND ABANDONED (1)

Directional Wellbores

InSAR Point Group AOI Boundaries
- Cavern AOI (Symbol Orientation A)
- Cavern AOI (Symbol Orientation B)
- Monument AOI

Historical Cavern Extent

Vertical & East-West 2-D Measurement Point

2-D Calculation Grid

Top of Salt Contours (CI = 500', subsea depth)
- 1,500' Contour
- All Other Contours

Appendix B – Vertical & East-West Displacement Time Series – AOI Point Groups

Averaged Vertical Displacement Time Series - AOI Point Groups

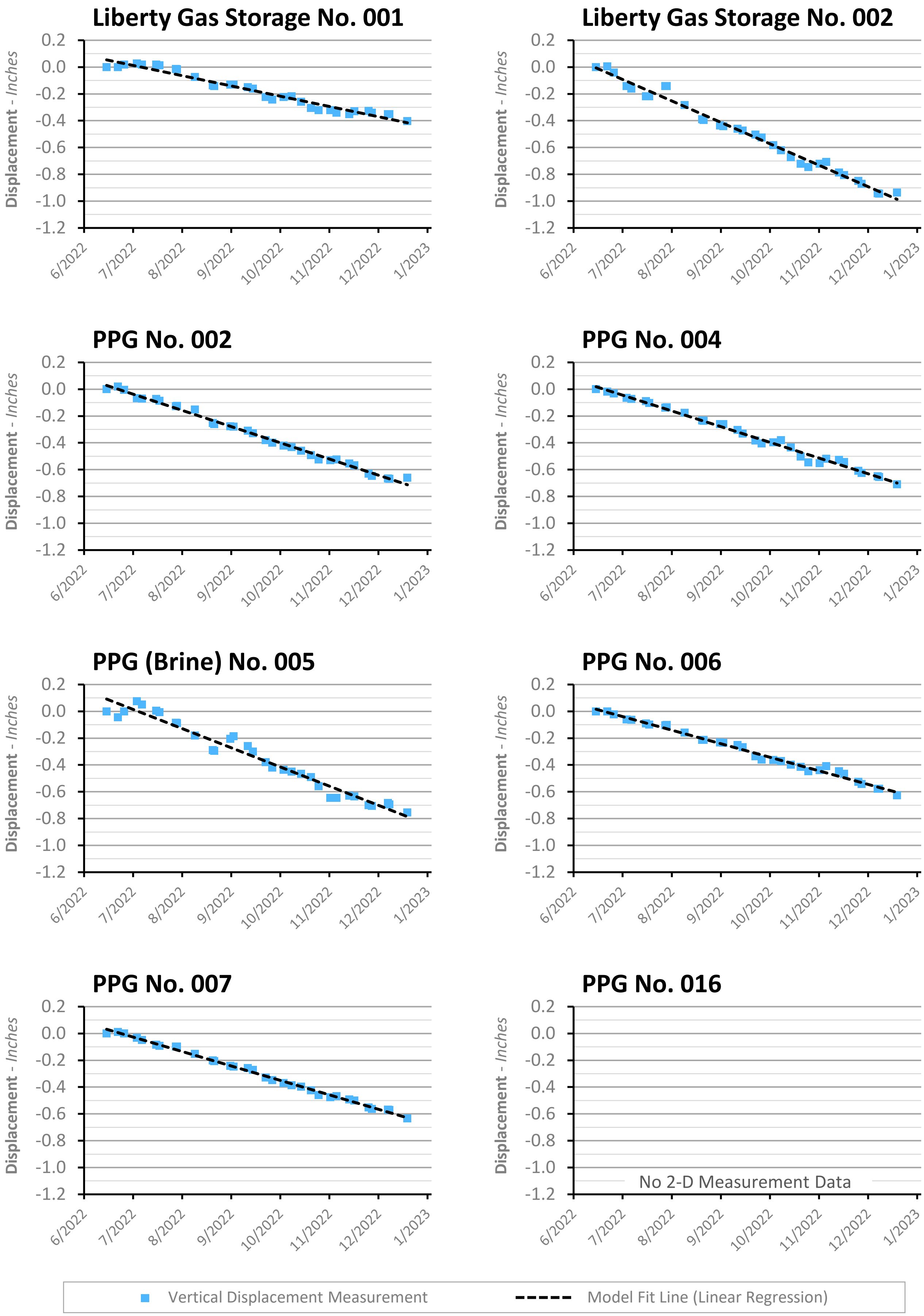

Averaged Vertical Displacement Time Series - AOI Point Groups

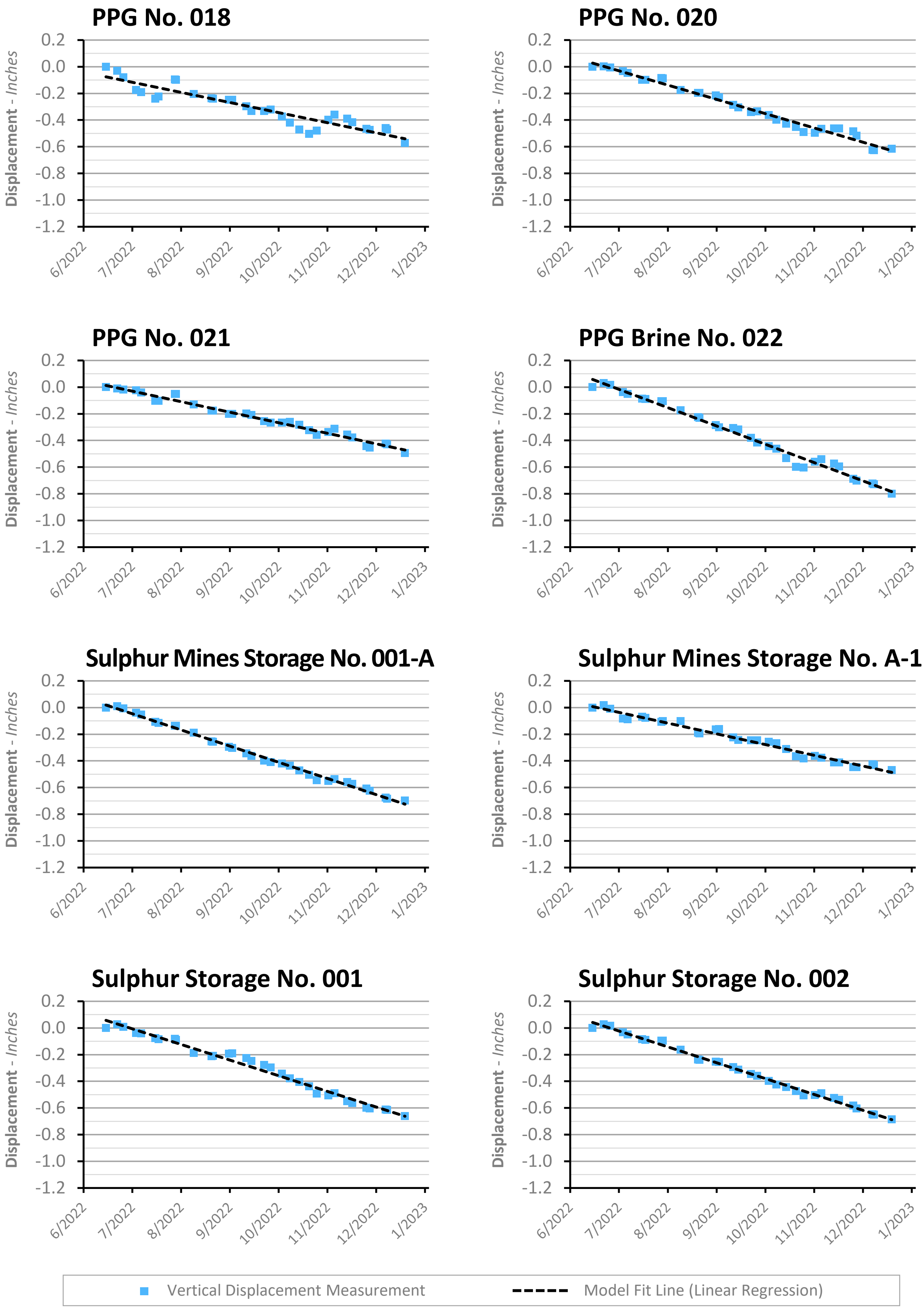

Averaged Vertical Displacement Time Series - AOI Point Groups

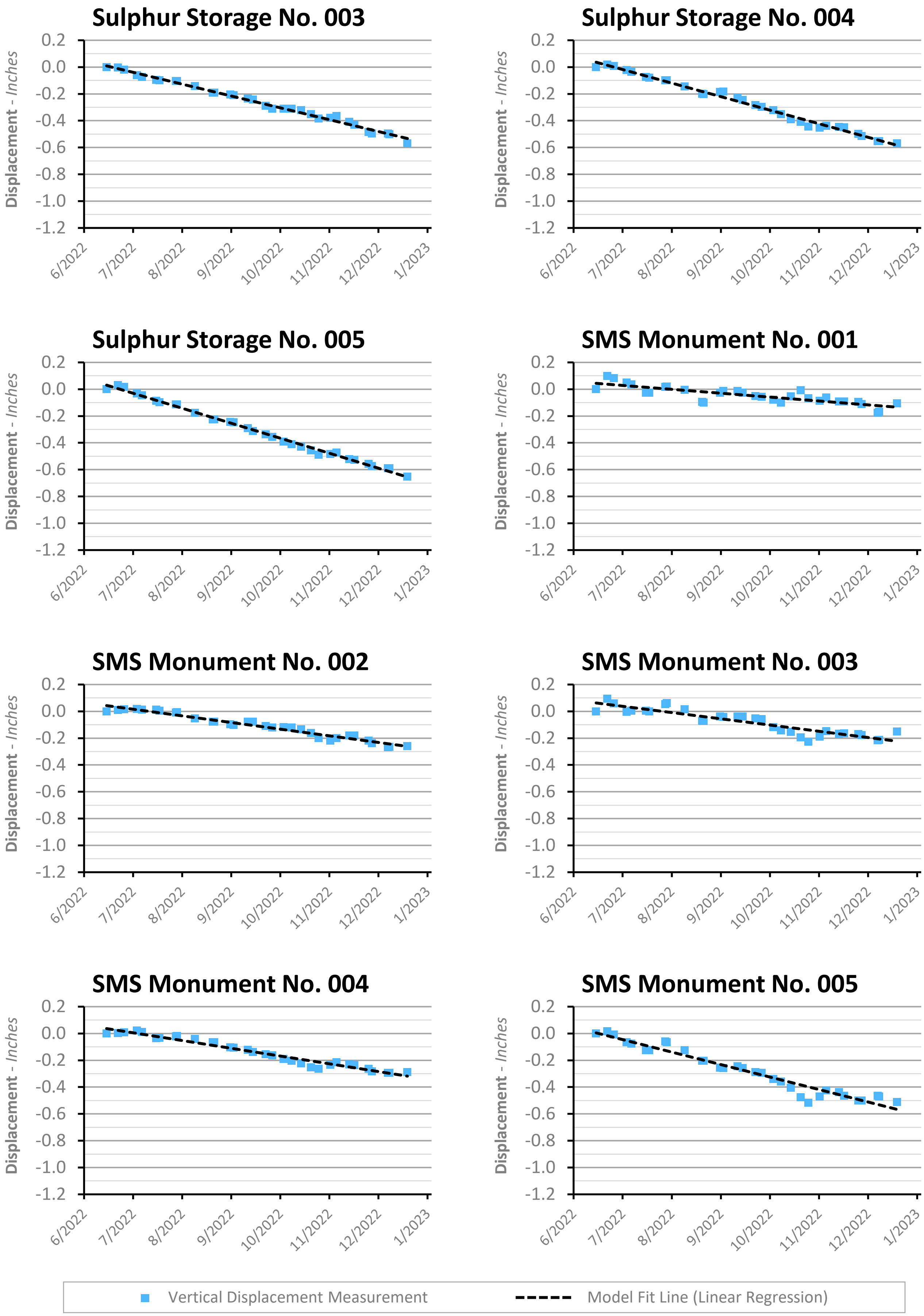

Averaged Vertical Displacement Time Series - AOI Point Groups

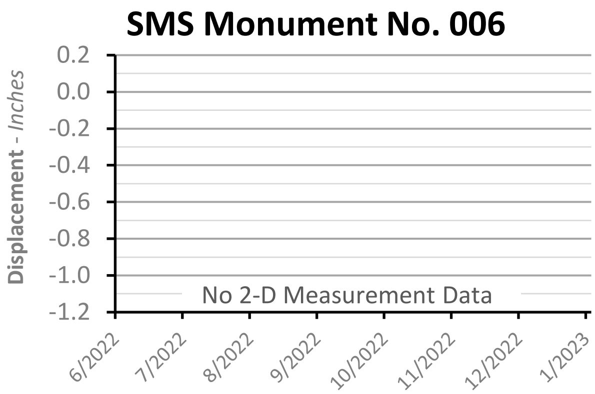

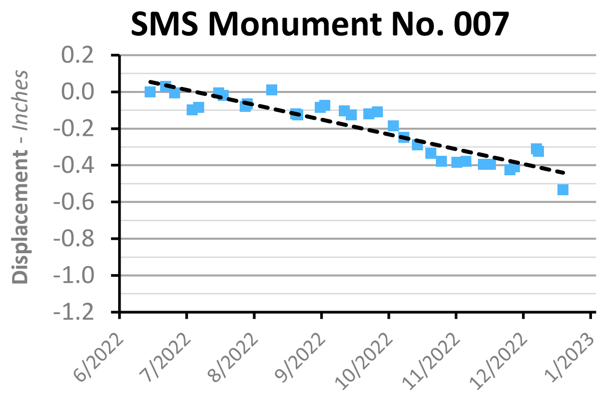

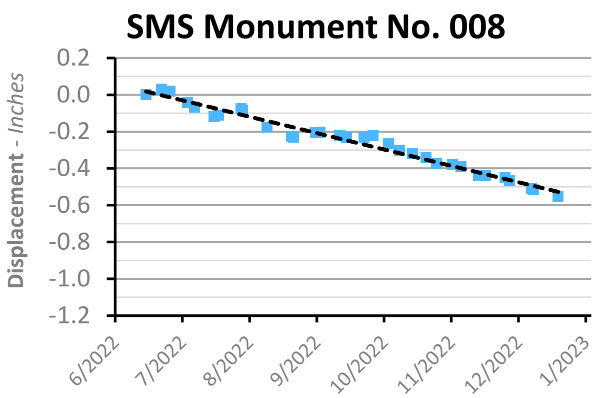

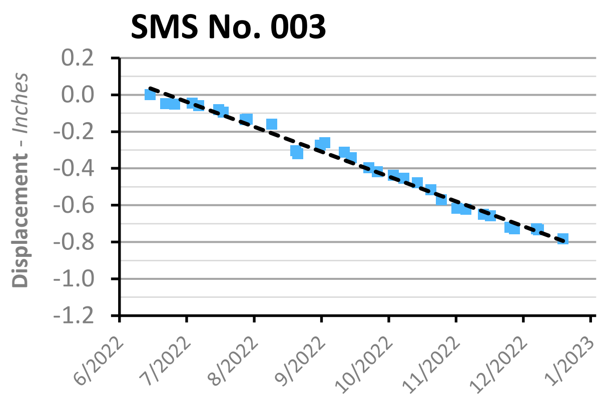

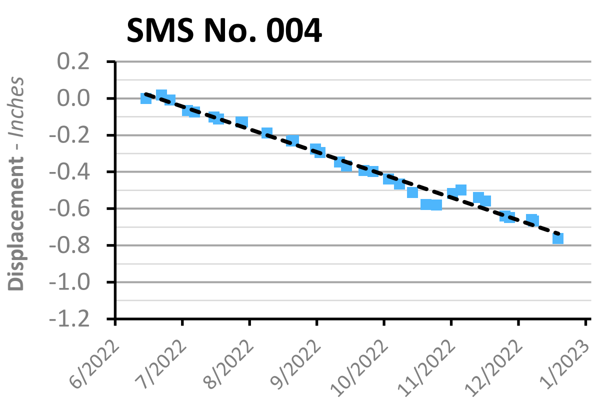

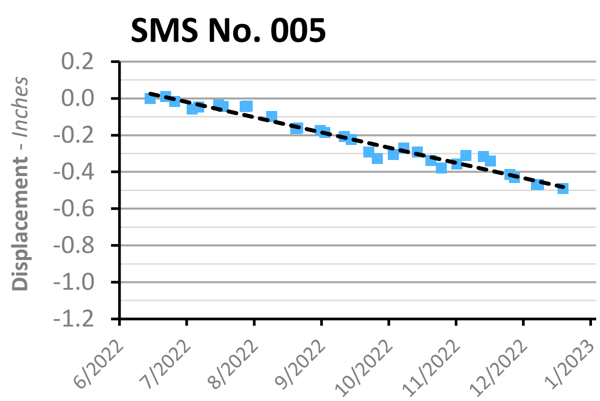

Vertical Displacement Measurement   Model Fit Line (Linear Regression)

Averaged East-West Displacement Time Series - AOI Point Groups

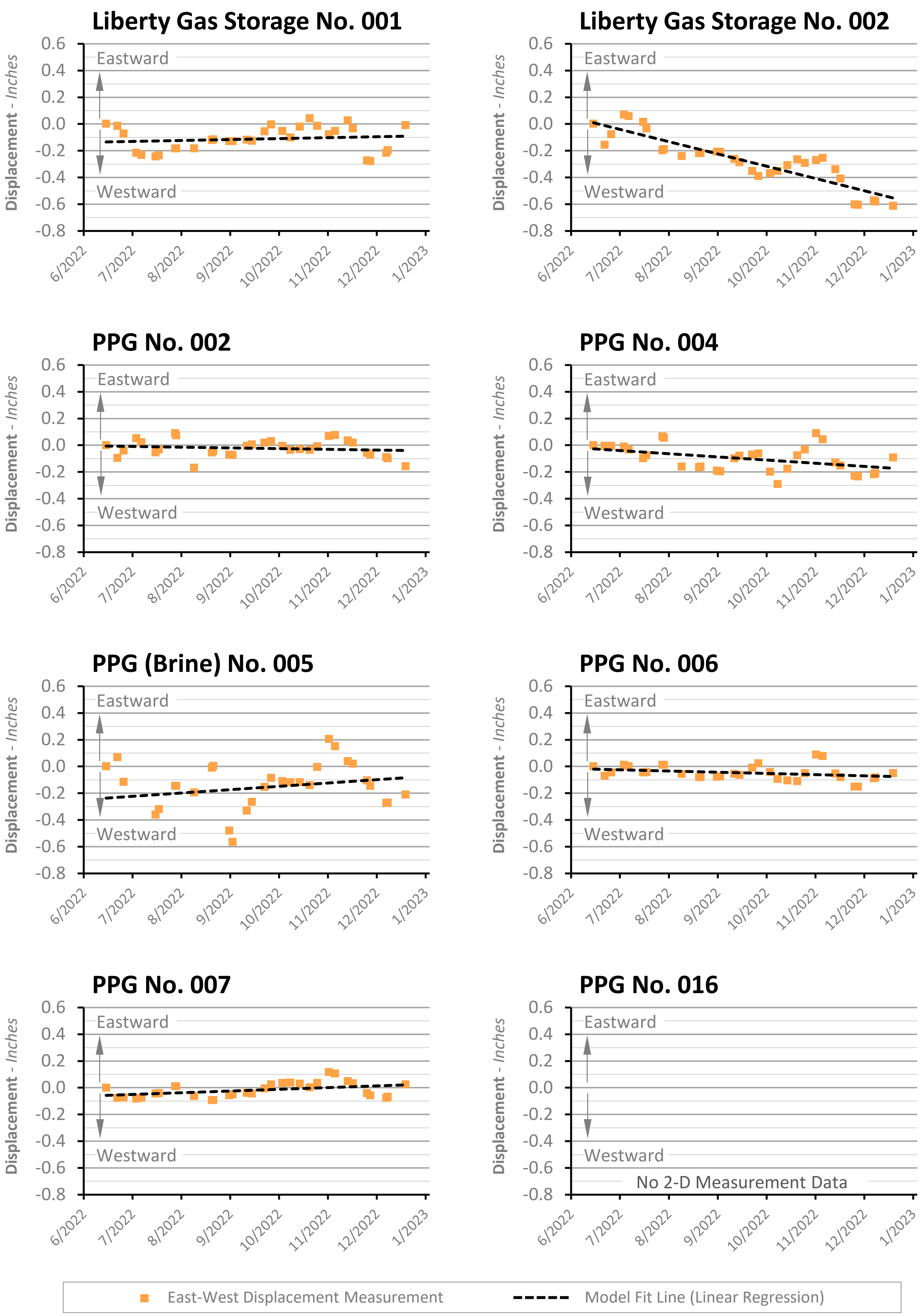

Averaged East-West Displacement Time Series - AOI Point Groups

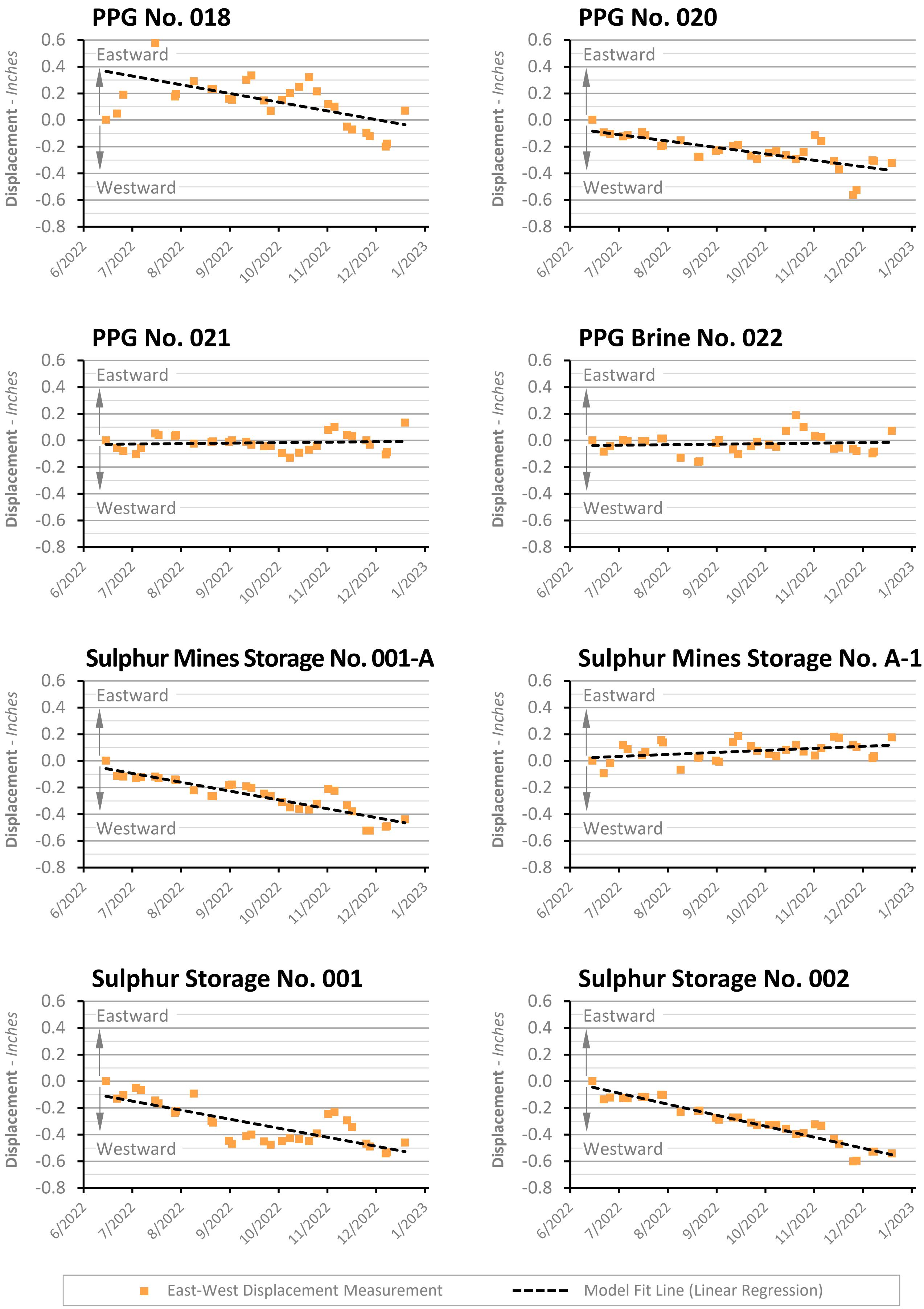

Averaged East-West Displacement Time Series - AOI Point Groups

Sulphur Storage No. 003

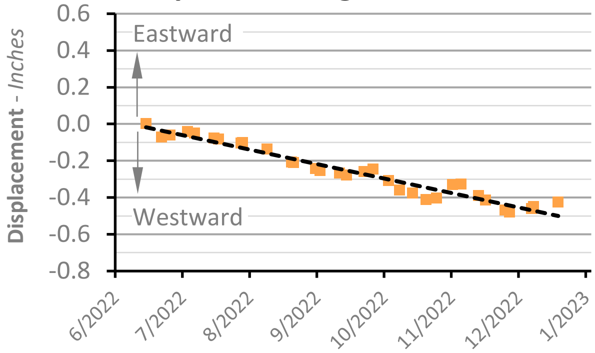

Sulphur Storage No. 004

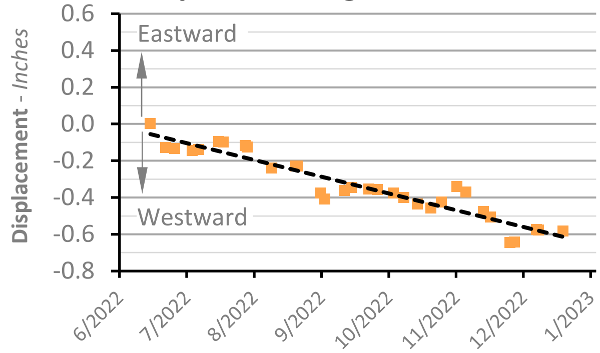

Sulphur Storage No. 005

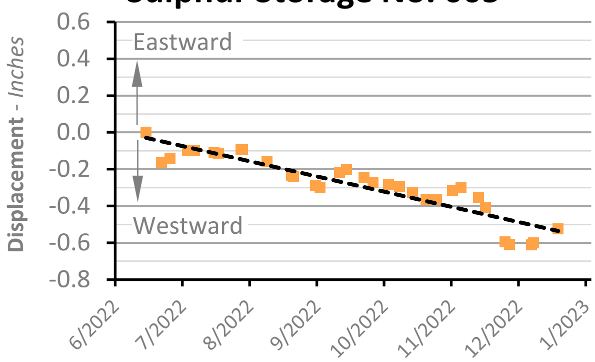

SMS Monument No. 001

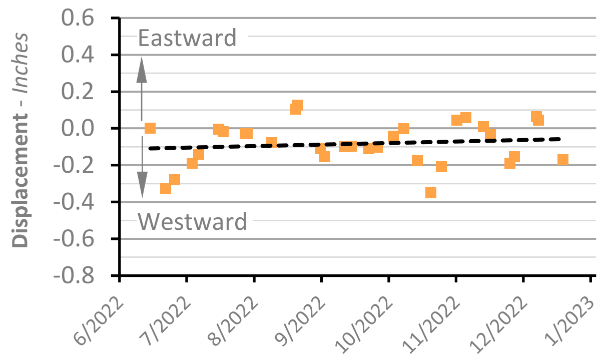

SMS Monument No. 002

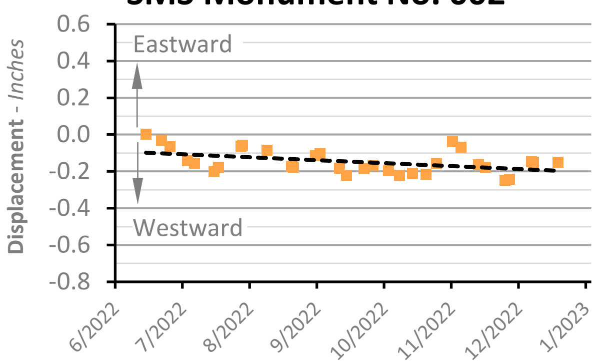

SMS Monument No. 003

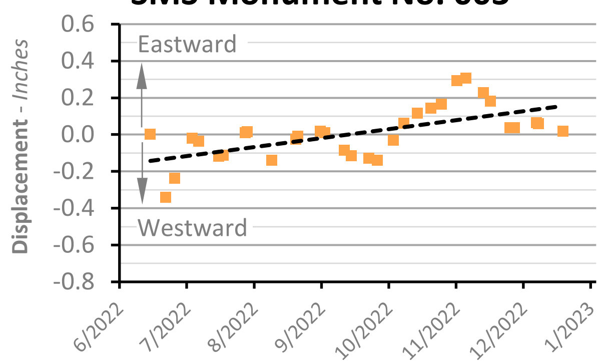

SMS Monument No. 004

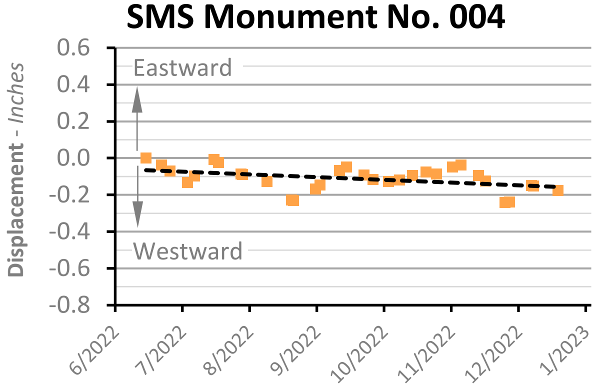

SMS Monument No. 005

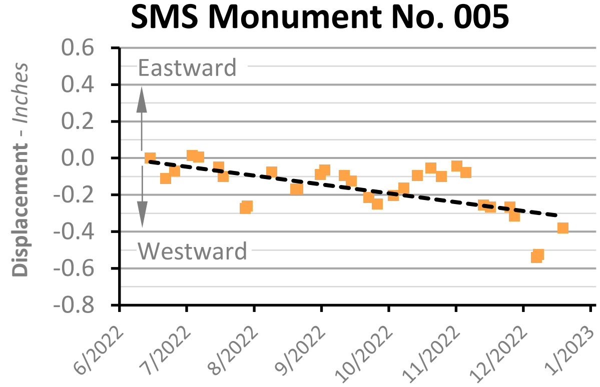

■ East-West Displacement Measurement   - - - - Model Fit Line (Linear Regression)

Averaged East-West Displacement Time Series - AOI Point Groups

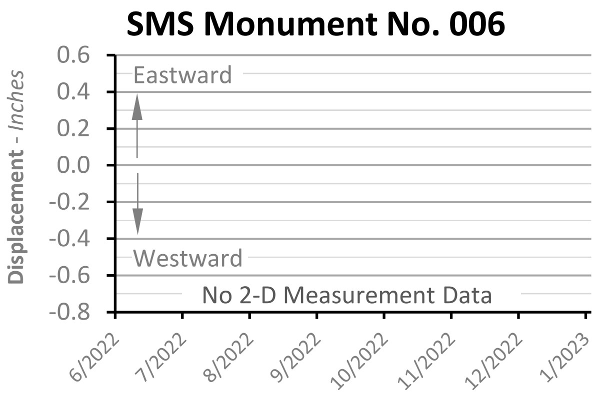

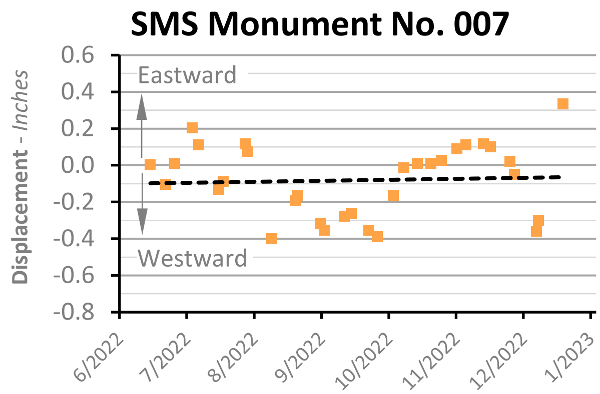

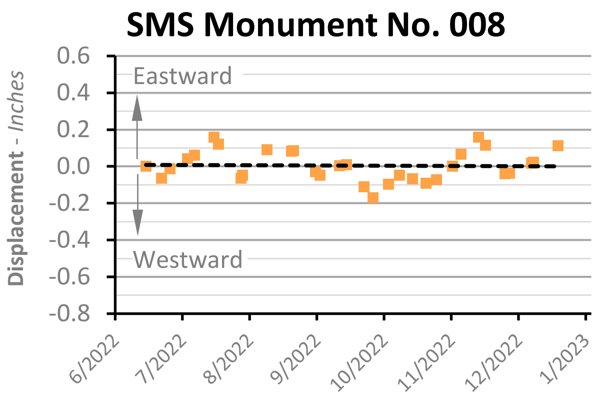

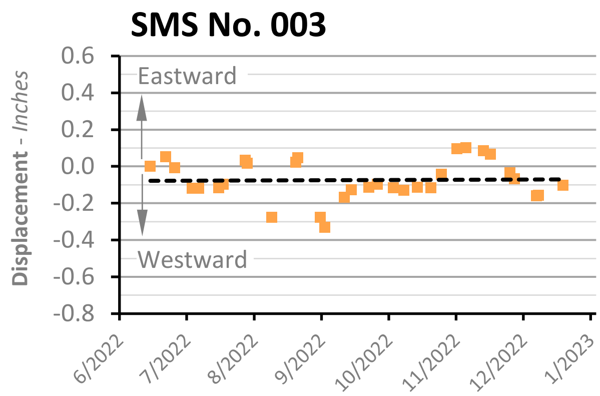

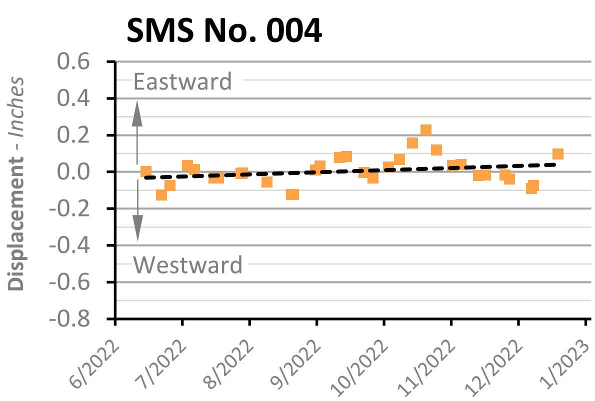

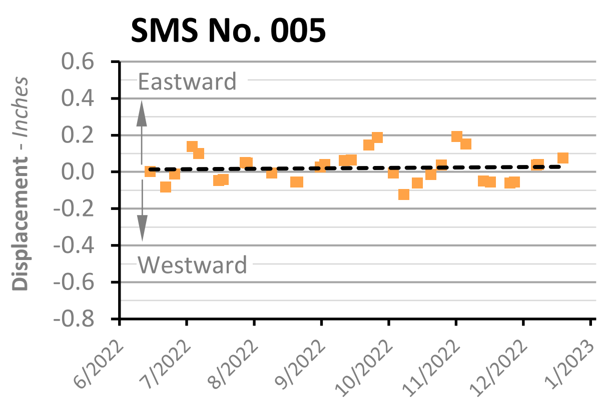

■ East-West Displacement Measurement ---- Model Fit Line (Linear Regression)

Appendix C – Map of Vertical Displacement Velocity Contours (Inches/year)

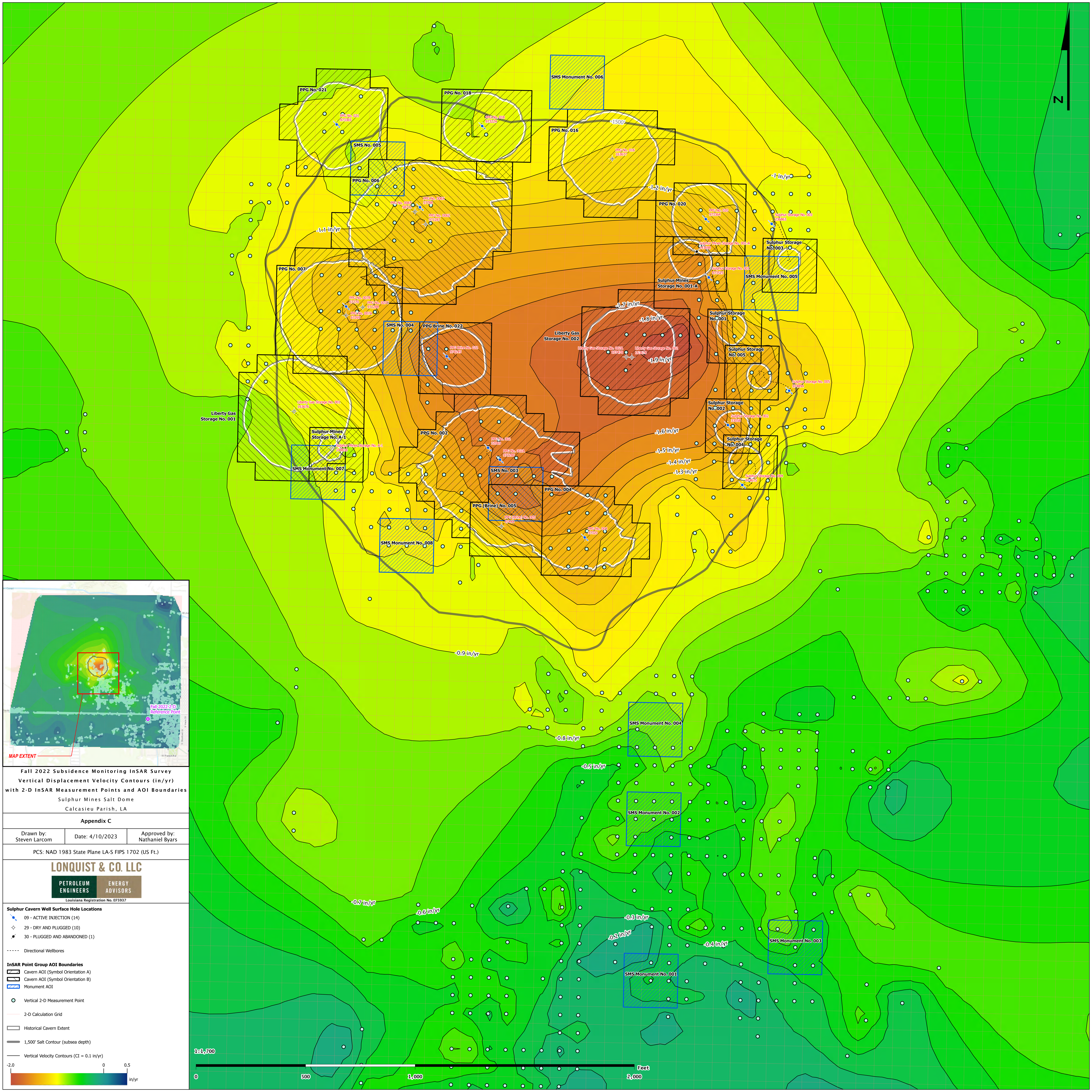

Fall 2022 Subsidence Monitoring InSAR Survey
Vertical Displacement Velocity Contours (in/yr)
with 2-D InSAR Measurement Points and AOI Boundaries
Sulphur Mines Salt Dome
Calcasieu Parish, LA

Appendix C

Drawn by: Steven Larcom	Date: 4/10/2023	Approved by: Nathaniel Byars

PCS: NAD 1983 State Plane LA-S FIPS 1702 (US Ft.)

LONQUIST & CO. LLC
PETROLEUM ENGINEERS | ENERGY ADVISORS
Louisiana Registration No. EF5937

Sulphur Cavern Well Surface Hole Locations
- 09 - ACTIVE INJECTION (14)
- 29 - DRY AND PLUGGED (10)
- 30 - PLUGGED AND ABANDONED (1)
- Directional Wellbores

InSAR Point Group AOI Boundaries
- Cavern AOI (Symbol Orientation A)
- Cavern AOI (Symbol Orientation B)
- Monument AOI
- Vertical 2-D Measurement Point
- 2-D Calculation Grid
- Historical Cavern Extent
- 1,500' Salt Contour (subsea depth)
- Vertical Velocity Contours (CI = 0.1 in/yr)

-2.0 0 0.5 in/yr

Appendix D – Map of East-West Displacement Velocity Contours (Inches/year)

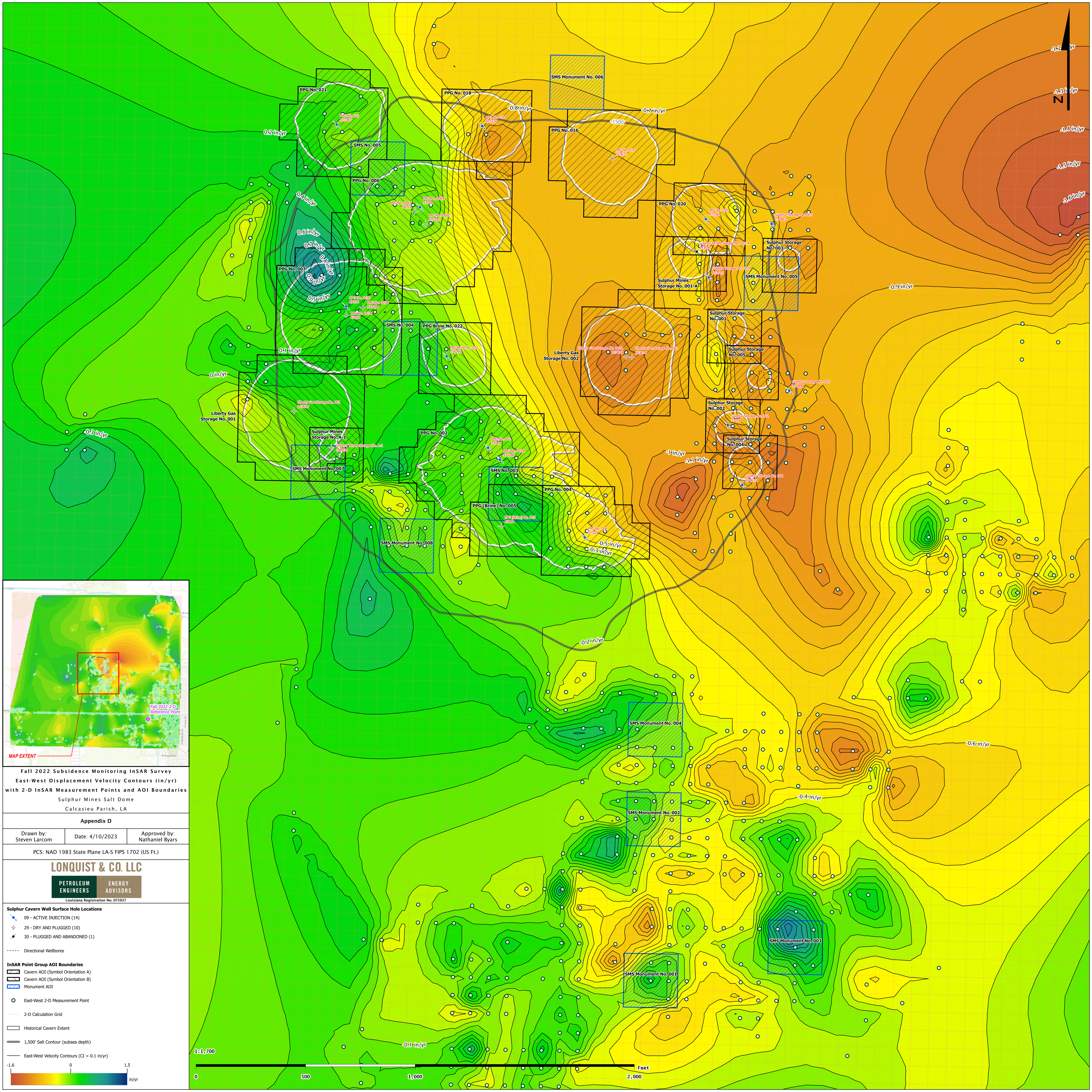

Fall 2022 Subsidence Monitoring InSAR Survey
East-West Displacement Velocity Contours (in/yr)
with 2-D InSAR Measurement Points and AOI Boundaries
Sulphur Mines Salt Dome
Calcasieu Parish, LA

Appendix D

Drawn by: Steven Larcom	Date: 4/10/2023	Approved by: Nathaniel Byars

PCS: NAD 1983 State Plane LA-S FIPS 1702 (US Ft.)

LONQUIST & CO. LLC
PETROLEUM ENGINEERS | ENERGY ADVISORS
Louisiana Registration No. EF5937

Sulphur Cavern Well Surface Hole Locations
- 09 - ACTIVE INJECTION (14)
- 29 - DRY AND PLUGGED (10)
- 30 - PLUGGED AND ABANDONED (1)
- Directional Wellbores

InSAR Point Group AOI Boundaries
- Cavern AOI (Symbol Orientation A)
- Cavern AOI (Symbol Orientation B)
- Monument AOI
- East-West 2-D Measurement Point
- 2-D Calculation Grid
- Historical Cavern Extent
- 1,500' Salt Contour (subsea depth)
- East-West Velocity Contours (CI = 0.1 in/yr)

-1.6 | 0 | 1.5 in/yr

Appendix E – TRE-Altamira InSAR Analysis of Ground Displacement

TRE ALTAMIRA
A CLS Group Company

InSAR Analysis of Ground Displacement over Sulphur Mine, Louisiana

December 2022 Update

Technical Report

Report Specifications

Client:	**Lonquist & Co. LLC**
Attention:	Nathaniel Byars, P.E.
Address:	12912 Hill Country Blvd. Suite F-200, Austin Texas 78738

Reference:	
Title:	InSAR Analysis of Ground Displacement over Sulphur Mine, Louisiana – December 2022 Update
TRE ALTAMIRA Delivery Reference:	JO22-2044-CA
Client Reference (#PO- date):	TREA_LON_2022_019R2 (November 2022)

Prepared by:	**TRE ALTAMIRA Inc.**
Address:	#410 - 475 West Georgia Street Vancouver, BC, V6B 4M9, Canada
Author(s):	Emma Cunningham
Verified by:	Hannah Raffler
Approved by:	Ajinkya Koleshwar
Date:	05 April 2023
Document number and version:	3.0

Executive Summary

This report describes the results of the InSAR analysis over the Sulphur Mine salt dome in Louisiana, USA. TRE-Altamira used its SqueeSAR® algorithm to process low-resolution Sentinel-1 (SNT) and high-resolution TerraSAR-X (TSX) radar imagery to assess ground displacement from 04 October 2016 – 20 December 2022. The following points summarize the main findings:

- Subsidence was observed over the entire dome with the highest magnitude of displacement rates measured over the east side of the dome adjacent to the Liberty Gas Storage No.002 monument (-1.88 in/yr).
- Westward displacement is concentrated over the east side of the dome with the highest rates measured adjacent to the Liberty Gas Storage No. 002 monument (1.15 in/yr).
- Average time series indicate that monuments: Liberty Gas Storage No. 002, PPG Brine No.022, and PPG No. 002A, have the highest magnitudes of subsidence.
- Average time series indicate that monuments: Liberty Gas Storage No. 002, Sulphur Storage No. 002, and Sulphur Storage No. 005 are observed with the highest magnitude of lateral displacement toward the west.
- The subsidence trends extend beyond the salt dome to the south-east of the dome.

Ongoing monitoring over the site is occurring with a frequency of 11 and 12 days with the TerraSAR-X and Sentinel-1 satellites, respectively. Monitoring frequency using a combination of TerraSAR-X and PAZ satellites will occur every 4 and 7 days starting in mid-late April 2023, once a baseline of ~13 images has been acquired.

Lonquist will be performing a further evaluation of these datasets to be provided under a separate cover. Additional analysis and conclusions will be presented in the context of the site history, cavern layout and dome structure, historical level surveys, InSAR measurement point coverage, and comparison of current and past subsidence trends across the dome.

Table of Contents

Acronyms and Abbreviations

AOI	Area of Interest
ATS	Average Time Series
CS	Cross-Section
DEM	Digital Elevation Model
DInSAR	Differential Interferometric SAR
DS	Distributed Scatterer(s)
GIS	Geographic Information System
InSAR	Interferometric Synthetic Aperture Radar
LOS	Line of Sight
MP	Measurement Point
NR	Natural Reflector
PS	Permanent Scatterer(s)
SAR	Synthetic Aperture Radar
SNT	Sentinel Satellite
SqueeSAR®	The most recent InSAR algorithm patented by TRE
TS	Time Series
TSX	TerraSAR-X satellite

1. Introduction

Lonquist & Co. LLC (Lonquist) contracted TRE-Altamira Inc. (TREA) to carry out a 2-D InSAR analysis of ground movement over the Sulphur Mines Salt Dome in Louisiana, USA. The salt dome is located approximately 2 miles north-west of the town of Sulphur and the area of interest (AOI) processed for the analysis encompasses 13.70 mi^2 (Figure 1). The AOI covers the main assets including the salt dome, cavern well pads, and on-site levelling monuments. Much of the AOI is vegetated with minimal topography and urban areas concentrated in the south-east. The InSAR analysis used imagery obtained from the low-resolution Sentinel-1 (SNT) satellite from an ascending orbit during the period October 2016 – December 2022 and high-resolution TerraSAR-X satellite from a descending orbit during the period June 2022 – December 2022. This document describes the results of the 2-D analysis.

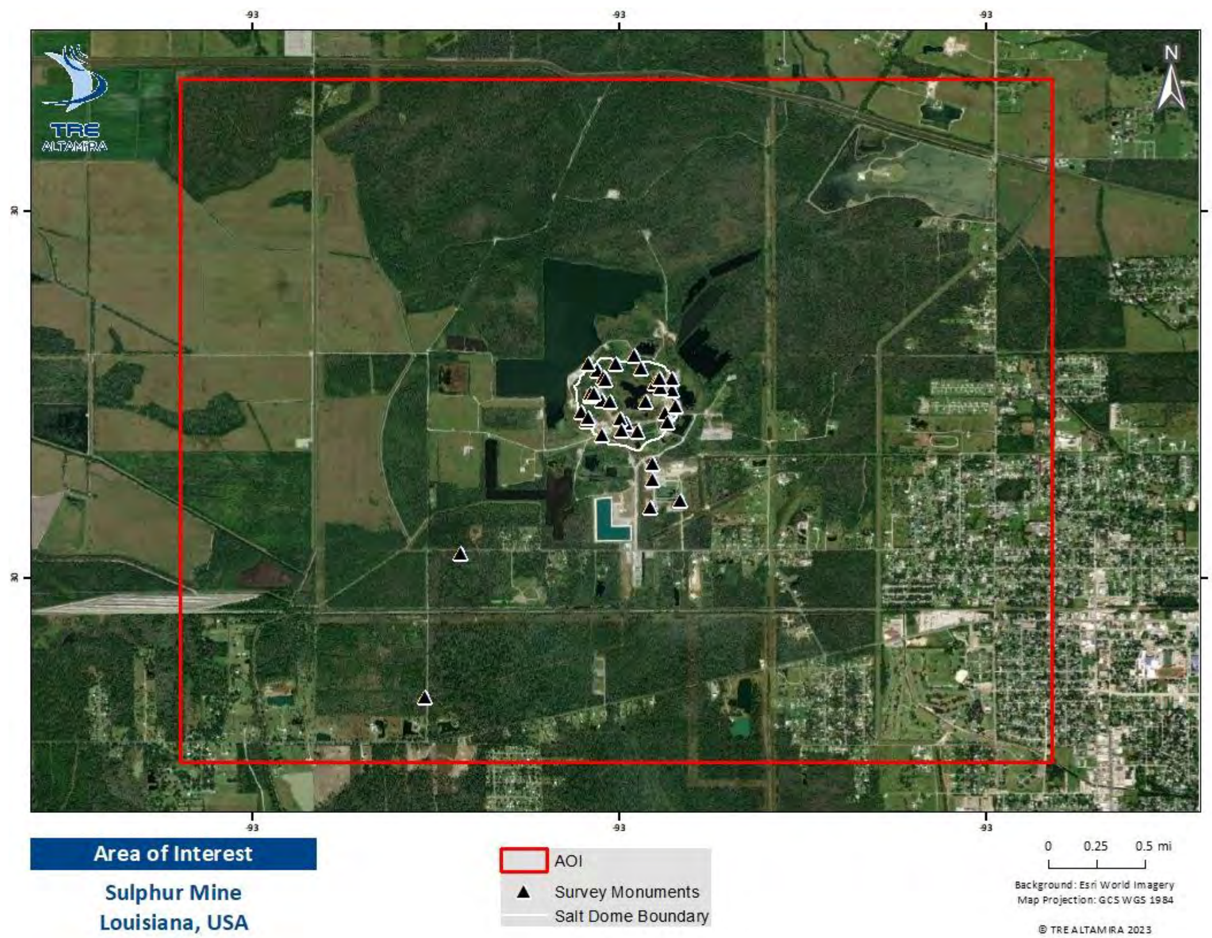

Figure 1: Area of interest and main assets of interest.

2. Radar Imagery

The radar data used for the current analysis consists of low-resolution (65x16 ft pixel resolution) images acquired by the Sentinel (SNT) satellite between October 2016 and December 2022 from an ascending (ASC) orbit, and high-resolution (3x3 ft) images acquired by the TerraSAR-X satellite between June 2022 and December 2022 from a descending (DESC) orbit.

Satellite orbits are referred to as ascending or descending according to the flight direction of the satellite, from south to north (imaging to the east) and from north to south (imaging to the west), respectively. The satellite Line of Sight (LOS) is inclined with respect to the vertical and the north-south direction (Figure 3) and is indicated as θ (theta) in Table 1. InSAR measurements are 1-D and correspond to the projection of the real vector of displacement onto the LOS (Figure 3).

Satellite	Band	Wavelength [in]	Pixel Resolution [ft]	Revisit frequency [days]
SNT	C-band	2.32	65 x 16	12
TSX/PAZ (*Spotlight*)	X-band	1.22	3 x 3	11

Table 1: Satellite characteristics

Satellite	Orbit	LOS Angle (Θ)	# of Images	Date Range
SNT	Ascending	42.52^{o}	166	04 Oct 2016 – 20 Dec 2022
TSX	Descending	17.18^{o}	18	16 Jun 2022 – 20 Dec 2022

Table 2: Satellite acquisition parameters and image acquisition information.

Figure 2: Temporal distribution of the radar images processed over the site.

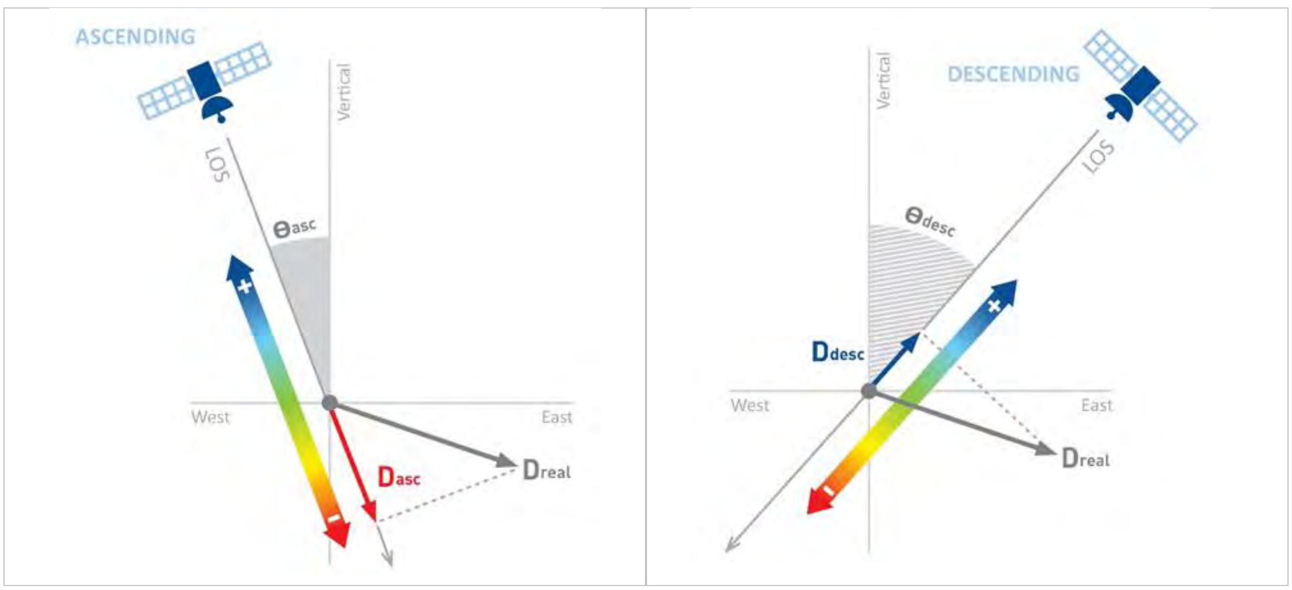

Figure 3: Ascending and descending acquisition geometries. InSAR measures the projection of real movement (Dreal) onto the satellite Line of Sight (LOS). The same real movement (Dreal) produces a different value from a different LOS (different inclination or different acquisition geometries). Positive values are indicated with colours from green to blue and denote movement towards the satellite; negative values and colours from green to red indicate movement away from the satellite.

3. Results

The SqueeSAR® processing of the radar imagery produced full resolution measurements in the form of point clouds, one for each orbit (ascending and descending). Each measurement point (MP) comprises a time series of displacement (i.e., cumulative displacement with respect to the first radar image of the analysis), average displacement rate, and acceleration over the full period (October 2016 – December 2022 for SNT and June 2022 – December 2022 for TSX).

Ascending and descending orbit measurements are 1-D (Line-of-sight – LOS) readings and represent the projection of real displacement onto the LOS (Figure 3). Spatially and temporally overlapping LOS results are then combined on a common spatial grid (82 x 82 ft cell) to produce 2-D vertical and east-west ground displacement measurements.

This section provides an overview of the LOS and 2D results, while Section 4 provides detailed observations over the salt dome. Refer to Appendix 1 for the list of deliverables and Appendix 2 for additional information on the SqueeSAR® technique.

3.1. Line of Sight (LOS) Results

An overview of the ascending and descending LOS results are shown in Figure 4 and Figure 5, respectively, where the measurement points are colour-coded according to the displacement rate between October 2016 – December 2022 (ascending) and June 2022 – December 2022 (descending). In the following figures, negative values (from yellow to red) indicate movement away from the satellite, while positive values (from light blue to dark blue) indicate movement towards the satellite (Figure 3). The analysis provides good coverage over most of the dome, including the pads and near most monuments.

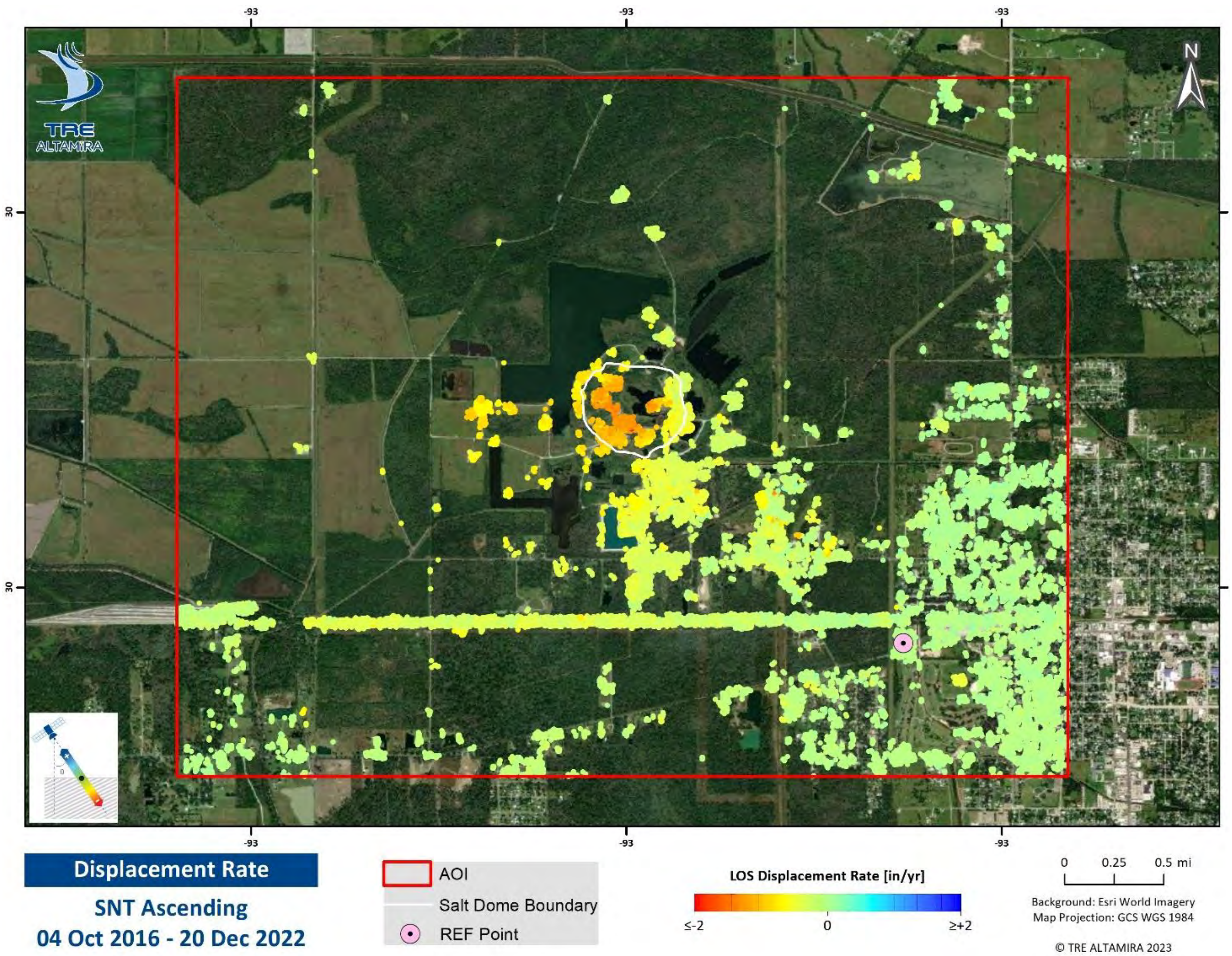

Figure 4. Sentinel ascending LOS SqueeSAR annual displacement rate (October 2016 - December 2022).

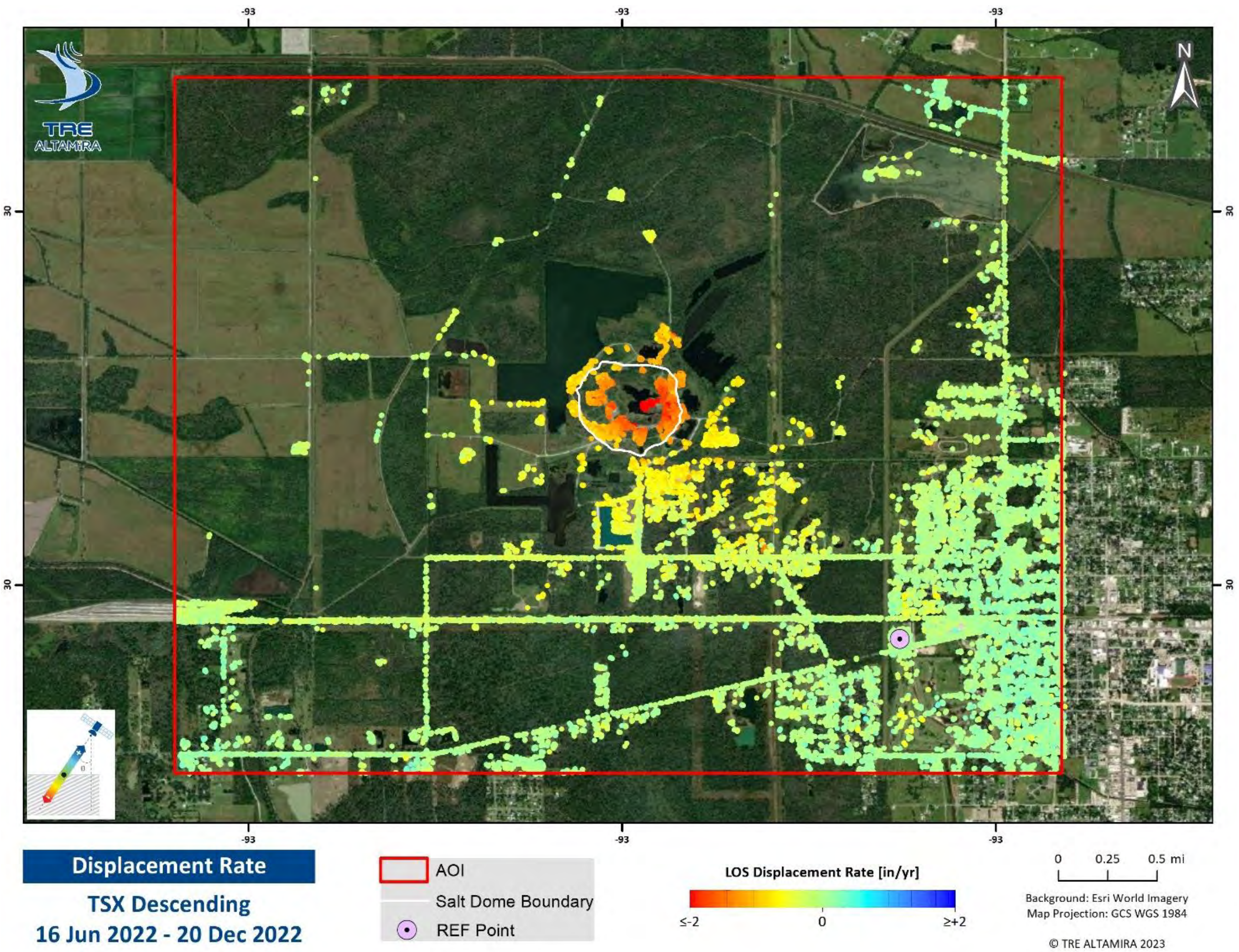

Figure 5. TerraSAR-X descending LOS SqueeSAR annual displacement rate (June 2022 - December 2022).

SqueeSAR measurements are differential compared to a local reference point (REF) and provided with two precision indices:

- Displacement rate standard deviation (V_STDEV), which provides an indication of the error bar associated to the annual rate measurements with respect to the reference point.
- Time series error bar (STD_DEF), which provides an indication of the error bar associated to the displacement time series of each measurement point.

A summary of the LOS SqueeSAR results, REF location and precision indices obtained with the analysis are reported in Table 3.

Analysis characteristics	LOS Ascending (SNT)	LOS Descending (TSX)
Period covered	10/04/2016 - 12/20/2022	06/16/2022 - 12/20/2022
N. of images processed	166	18
Reference point location (WGS84)	X = -93.392732 Y = 30.235768	X = -93.392611 Y = 30.235862
Number of measurement points (PS/DS)	25,761	28,635
Average Point Density	1,880 pts/mi^2	2,090 pts/mi^2
Average displacement rate standard deviation (V_STDEV)	± 0.01 in/yr	± 0.13 in/yr
Average time series error bar (STD_DEF)	± 0.20 in	± 0.03 in

Table 3: Summary of the SqueeSAR analyses characteristics.

3.2. 2-D (Vertical and East-West) Results

The ascending and descending LOS results are combined to produce 2-D measurements (vertical and east-west) for the period in common covered by the two LOS data sets (16 June 2022 – 20 December 2022).

As satellites identify different targets on the ground from the ascending and descending orbits the procedure requires the use of a common spatial grid to combine the LOS results. The area of interest is divided into a regular grid (82 x 82 ft cells for this analysis) and all ascending and descending points within a cell are averaged. Consequently, 2-D measurements are generated only where LOS measurements from both orbits fall within a grid cell. This entails that the measurements are cells of a grid, not individual radar targets.

An overview of the 2-D SqueeSAR results are shown in Figure 6 and Figure 7, where MPs are colour-coded according to the vertical and east-west displacement rates, respectively. In the vertical dataset, negative values (from yellow to red) indicate downward surface displacement (subsidence), while positive values (from pale to dark blue) indicate upward surface displacement (uplift). In the east-west dataset, negative values (from yellow to red) indicate westward motion, while positive values (from pale to dark blue) indicate eastward motion. InSAR is not sensitive to monitoring north-south movement.

As for the LOS results, 2-D measurements are calculated with respect to a reference point (REF) and provided with a precision index, the standard deviation of the displacement rate. A summary of the 2-D SqueeSAR results, REF location and precision indices are reported in Table 4.

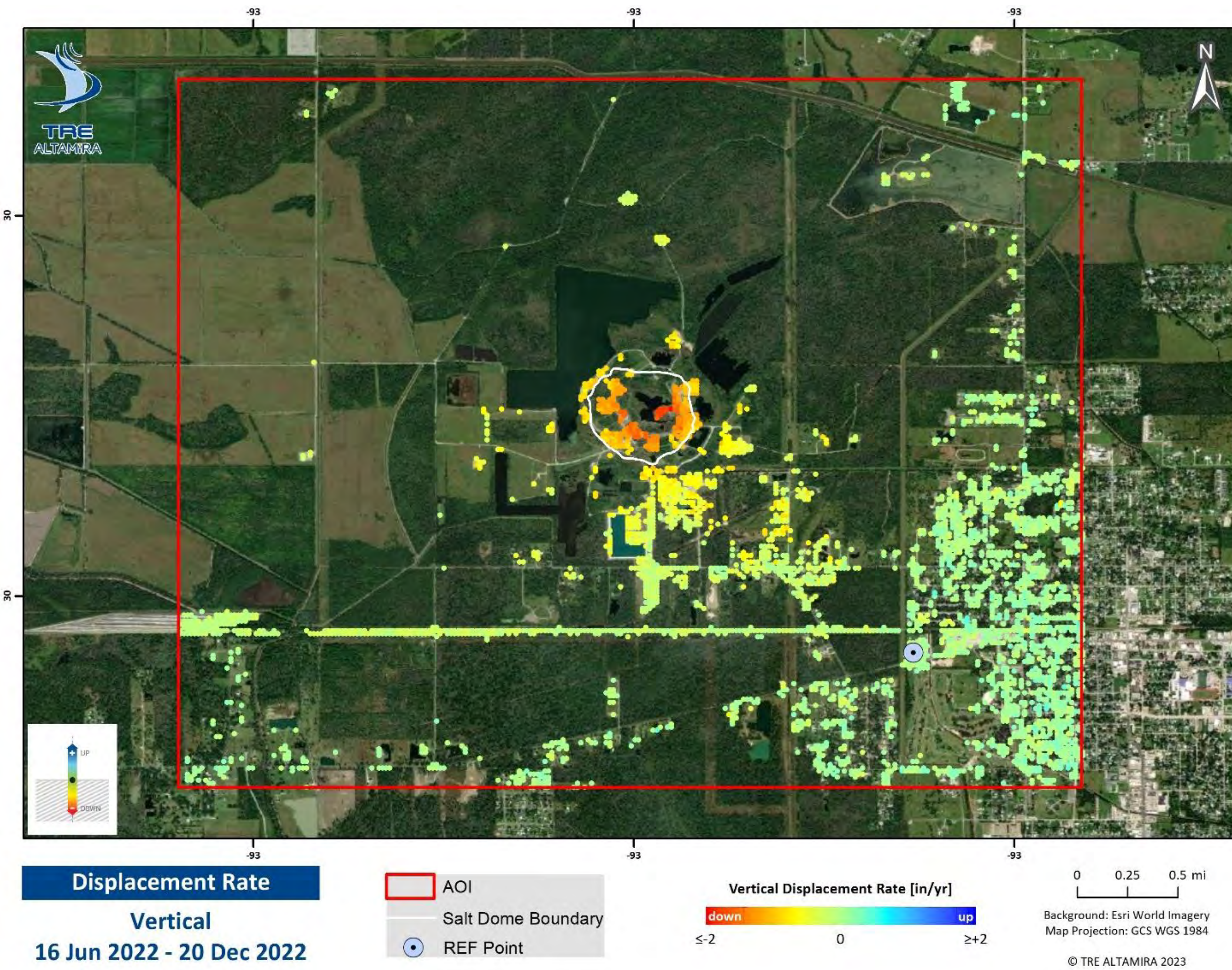

Figure 6: Vertical annual displacement rate (June 2022 - December 2022).

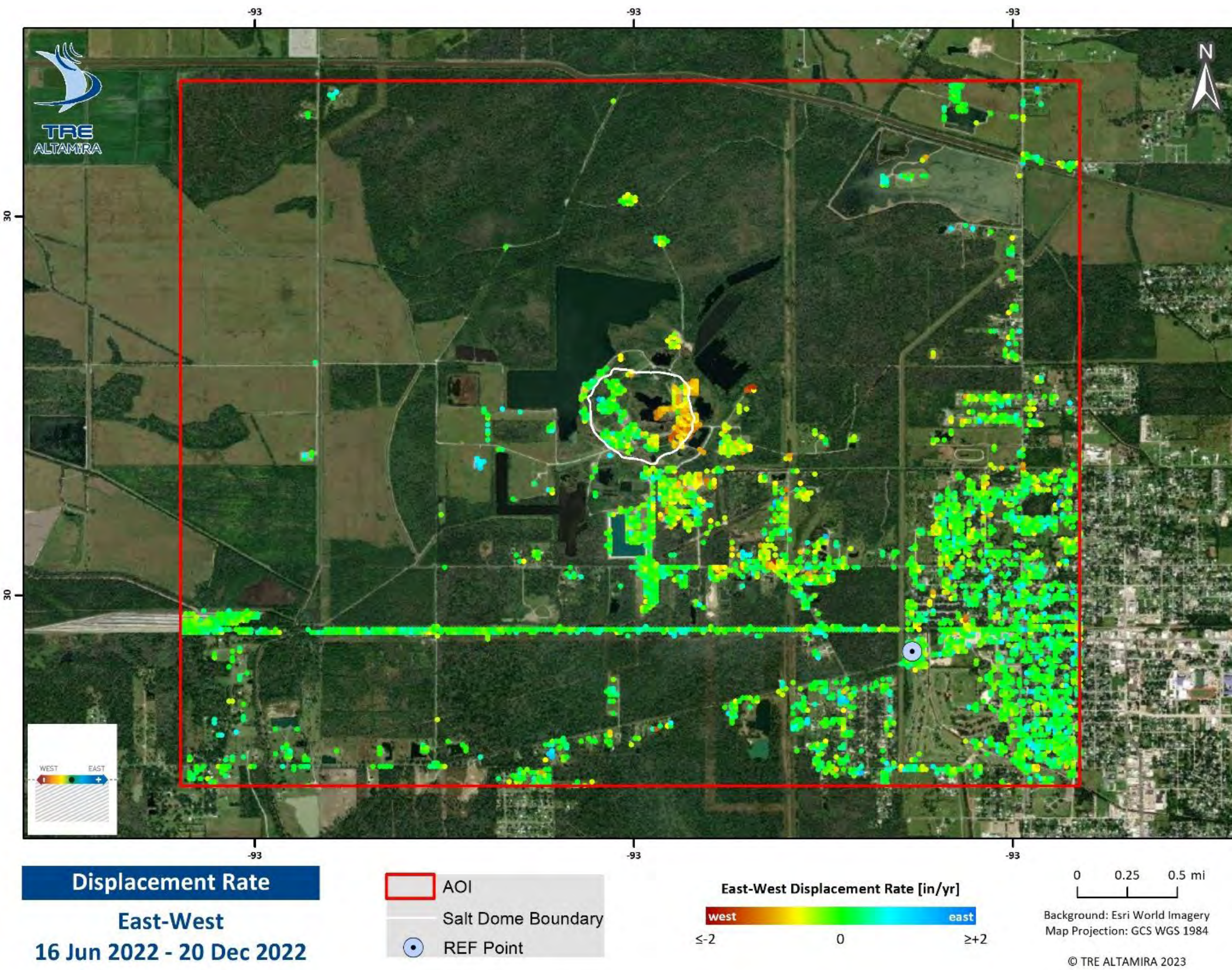

Figure 7: East-West annual displacement rate (June 2016 - December 2022).

Analysis characteristics	Vertical	East-West
Period covered	16 June 2022 – 20 December 2022	
N. of images	32	
Reference point location (WGS84)	X = -93.392842 Y = 30.235753	
Number of cells	3,536	
Cell size	82 x 82 ft	
Average displacement rate standard deviation (V_STDEV)	±0.02 in/yr	±0.05 in/yr

Table 4: Summary of the 2-D SqueeSAR analysis.

4. Observations

This section provides ground displacement observations based on the 2-D results (vertical and east-west) over the area of interest, by means of average time series (ATS) and cross-sections (CS) where appropriate.

The ATS calculates the average displacement of all measurement points within a polygon to provide an overview of displacement over an area. The displacement rate and cumulative displacement values are displayed in the legend at the top of each figure in imperial units.

A CS profile highlights displacement rates along a surface profile by averaging all measurement points within a buffered distance.

4.1. Average Time Series near Monuments

ATS around each levelling survey monument calculate the average displacement of all measurement points that fall within 100 feet of each monument. The locations of the levelling ATS polygons are shown in Figure 8 and Figure 10 along with the vertical and east-west displacement rates, respectively. The ATS showing the highest magnitude displacement rates are highlighted in red and the time series are shown in Figure 9 and Figure 11. The highest magnitude displacement rates are observed at Liberty Gas Monument No.002, reaching -1.88 in/yr of subsidence and -1.15 in/yr of lateral movement towards the west. A summary of displacement rates within all ATS polygons is shown in Table 5 and the individual average time series are shown in Appendix 3. A lack of measurement points is observed over some monuments due to the surface characteristics of those areas (i.e., vegetation cover).

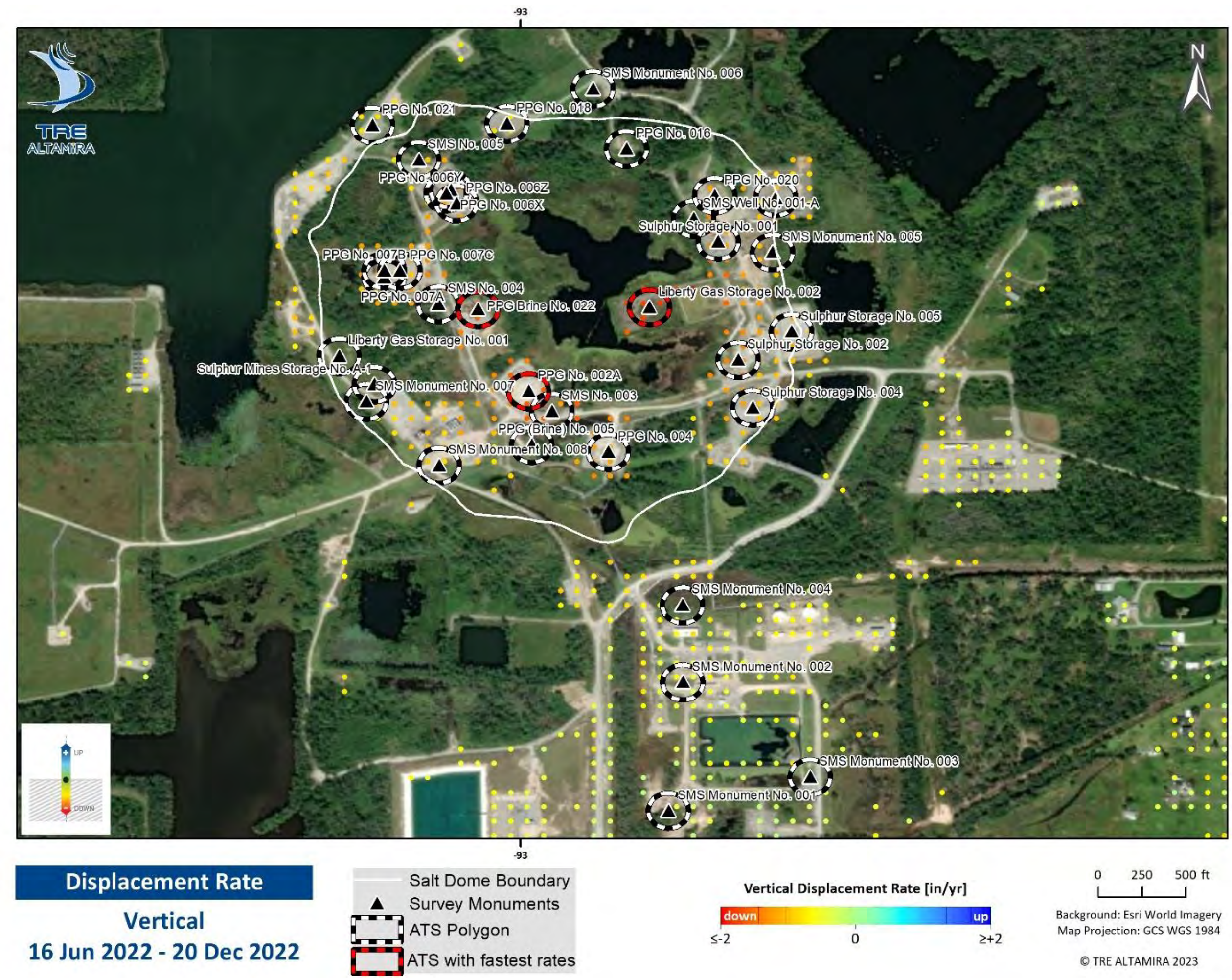

Figure 8. Locations of the ATS polygons around monuments located over the dome. ATS showing the highest Vertical displacement rates are highlighted in red.

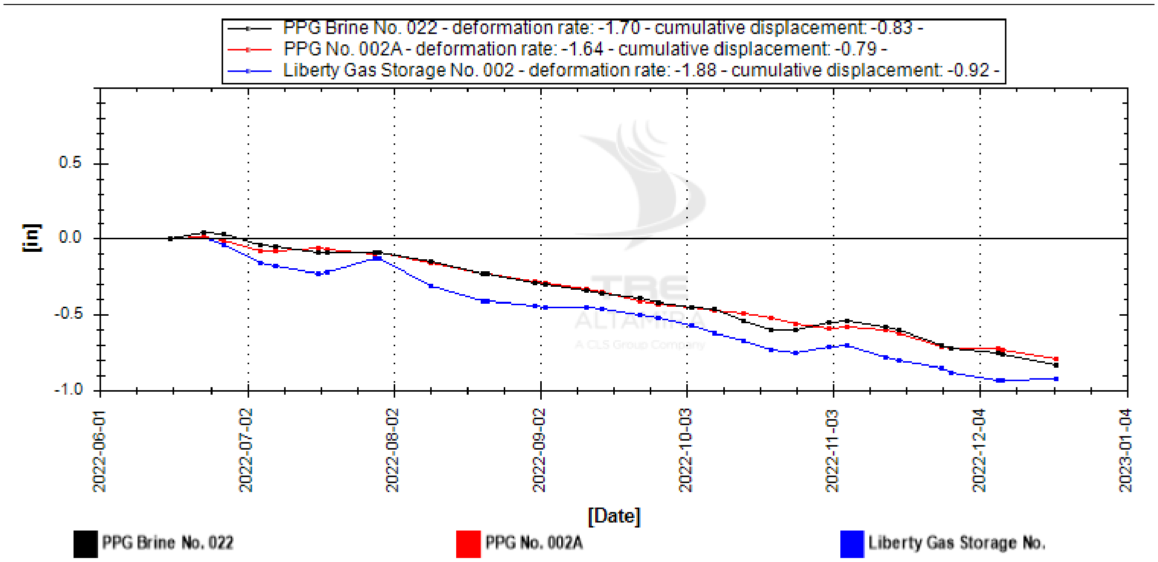

Figure 9. Average time series of monuments PPG Brine No.022, PPG No. 002A, and Liberty Gas Storage No. 002 showing the fastest rates of subsidence.

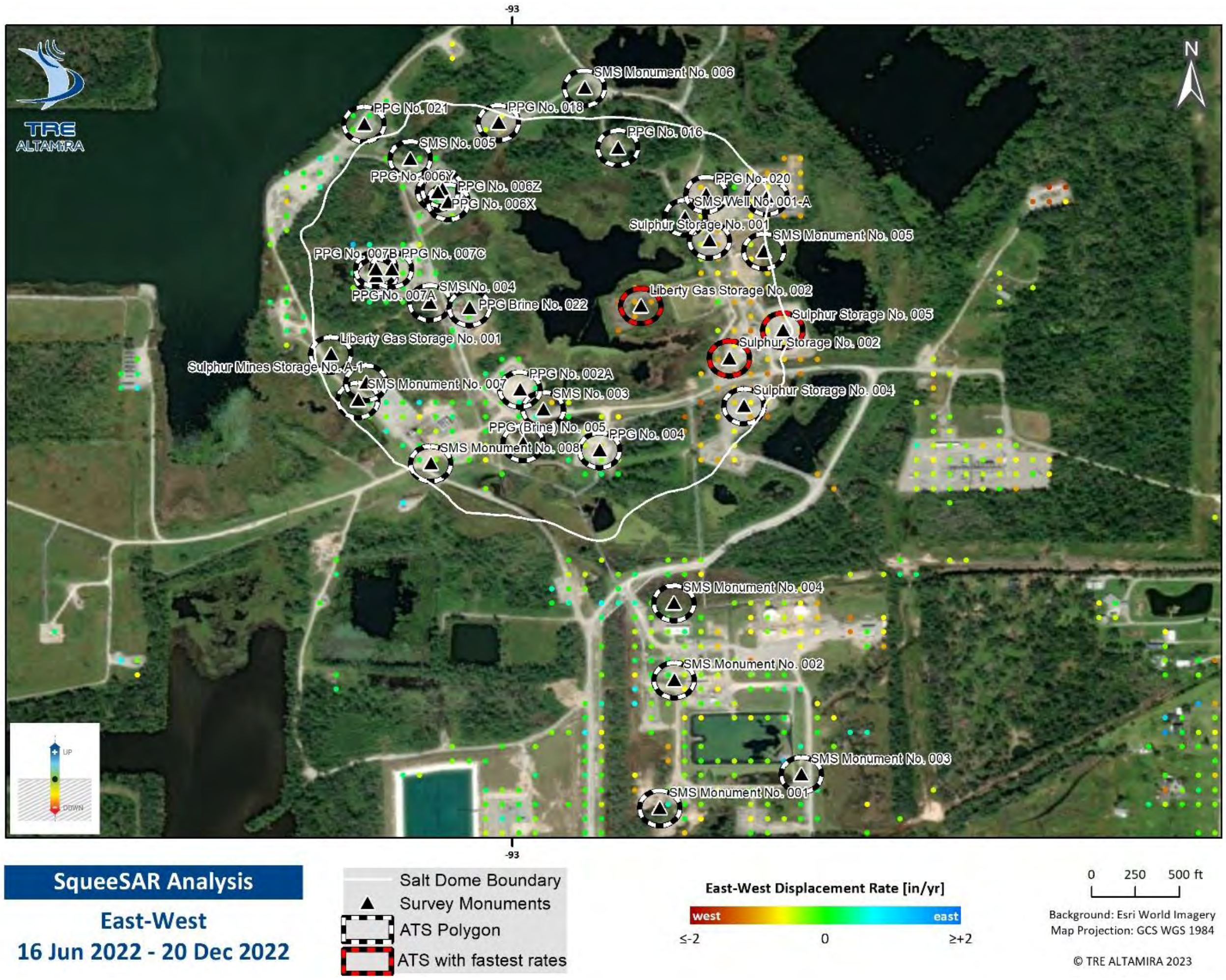

Figure 10.Locations of the ATS polygons around monuments located over the dome. ATS showing the highest East-West displacement rates are highlighted in red.

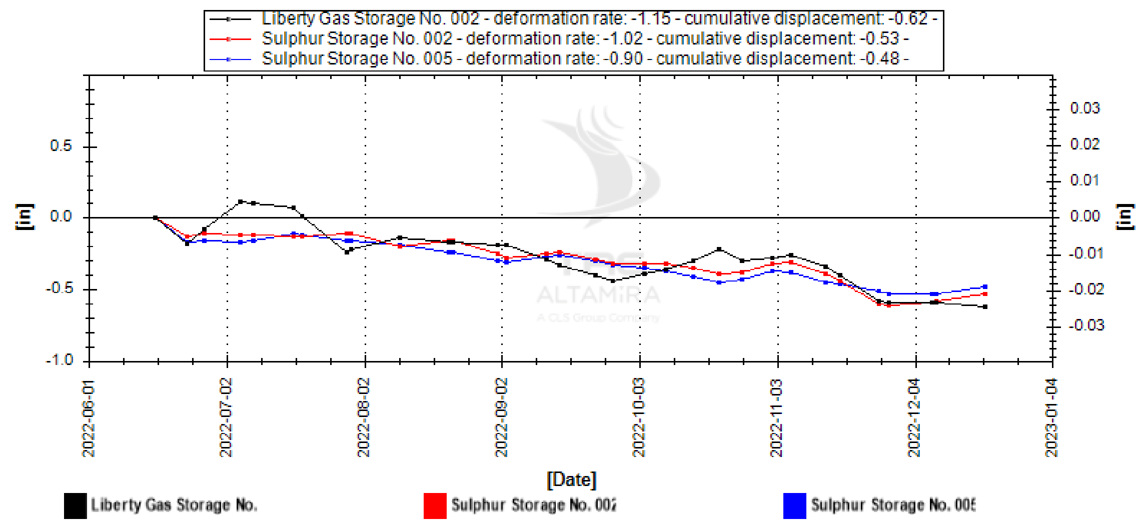

Figure 11. Average time series of monuments Sulphur Storage No.002, Sulphur Storage No.005 and Liberty Gas Storage No. 002 showing the fastest rates of lateral displacement towards the west.

Table 5. Summary of the Vertical and East-West displacement rates and associated standard deviation values observed within each of the levelling ATS polygons.

Monument	VERT Displacement Rate ± Standard Deviation (in/yr)	EW Displacement Rate ± Standard Deviation (in/yr)
SMS-Monument N0.001	-0.48 ± 0.02	0.46 ± 0.05
SMS-Monument No.002	-0.54 ± 0.01	-0.38 ± 0.04
SMS-Monument No.003	-0.45 ± 0.02	0.31 ± 0.04
SMS-Monument No.004	-0.74 ± 0.01	-0.21 ± 0.04
SMS-Monument No.005	-1.12 ± 0.02	-0.57 ± 0.06
SMS-Monument No.007	-1.02 ± 0.02	0.17 ± 0.06
SMS-Monument No.008	-0.99 ± 0.02	-0.12 ± 0.05
SMS-Well No.001	-1.41 ± 0.02	-0.50 ± 0.04
SMS No.003	-1.58 ± 0.02	-0.14 ± 0.06
SMS No.004	-1.35 ± 0.02	0.08 ± 0.05
SMS No. 005	-1.03 ± 0.02	0.05 ± 0.06

Sulphur Storage No.001	-1.46 ± 0.02	-0.87 ± 0.04
Sulphur Storage No.002	-1.54 ± 0.02	-1.02 ± 0.04
Sulphur Storage No.003	-1.05 ± 0.01	-0.80 ± 0.04
Sulphur Storage No.004	-1.18 ± 0.02	-0.89 ± 0.05
Sulphur Storage No.005	-1.24 ± 0.02	-0.90 ± 0.05
PPG No.002A	-1.64 ± 0.02	-0.05 ± 0.05
PPG No.004	-1.35 ± 0.02	-0.47 ± 0.05
PPG No.006X	-1.24 ± 0.02	-0.07 ± 0.05
PPG No.006Y	-1.25 ± 0.02	-0.02 ± 0.05
PPG No.06Z	-1.29 ± 0.02	-0.04 ± 0.05
PPG No.007A	-1.30 ± 0.02	0.25 ± 0.05
PPG No.007B	-1.30 ± 0.02	0.20 ± 0.05
PPG No.007C	-1.27 ± 0.02	0.07 ± 0.06
PPG No.018	-0.90 ± 0.02	-0.78 ± 0.06
PPG No.020	-1.24 ± 0.02	-0.78 ± 0.05
PPG No.021	-0.92 ± 0.02	-0.03 ± 0.05
PPG Brine No.022	-1.70 ± 0.02	0.01 ± 0.05
Liberty Gas Storage No. 002	-1.88 ± 0.02	-1.15 ± 0.06

4.1. Cross- Sections over Dome

Cross-section profiles (CS) highlight the displacement rate along a surface profile by averaging all measurement points within a buffered distance (200 feet) of the CS line. Three cross-section lines were drawn: A-A' along the north and west portions of the dome, B-B' along the east side of the dome, and C-C' along the southern portion of the dome. The locations of the surface profiles are shown in Figure 12 visualized with the vertical displacement rates. Closeups of the cross-sections and the associated surface profiles are shown in Figure 13 through Figure 20

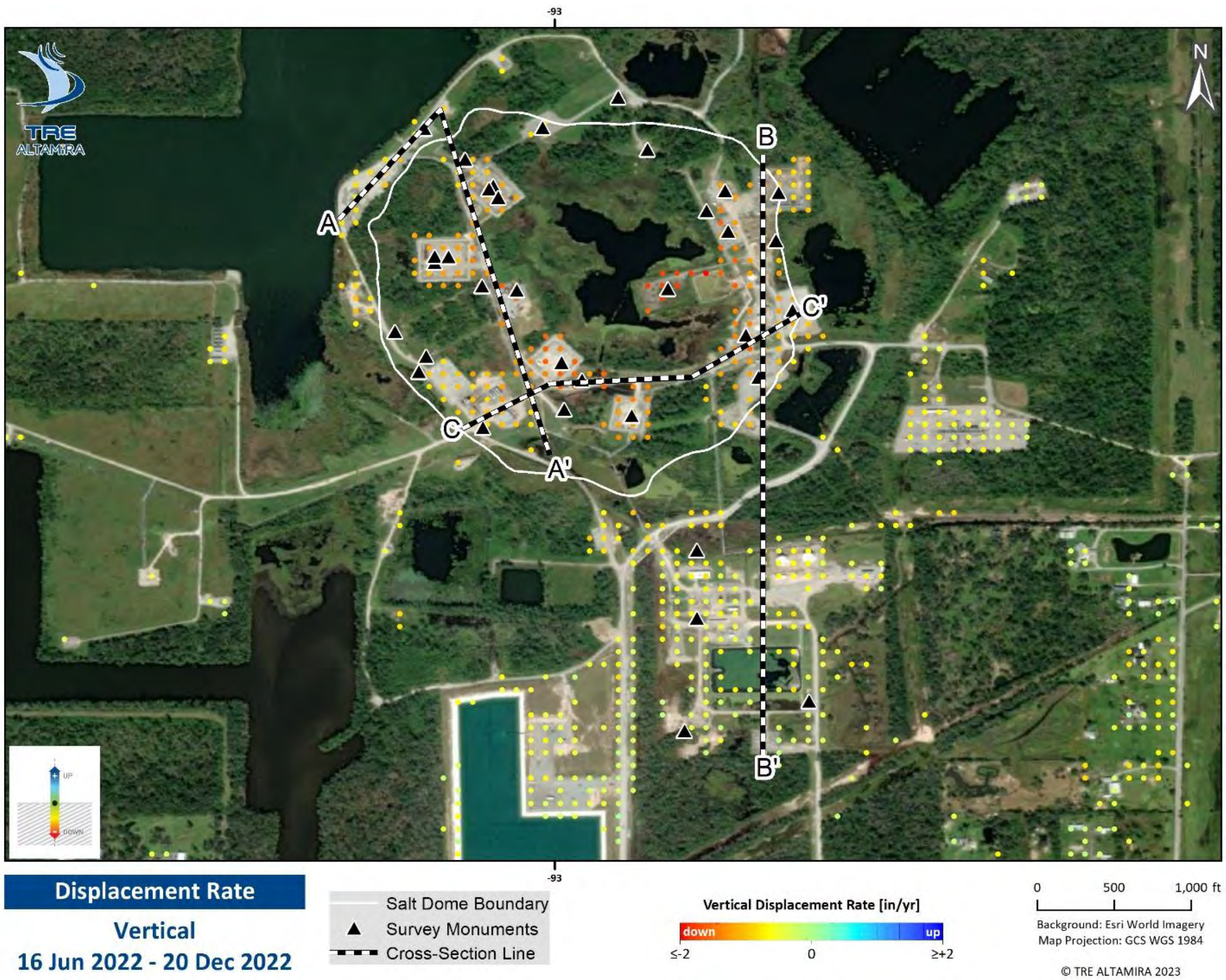

Figure 12. Locations of the cross-section lines within the AOI.

Figure 13. Closeup of Cross-Section A-A' over the north and west sides of the dome.

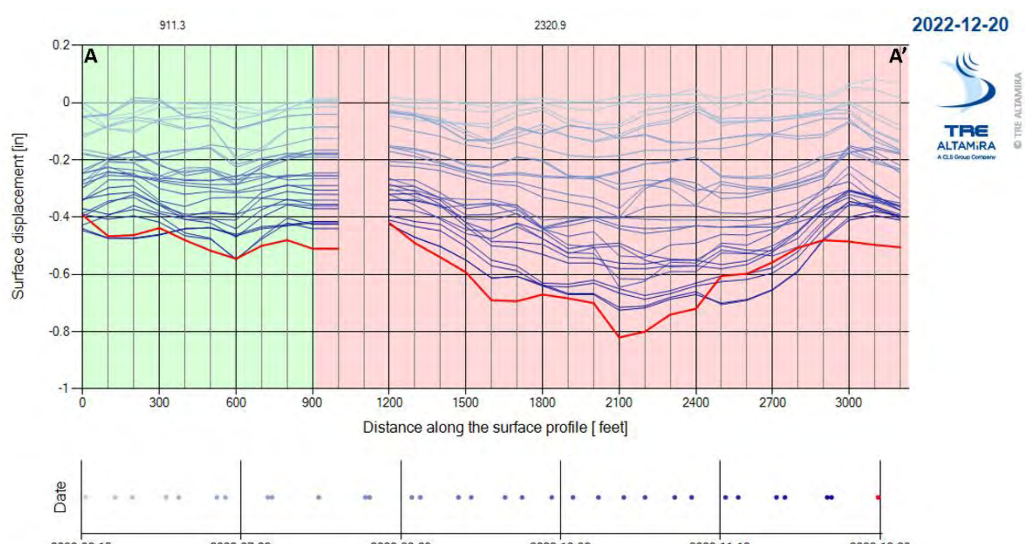

Figure 14. Surface profile of cross-section A-A' showing Vertical displacement. Negative values indicate subsidence while positive values indicate uplift. The green shading represents the N-W section of the CS line while the red shading represents the southern section.

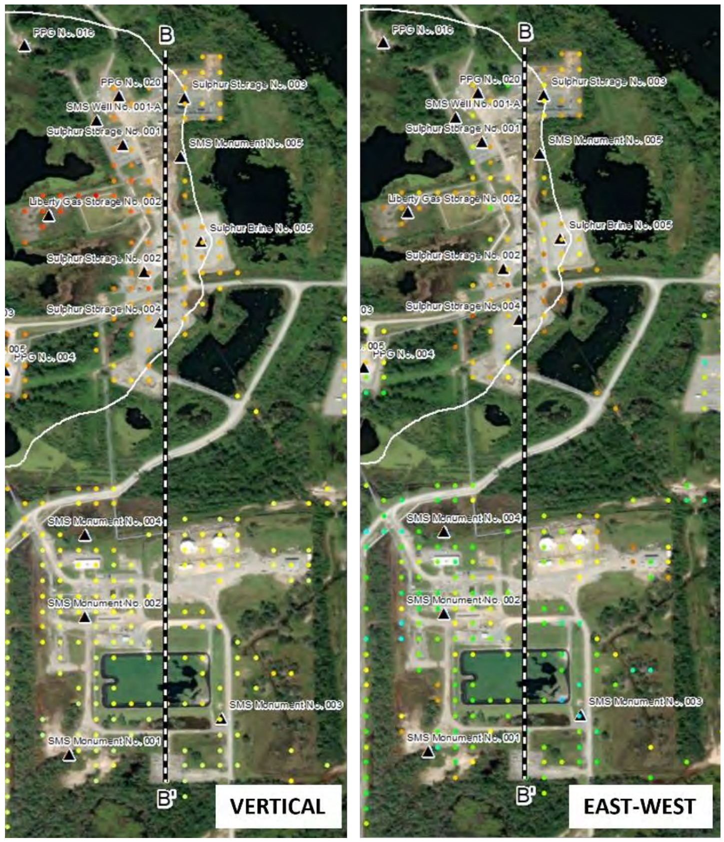

Figure 15. Closeup of Cross-Section B-B’ along the east side of the dome.

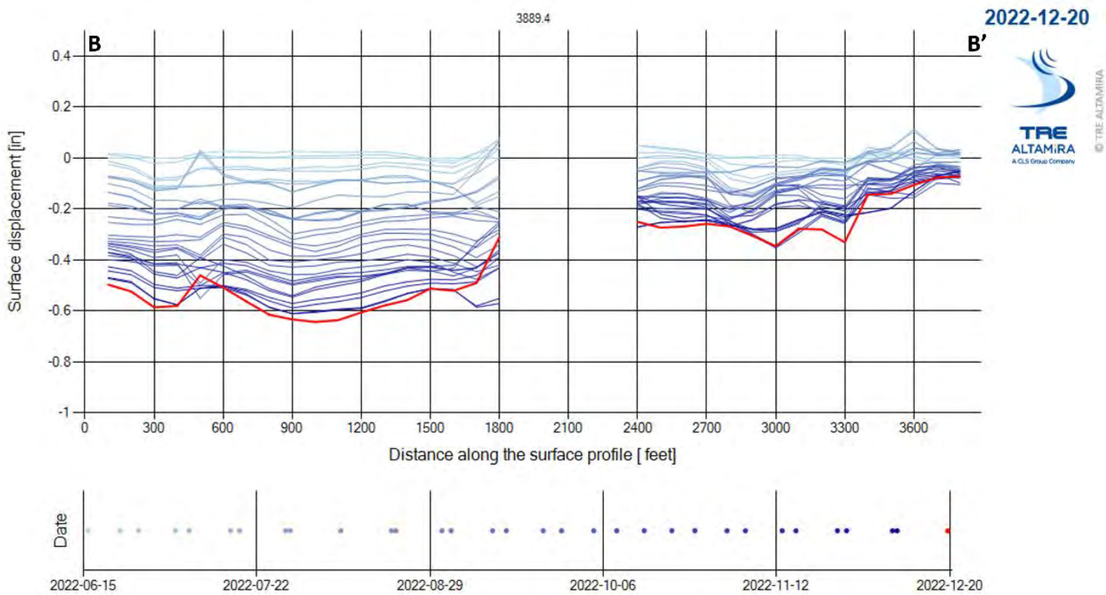

Figure 16. Surface profile of cross-section B-B' showing Vertical displacement. Negative values indicate subsidence and positive values indicate uplift.

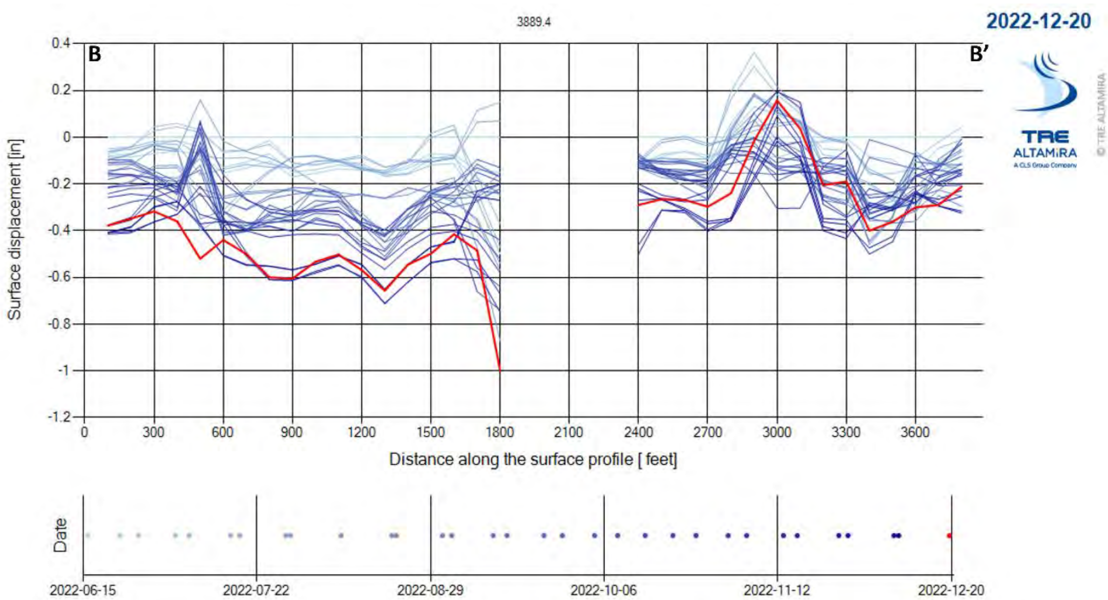

Figure 17. Surface profile of cross-section B-B' showing East-West displacement. Negative values indicate lateral displacement towards the west and positive values indicate lateral displacement towards the east.

Figure 18. Close-up of cross-section C-C' along the southern side of the dome.

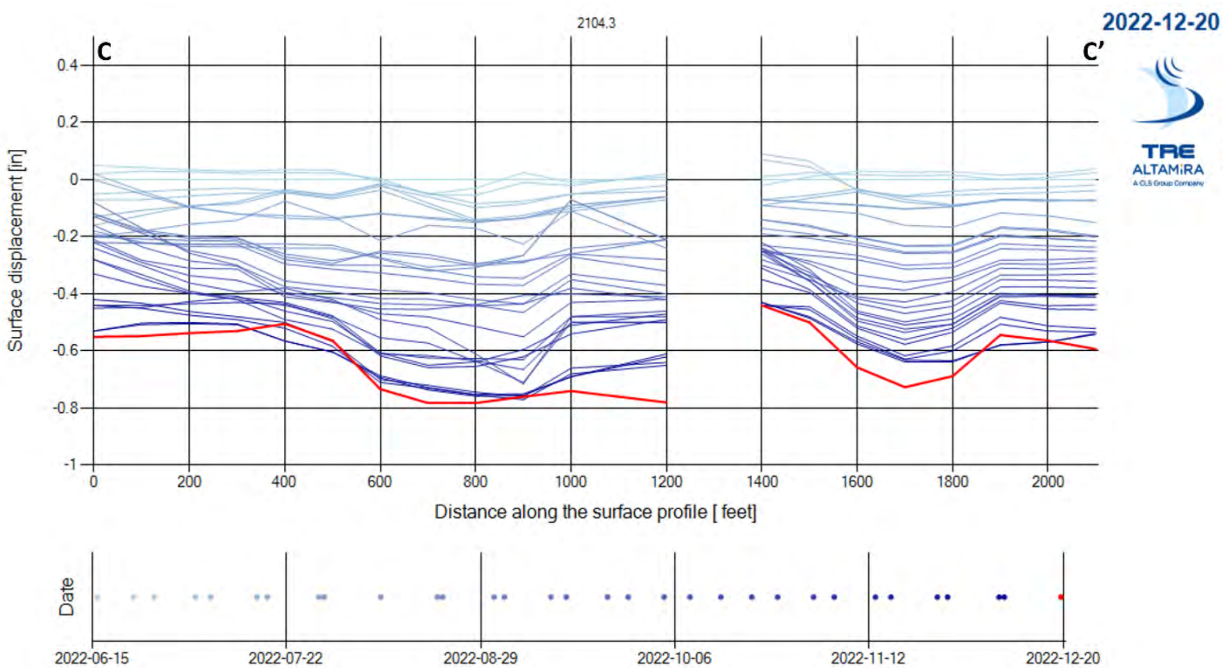

Figure 19. Surface profile of cross-section C-C' showing Vertical displacement. Negative values indicate subsidence and positive values indicate uplift.

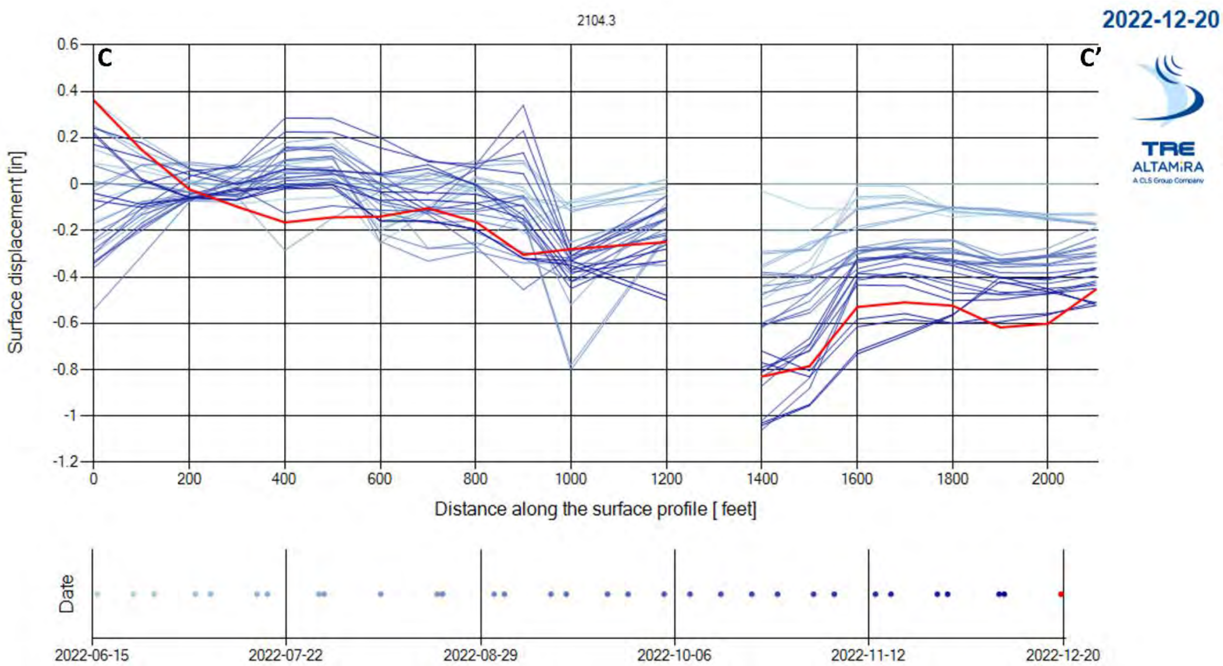

Figure 20. Surface profile of cross-section C-C' showing East-West displacement. Negative values indicate lateral displacement towards the west and positive values indicate lateral displacement towards the east.

5. Summary

TREA carried out an analysis of ground displacement over the Sulphur Mine Salt Dome using low resolution SNT imagery covering a 6-year and 2-month period (04 October 2016 – 20 December 2022) and high resolution TSX imagery covering a 6-month period (16 June 2022 - 20 December 2022). The results confirm the presence of a subsidence bowl, with maximum subsidence rates observed near the Liberty Gas Storage No.002 monument. A subsidence trend extends past the salt dome boundary and towards the west and southern regions of the AOI. Lateral displacement in the western direction was observed over the eastern portion of the dome, with maximum displacement rates observed near the Liberty Gas Storage No.002 monument.

The SNT and TSX satellites continue to acquire imagery every 12 and 11 days, respectively. Ongoing monitoring over the site is occurring with a frequency of 11 and 12 days. Monitoring frequency using a combination of TSX and PAZ satellites will occur every 4 and 7 days starting in mid-late April 2023, once a baseline of ~13 images has been acquired.

Lonquist will be performing a further evaluation of these datasets to be provided under a separate cover. Additional analysis and conclusions will be presented in the context of the site history, cavern layout and dome structure, historical level surveys, InSAR measurement point coverage, and comparison of current and past subsidence trends across the dome.

Appendix 1: Delivered Files

All results are delivered via TREmaps® web platform (https://signin.main.tremaps.com/login/#/) our proprietary online GIS platform to view and interrogate the SqueeSAR data. For login instructions and main functionalities, please use the Help page (https://en.ums.tre-altamira.com)

Table 6 lists the deliverables including the present report, the InSAR data files and an updated version of the TRE toolbar, a software tool for assisting with the loading, viewing and interrogation of the data in ESRI ArcGIS 10.x software (for set-up procedure and functionalities, see the attached manual *TREToolbarSetup_5.0.pdf*).

The SqueeSAR data is provided in shapefile (.shp) format, imperial units and NAD 1983 State Plane Louisiana South FIPS 1702 ft coordinate system. The shapefile of each elaboration contains details about the measurement points, such as displacement rate, acceleration rate, cumulative displacement, and quality indexes. The information associated within the database files (dbf) are described in Table 7.

Description		File name
SqueeSAR Data	**ASC**	SULPHUR_SNT_T136_A_CA6908A002S.shp
	DESC	SULPHUR_TSX_T29_D_CA6908A005S.shp
	2D	SULPHUR_MINE_SNT_TSX_VERT_CA6908A006V.shp SULPHUR_MINE_SNT_TSX_EAST_CA6908A007E.shp
Technical Report		TREA Lonquist – Sulphur Mine InSAR Monitoring Report Dec2022.pdf

Table 6: List of deliverables.

Field	Description
CODE	Measurement Point (MP) identification code.
HEIGHT	Topographic Elevation referred to input DEM [ft].
H_STDEV*	Height standard deviation of the measurement point [ft].
VEL	MP displacement rate [in/yr]. – **LOS:** Positive values correspond to motion toward the satellite; negative values correspond to motion away from the satellite. – **Vertical (VEL_V):** Positive values indicate uplift; negative values indicate downward movement. – **E-W Horizontal (VEL_E):** Positive values indicate eastward movement; negative values westward movement.
V_STDEV	Displacement rate standard deviation [in/yr].
ACC	Acceleration rate [in/yr^2].
A_STDEV	Standard deviation of the acceleration value [in/yr^2].
COHERENCE*	Quality measure between 0 and 1.
STD_DEF*	Displacement time series error bar [in]
EFF_AREA*	This parameter represents the effective extension of the area [ft^2] covered by Distributed Scatterers (DS). For permanent scatterers (PS), its value is set to 0.
Dyyyymmdd	Series of columns that contain the displacement values of successive acquisitions relative to the first acquisition available [in].

Table 7: Description of the fields contained in the LOS and 2D database. *Field is only present in LOS data sets.

Appendix 2: Technique Description

6. SqueeSAR®

SqueeSAR® is the advanced multi-image InSAR algorithm patented by TREA that provides high precision measurements of ground displacement in the form of a point cloud. By analyzing a stack of SAR images acquired over a site, the SqueeSAR algorithm identifies and measures the movement of radar reflectors on the ground surface that remain visible and coherent throughout the period of the analysis.

Radar reflectors belong to two different families (Figure 21):

- Permanent Scatterers (PS): point-wise radar targets characterized by highly stable radar signal returns (e.g. buildings, rocky outcrops, infrastructures, etc.)
- Distributed Scatterers (DS): patches of ground exhibiting a lower but homogenous radar signal return (e.g. rangeland, debris fields, arid areas, etc.). DS are represented as individual points, but the information does not refer to a single target, but rather to the patch of ground associated with each DS (the size [km2] but not the exact shape of the patch is provided).

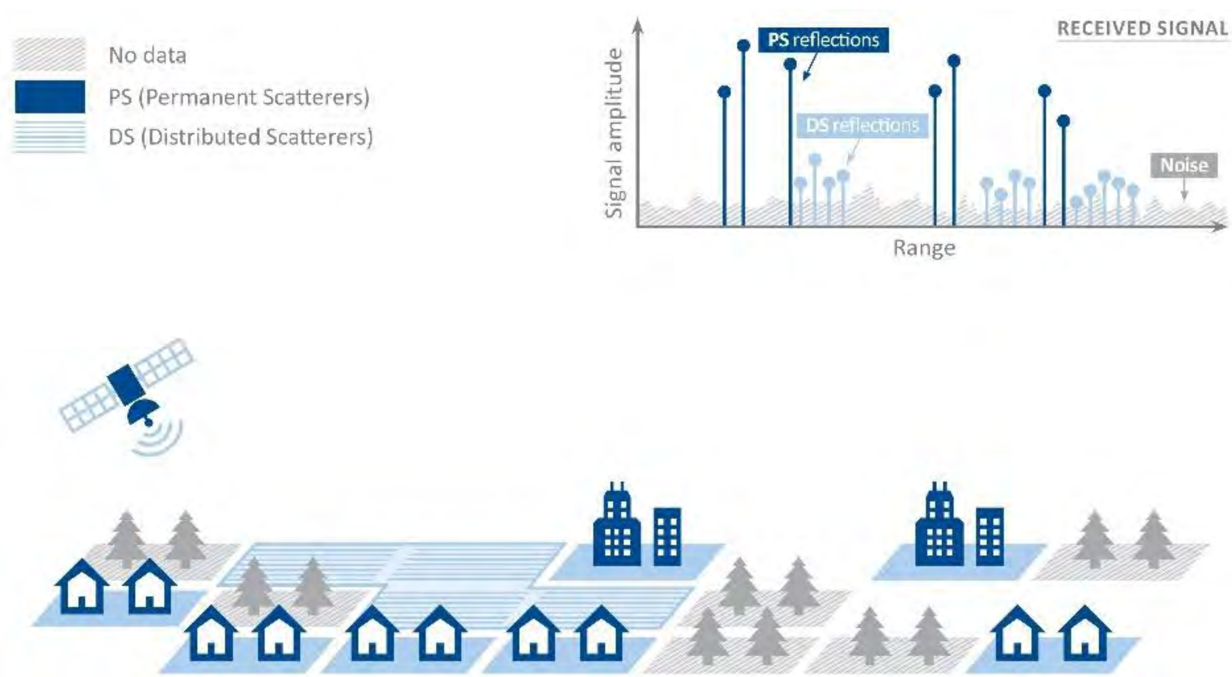

Figure 21: Schematic of PS and DS radar targets.

6.1. 1-D (LOS) Measurements

SAR satellites image the ground from ascending and descending orbits, according to the flight direction, from south to north (imaging to the east) and from north to south (imaging to the west) respectively (Figure 22). InSAR measures the projection of the real vector of displacement onto the satellite line-of-sight (LOS) and provides 1-D measurements along the LOS, which is inclined with respect to the vertical and north-south direction (θ and δ angle, respectively).

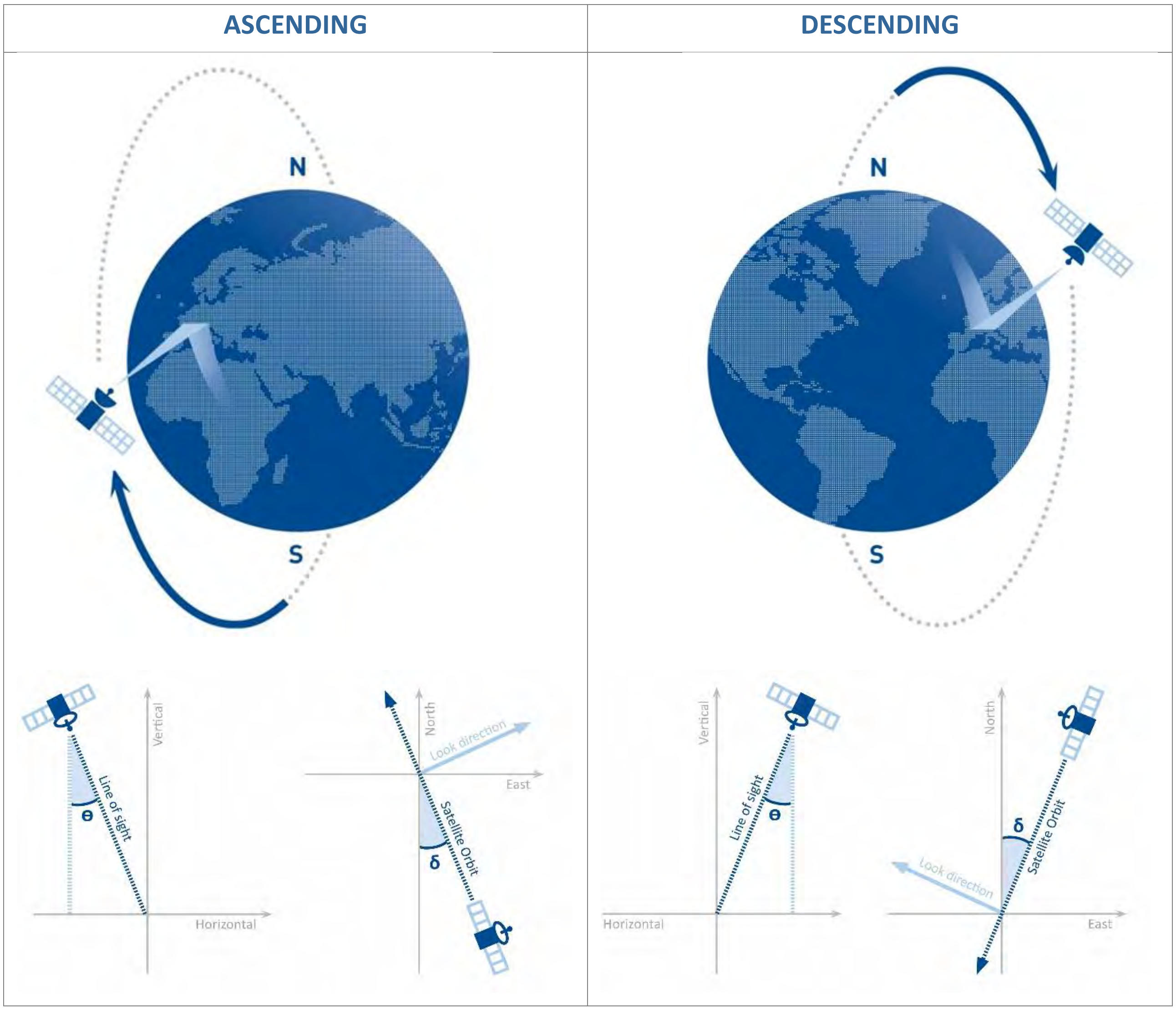

Figure 22: SAR satellites image the ground from ascending and descending orbits, according to the flight direction, from south to north (imaging to the east) and from north to south (imaging to the west), respectively. The satellite Line Of Sight (LOS) is inclined with respect to the vertical and north-south direction (θ and δ angle, respectively).

As SqueeSAR measurements are 1-D (i.e. away or toward the satellite), the sign and value of the displacement depends on the orientation of the real displacement with respect to the LOS (Figure 23). Negative values (from green to red) indicate movement away from the satellite, while positive values (from green to blue) indicate movement towards the satellite. A same displacement produces different readings when viewed from different LOS angles (Figure 23).

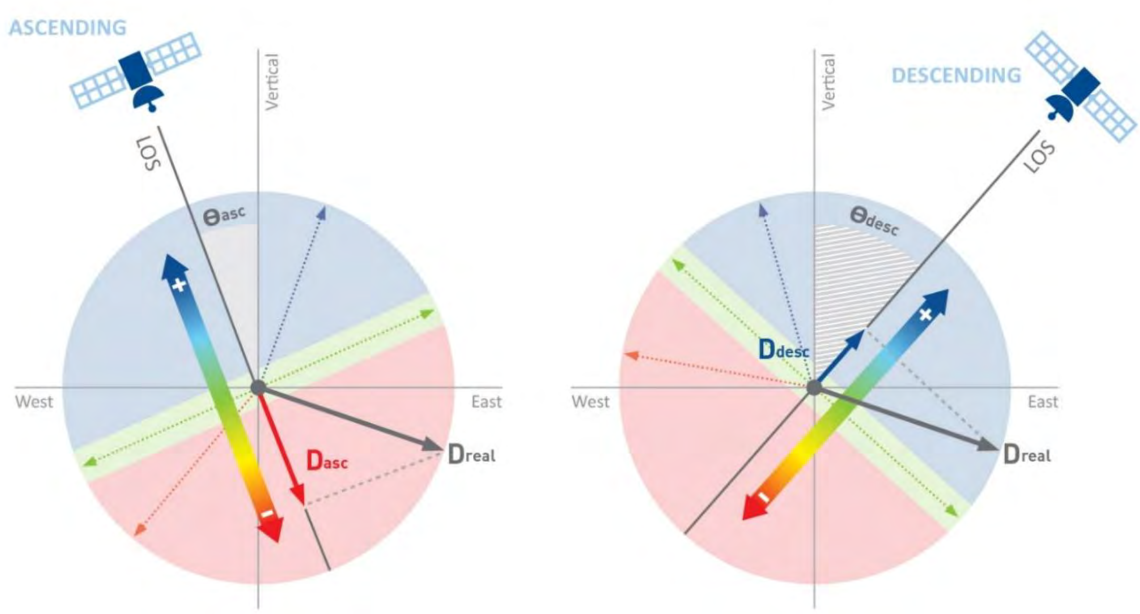

Figure 23: SqueeSAR measures the projection of real movement (Dreal) onto the LOS. The same real movement (Dreal) produces a different value from a different LOS (different inclination or different orbits). Real displacement vectors (Dreal) within the blue areas will produce positive LOS measurements while those within the red areas will produce negative LOS values. Real displacement vectors within the green band (i.e. perpendicular to the satellite LOS) will produce small (i.e. close to zero) LOS measurements.

SqueeSAR measurements are differential in space and time: spatially they are related to a local reference point (REF) and temporally to the date of the first available satellite image. The REF is assumed to be motionless and selected for its radar properties to optimize the quality of the measurements. It corresponds to a radar target with a high coherence signal in all the images of the archive and that is not affected by displacement rate variations (non-linear movement or cyclical deformations) in the analysis period. The selection of the REF is imagery-dependent. If the imagery changes (number of images and/or time span), the MP selected as the REF can change. The absolute movement of the REF point can be defined only with calibration to a GNSS network.

For each measurement point (MP), SqueeSAR provides the following main information:

- Position and elevation estimated with respect to the input DEM [ft].

– Displacement time series (TS) representing the evolution of the displacement for each acquisition date [mm or in] and measured along the LOS direction.

– Annual average displacement rate [in/yr], calculated from a linear regression of the displacement time series over the analysis period and referred to the REF.

SqueeSAR is best suited for displacement rates < 3.3ft /yr.

6.1.1. Measurement Point Density and Coverage

The density and distribution of MPs identified by the analysis depends on the resolution of the imagery, the surface characteristics, changes over time and topography of the area. In detail, MP density and coverage increases with satellite resolution and decreases over (Figure 24):

– Vegetated and low reflectivity areas (i.e., areas where the signal backscattered to the satellite is low).

– Areas affected by temporal decorrelation (i.e. radar signal is not coherent over time), which is generally associated with rapid surface changes (such as active operations areas), seasonal surface changes (such as floods or snow-coverage) or fast movement (displacement rate >3.3ft/yr)

– Areas where the satellite has visibility limitations, because of the Line of Sight (LOS) orientation with respect to the local topography.

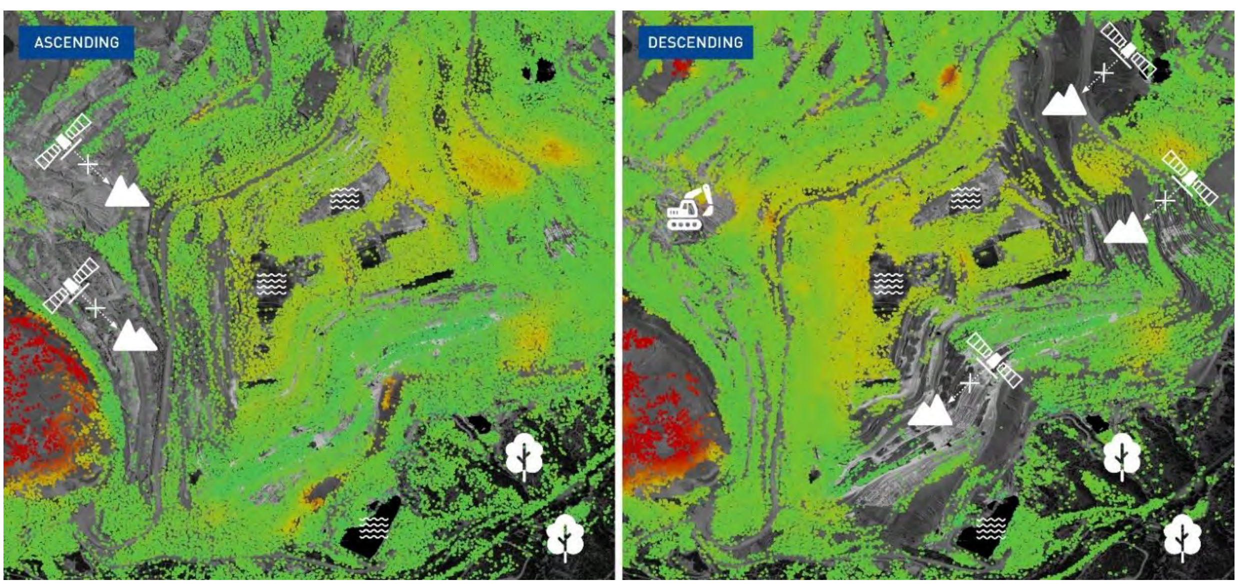

Figure 24: Example of point coverage over a mine site. The MPs coverage is low over areas with vegetation, areas of surface operations or where the visibility is limited due to the orientation of the slope with respect to the satellite line of sight. Generally, west-facing slopes have a better coverage in ascending orbit while east-facing slopes has a better visibility on descending orbit.

6.1.2. Measurement Precision

SqueeSAR can measure displacement with precision up to one-hundredth of an inch. The precision depends on a correct phase unwrapping and atmospheric contribution estimation and increases with the quality of the imagery and the coherence of the signal. In particular, the precision:

- Increases with the number of processed images, the length of the period of the analysis, the frequency of acquisitions, the coherence of the signal (i.e. the absence of vegetation or surface disturbances) and the density of points.
- Decreases with the presence of gaps in the acquisitions, strong atmospheric disturbances and surface variations in the period of the analysis (e.g. snow, floods, changes to the ground surface).

Typical displacement precision values obtained with a dataset of at least 30 images are reported in Table 8. SqueeSAR LOS measurements are provided with two displacement precision indices:

– The displacement rate standard deviation (V_STDEV), which provides an indication of the precision of the annual deformation rate with respect to the REF. Given the standard deviation (σ), and assuming that the errors are normally distributed (Gaussian), 95% of the rate values tend to be included in a ±2σ range. The displacement rate standard deviation increases with the distance of the point from the REF.

– The time series error bar (STD_DEF), which provide an indication of the precision of single displacement measurements. It depends on the coherence of the phase signal over time: the higher the coherence, the higher the precision of the measurements. This parameter is calculated as standard deviation of the residuals with respect to an analytic model (i.e. how well the model fits the displacement time series). The model is selected individually for each MP with an advanced Model Order Selection technique that take into consideration the quality of the imagery (number of images, time span and possible gaps in the acquisitions).

LOS measurements	Displacement rate standard deviation	Error bar of single measurement
Precision	±0.04 in/yr	±0.20 in

Table 8: Typical precision values for a MP less than 0.62 mi from the REF and a data set of at least 30 SAR scenes.

While the precision of the displacement measurements is within the order of one-hundredth of an inch, the location of individual measurement points is known with metric accuracy and depends on the satellite system being used (Table 9) As for the measurement precision, the location accuracy increases with the quality of the imagery, the coherence of the signal and the density of points.

Satellite	Band	Wavelength [in]	Resolution RGxAZ [ftxft]	North-South [ft]	East-West [ft]	Elevation [ft]
ERS - ENVI	C-band	2.20	65x16	± 6	± 23	± 5
RSAT (*Standard Beam*)	C-band	2.20	65x16	± 6	± 23	± 5
SNT	**C-band**	**2.32**	**16x65**	**± 26**	**± 39**	**±26**
CSK	X-band	1.23	10x10	± 3	± 3	±1.6
TSX (*Stripmap*)	X-band	1.22	10x10	± 3	± 10	± 5
TSX (*Spotlight*)	**X-band**	**1.22**	**3x3**	**± 1.6**	**± 10**	**± 5**
ALOS-1 (*Fine Beam*)	L-band	9.29	54x54	± 5	± 10	± 3
ALOS-2 (*Fine SM3 Beam*)	L-band	9.37	32x32	± 5	± 10	± 3

Table 9: Typical precision values (1 sigma) associated to the UTM coordinates of a MP at mid-latitudes. Values are referred to a MP less than 0.62 mi from the REF and a data-set of at least 30 SAR scenes. Satellites used in this analysis are in bold.

6.1.3. Fast Movements and Phase Unwrapping

SqueeSAR is best suited to measure displacement rates below 3.3 ft/yr. In a case of rapid deformation, the measurements can be affected by phase unwrapping inaccuracies.

Figure 25 represents a schematic of a radar target affected by a phase unwrapping error. The target is represented at an initial distance R_0 (in blue), while in red there are three possible cases that are shifted by different amounts. Without prior information, the radar system is not able to estimate the correct number of wavelengths ($n\lambda$), therefore, all three cases will produce equivalent ΔRs.

In theory, on a single isolated radar target, only displacement that is below half a wavelength can be correctly detected. A greater displacement may be underestimated. In extreme cases, if the target moved exactly half a wavelength between two acquisitions the target would still be observed as perfectly stable.

These theoretical limits refer to movements affecting single isolated radar targets. The limits increase significantly in cases where the movement is spatially correlated and the MP density is adequate. Figure 26 shows a schematic of spatially correlated subsidence. When the radar target density is adequate, the phase can be correctly unwrapped and displacement exceeding the $\lambda/2$ limit can be measured. In cases where the radar target distribution is not adequate, incorrect phase unwrapping can occur and will usually cause displacement to be underestimated.

The temporal distribution of the acquisitions also impacts the phase unwrapping procedure: a higher acquisition frequency means a higher sampling frequency and thus the ability measure more rapid movement.

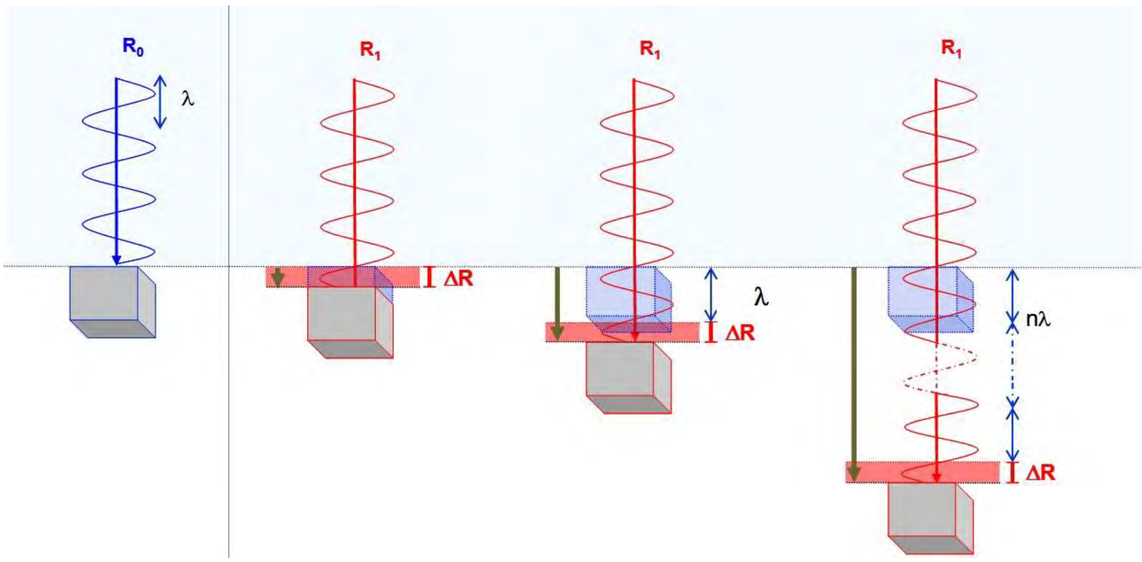

Figure 25: Schematic of a sinusoidal phase of the electromagnetic wave incident on a moving target (grey solid). Without prior information, it is not possible to estimate the correct number of wavelengths (nλ) which occur and in all three cases an equivalent ΔR shift is measured.

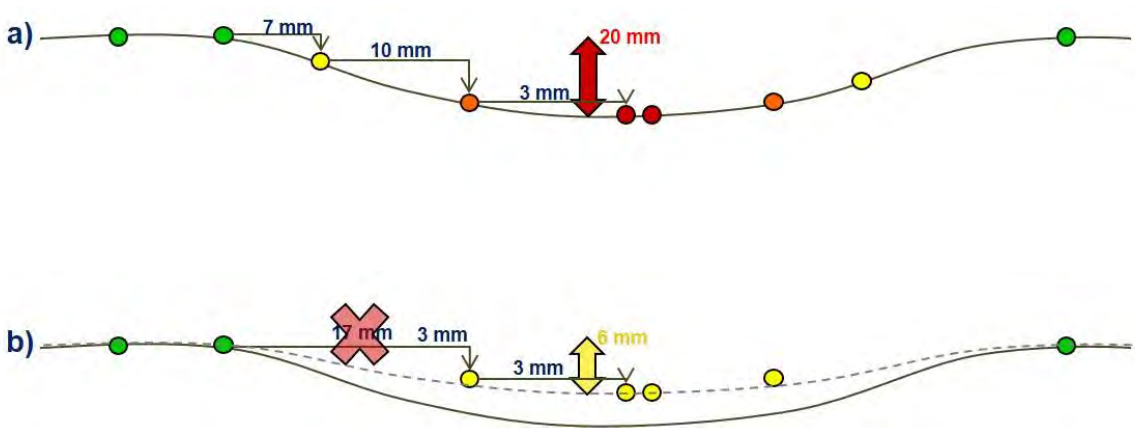

Figure 26: Schematic of spatially correlated subsidence. The MPs are colour-coded according to the displacement measured. Considering a X-band satellite (λ=1.22), a total displacement of 0.79 in (higher than the λ/2 limit of 0.61 in) can be measured when the MP are well distributed along the subsiding profile (a). When the MP distribution is not adequate, an underestimation of the real displacement occurs (b)

6.2. 2-D (Vertical and East-West) Measurements

The combination of 1-D (LOS) SqueeSAR results obtained from ascending and descending orbits over the same area and overlapping period, produces 2-D (vertical and east-west) measurements.

The estimation of the 2-D measurements requires the following steps and assumptions:

– Satellites travelling in ascending and descending orbits identify different radar targets on the ground, entailing that the 2-D procedure requires a spatial grid to capture MPs from both orbits within each cell. It is assumed that MPs that fall within the same cell are affected by the same motion. All MPs within a same cell are then averaged. This entails that the 2-D cells do not represent radar targets on the ground, but rather synthetic points located at the centre of the cells (Figure 27).

– A 2-D time series is calculated by combining all ascending and descending time series using trigonometry. Only cells that contain points from both input LOS data sets will produce a 2-D time series. This entails that the spatial coverage of the 2-D information is thus generally lower than that of the individual LOS data sets (Figure 27).

– Since the images are acquired on different dates from each orbit, the LOS displacement time series must be re-sampled in time. The final output includes all ascending and descending acquisition dates and covers the overlapping period in common for the two data sets.

– North-south movement cannot be measured with InSAR as SAR satellites are not sensitive to movement parallel to their travel direction.

As in LOS analyses, average annual displacement rates in a 2-D analysis are calculated from a linear regression of the displacement measured over the entire period of the study and all measurements are relative to a reference point that is assumed to be stable.

The convention for displacement sign and point colour is the following (Figure 28):

– In a vertical data set, negative values (from yellow to red) indicate downward displacement (subsidence), while positive values (from pale to dark blue) indicate upward displacement (uplift or heave).

– In an east-west data set, negative values (from yellow to red) indicate westward motion, while positive values (from pale to dark blue) indicate eastward motion.

Although 2-D measurements are generally easier to interpret than LOS data but they have a lower spatial resolution, which means that in detailed analysis of localized features it may be beneficial to use the full resolution LOS results.

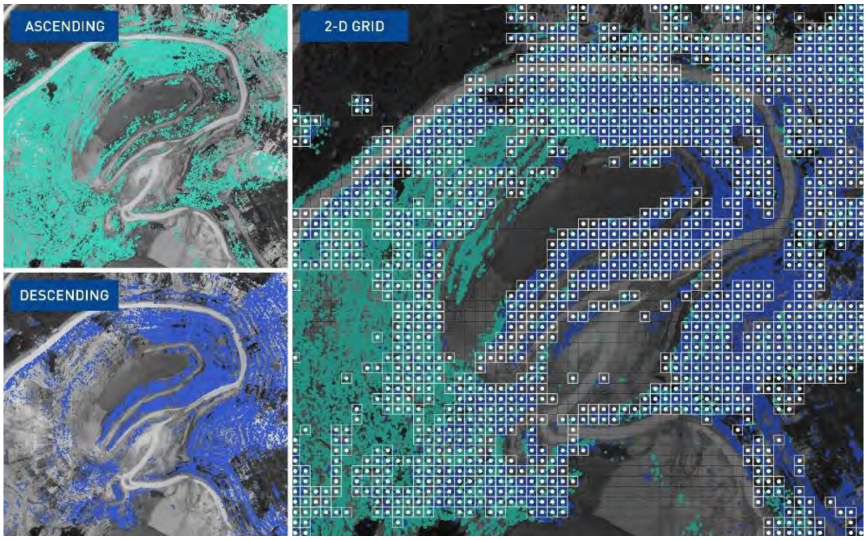

Figure 27: 2-D measurements are estimated by subsampling ascending and descending data on a common spatial grid. The measurements of all MPs contained within the same cell are averaged to produce 2-D measurement points located at the centre of the cell. The 2-D procedure only produces readings for cells containing MP from both orbits (white cells).

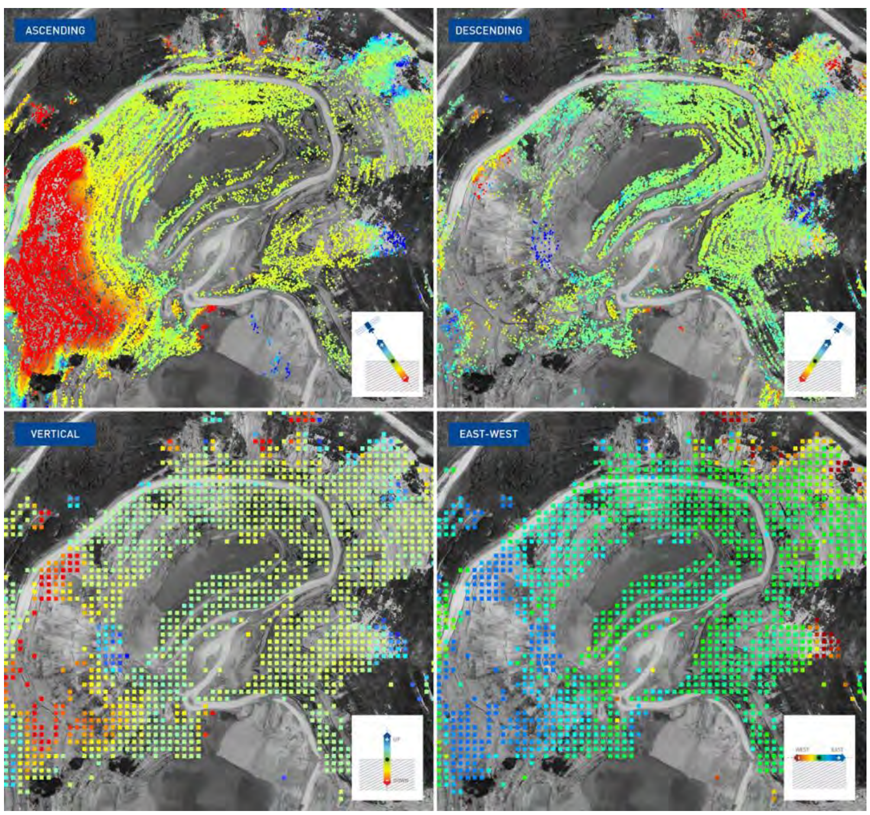

Figure 28: Ascending and descending LOS measurements correspond to the full resolution network of natural reflectors identified on the ground and provide the projection of the real movement to the specific LOS The combination of ascending and descending data produces a regular grid of vertical and east-west measurements.

6.3. SqueeSAR vs Other Surface Monitoring Techniques

When comparing SqueeSAR data with other measurements, the main characteristics to take into consideration are the following:

- SqueeSAR measurements are referred to a local REF. The REF is selected for its radar properties to optimize the quality of the measurements and corresponds to a radar target with high coherence signal and not affected by displacement rate variations in the period of the analysis. The "absolute" stability of the REF point can be verified with a GNSS network.
- SqueeSAR provides displacement measurements with precision in the order of one-hundredth of an inch but point location accuracy is in the order of feet.
- SqueeSAR provides a dense network of measurement points (from 259 to over 25,900 MP/mi^2, depending on the satellite resolution and the land cover) that is not achievable with other in-situ monitoring techniques. This dense network of natural benchmarks allows InSAR to provide very accurate relative movement (estimation of how a point is moving with respect to another point) but less accurate absolute measurements because all the measurements are referred to a local reference point.
- InSAR does not measure the full displacement vector but its projection onto the satellite line of sight. SqueeSAR measurements are 1-D (LOS) and an accurate estimation of the vertical motion component is only possible by combining LOS measurements obtained from ascending and descending orbits over the same area and overlapping period.
- InSAR is not sensitive to movement along the orbit direction (Azimuth), which is approximately north-south (i.e. SqueeSAR do not provide north-south measurements).

Table 10 reports a comparison between the main characteristics of InSAR measurements with respect to other conventional surface monitoring techniques.

Main Characteristics	SqueeSAR	Manual GNSS	Permanent GNSS	Levelling
Spatial density of points	259 - >125,900 points/mi^2	few points/mi^2	few points/mi^2	few points/mi^2
Measurement precision * [1σ]	± 0.20 in (LOS and vert)	± 0.40 in (horizontal) ± 0.80 in (vertical)	± 0.40 in (horizontal) ± 0.40 in (vertical)	±0.04-0.08 in **

Measurement accuracy	High relative accuracy but low absolute accuracy	High absolute accuracy	High absolute accuracy	High absolute accuracy
Location accuracy**	feet	inches	inches	inches
Components	1-D (LOS) and 2-D	3-D	3-D	1-D (vert)
Acquisition frequency	Weekly to monthly	Quarterly to yearly	Hourly to daily	Quarterly to yearly

Table 10: Main characteristics of InSAR and other conventional monitoring techniques. *Precision refers to the error bar of a single measurement (i.e. the consistency of repeated measurements). **Accuracy refers to how close a measurement is to the absolute value. GNSS precision values refer to a 1-hour static session.

In general, to perform a comparison of InSAR data with other measurements it is necessary:

1. To compare the measurements along a same direction.

– As InSAR provides 1-D (LOS) measurements, it is more rigorous to project 3-D measurements to the LOS direction. The projection of the LOS measurements to the vertical direction can be performed only under the assumption of negligible horizontal motion components. Alternatively, the use of SqueeSAR measurements obtained from ascending and descending orbits over the same area and overlapping period allows an accurate estimation of the vertical motion component.

2. Define a co-location rule between the InSAR measurement points and other stations/benchmarks

– In general, it is unusual for SqueeSAR measurement points to fall exactly at benchmark locations. It is therefore recommended to perform the comparison using all of the most coherent (highest quality) points located within a certain radius from the benchmark, rather than just an individual SqueeSAR point.

3. Use the same reference point or verify the absolute stability of the local InSAR reference point (REF)

4. Use the same reference period and consider the accuracy and frequency of the measurement techniques being compared.

6.3.1.1. Integration and Calibration of InSAR Data with a GNSS Network – Best Practices

InSAR and GNSS (Global Navigation Satellite System) are complementary techniques for monitoring surface movements and are generally integrated to take advantage of the strengths of both technologies, in terms of spatial density, precision and accuracy (Table 10). The integration of InSAR and GNSS measurements provides a high spatial density of information with optimal precision and accuracy of the measurements when a common reference system is used.

To achieve this, the SqueeSAR data is generally calibrated to an absolute GNSS network based on the following steps:

1) Projection of the GNSS measurements to the satellite LOS. The GNSS 3-D measurements are projected to the satellite 1-D LOS to create a GNSS LOS time series. This step allows a direct comparison of the two independent measurements (InSAR and GPS). The projection of the 3-D GNSS measurements onto the LOS direction can be calculated as follows:

$$D_{LOS} = D_{VERT}*V_{LOS} + D_{EW}*E_{LOS} + D_{NS}*N_{LOS}$$

with V_{LOS}, E_{LOS} e N_{LOS} are the LOS versors along the 3 directions and D_{VERT}, D_{EW} e D_{NS} are the 3 components of the GNSS measurements. The LOS versors are provided in the metadata associated to the SqueeSAR data (Figure 29) and represent the cosines of the angles between the LOS and the 3 coordinate axes.

2) Co-localization of the measurement points. Generally, GNSS benchmarks and InSAR points are not exactly co-located. Additionally, the accuracy of the InSAR point location is known to within a few metres (Table 9). The location of a GNSS benchmark is known with cm precision. For these reasons, InSAR measurement points (MP) within a certain radius of each GNSS are generally selected and used to calculate an average time series (ATS) for the overlapping period with the GNSS time series (one InSAR ATS for each GNSS). This step allows the comparison of data collected at a same location over a corresponding period.

3) Refence point stability check. GNSS measurements are absolute as they are connected to a global network, while InSAR data are referred to a local reference point (REF). GNSS measurements can be used to verify the "absolute" stability of the REF. If there is no GNSS station close to the REF, it is suggested to just verify the stability of the InSAR points in an area around a stable GPS station.

4) Absolute calibration. If the REF check highlights discrepancies between InSAR and GNSS measurements, the InSAR measurements are calibrated to the absolute GNSS network as follows:

– Plane removal (when only a linear regional trend is present): a difference in average velocity is calculated for each ATS and corresponding GNSS. The average velocity differences calculated for each ATS and GNSS pair is then used to estimate and remove a first order surface (plane) from all InSAR measurement points. The plane is statistically estimated at regional scale by minimizing the residuals of the differences between the ATS and corresponding GNSS.

– Time series calibration (when a not-linear regional trend is present): evaluation of an average time series of residuals by comparing the ATS to the corresponding GNSS time series at each location. All the time series of residuals obtained are then averaged to define a unique common time series of residuals (cRTS) at regional scale. This cRTS represents the movement of the local InSAR reference points with respect to the absolute GNSS reference frame. The cRTS is then removed from every InSAR MP time series.

$$D_{LOS} = D_{VERT} * V_{LOS} + D_{EW} * E_{LOS} + D_{NS} * N_{LOS}$$

Satellite info

Satellite	Wavelength	Satellite geometry	Sensor mode	Satellite track
SNT	5.55 cm	ASCENDING	IW	111

Acquisition geometry

Line of sight angle	**θ:**	35.75°	**δ:**	15.47°			
Line of sight versors	**V:**	0.812	**N:**	-0.156		**E:**	-0.563

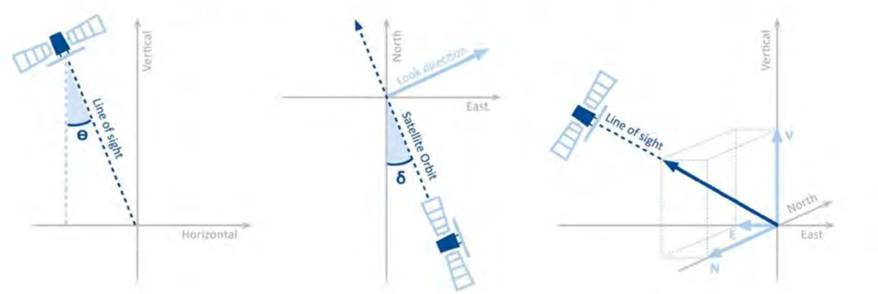

Figure 29: Example of metadata associated to the SqueeSAR measurements. LOS angles and versos can be used to transform a 3-D measurement (D_{VERT}, D_{EW} and D_{NS}) onto a LOS measurement (D_{LO}).

Appendix 3: Average Time Series over Monuments

The average time series plots showing the average displacement rates (vertical and east-west) within a 100-foot buffer of each monument are provided in Figure 30. The vertical displacement rates are shown in black and the east-west displacement rates are shown in red. For east-west displacement rates, negative values indicate movement towards the west and positive values indicate movement towards the east.

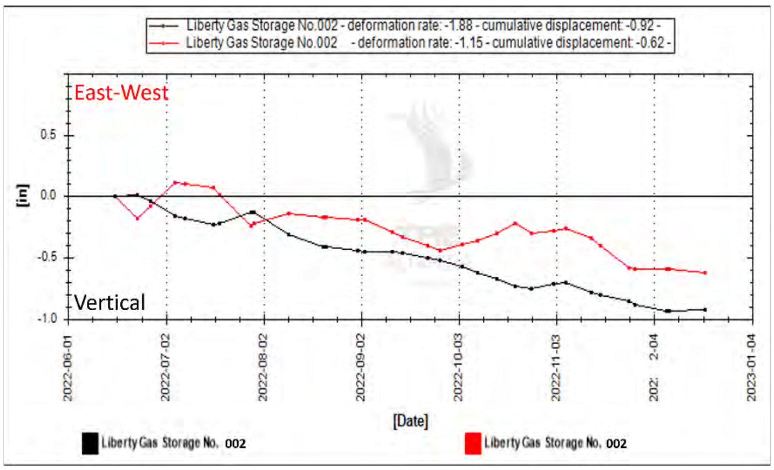

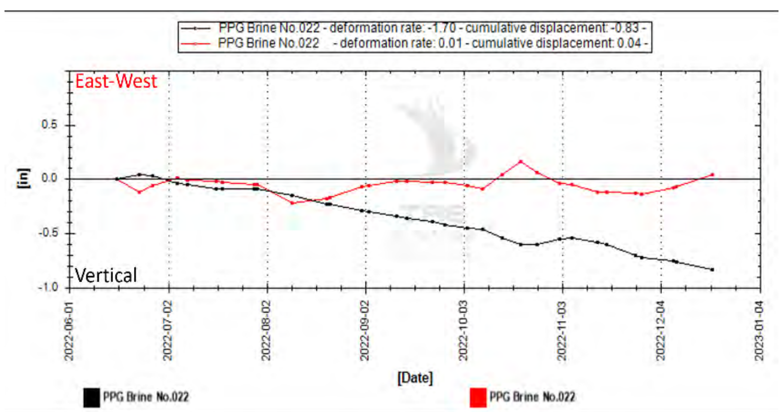

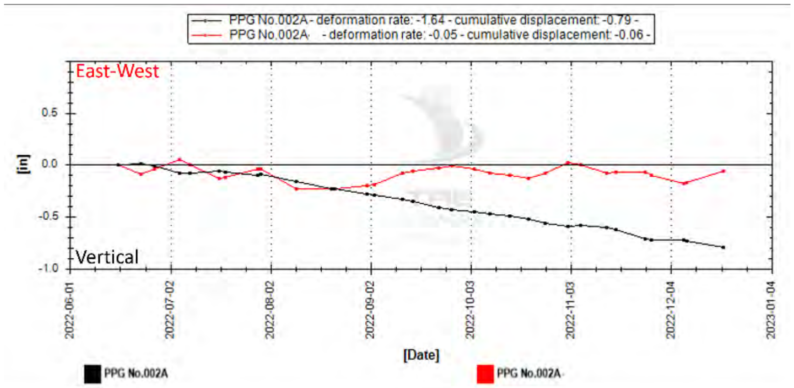
PPG No.002A - deformation rate: -1.64 - cumulative displacement: -0.79 -
PPG No.002A - deformation rate: -0.05 - cumulative displacement: -0.06 -
East-West
Vertical
[m]
[Date]
PPG No.002A
PPG No.002A

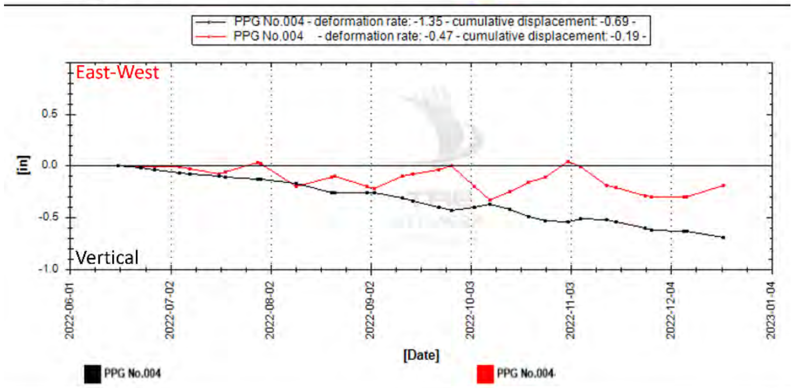
PPG No.004 - deformation rate: -1.35 - cumulative displacement: -0.69 -
PPG No.004 - deformation rate: -0.47 - cumulative displacement: -0.19 -
East-West
Vertical
[m]
[Date]
PPG No.004
PPG No.004

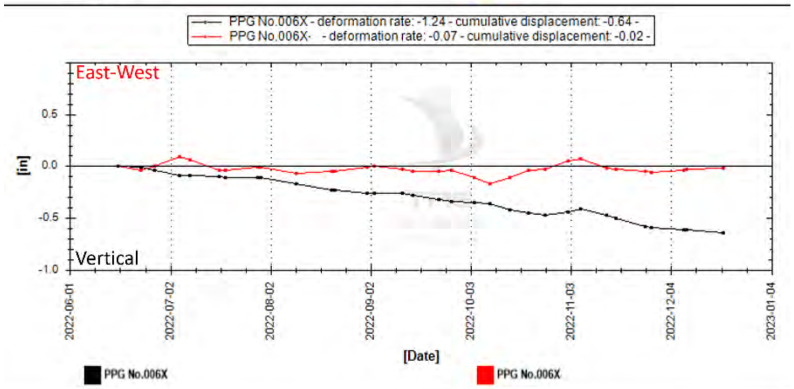
PPG No.006X - deformation rate: -1.24 - cumulative displacement: -0.64 -
PPG No.006X - deformation rate: -0.07 - cumulative displacement: -0.02 -
East-West
Vertical
[m]
[Date]
PPG No.006X
PPG No.006X

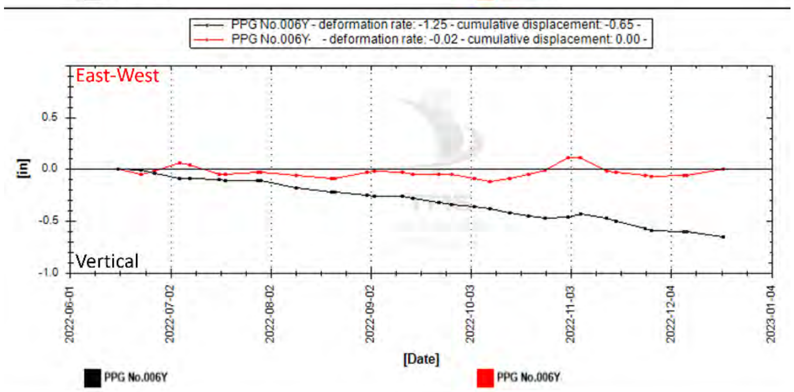
PPG No.006Y - deformation rate: -1.25 - cumulative displacement: -0.65 -
PPG No.006Y - deformation rate: -0.02 - cumulative displacement: 0.00 -
East-West
Vertical
[m]
[Date]
PPG No.006Y
PPG No.006Y

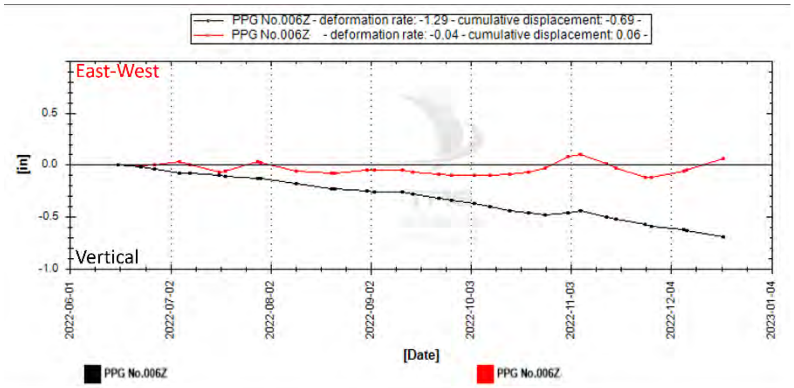
PPG No.006Z - deformation rate: -1.29 - cumulative displacement: -0.69 -
PPG No.006Z - deformation rate: -0.04 - cumulative displacement: 0.06 -
East-West
Vertical
[m]
0.5
0.0
-0.5
-1.0
2022-06-01
2022-07-02
2022-08-02
2022-09-02
2022-10-03
2022-11-03
2022-12-04
2023-01-04
[Date]
PPG No.006Z
PPG No.006Z

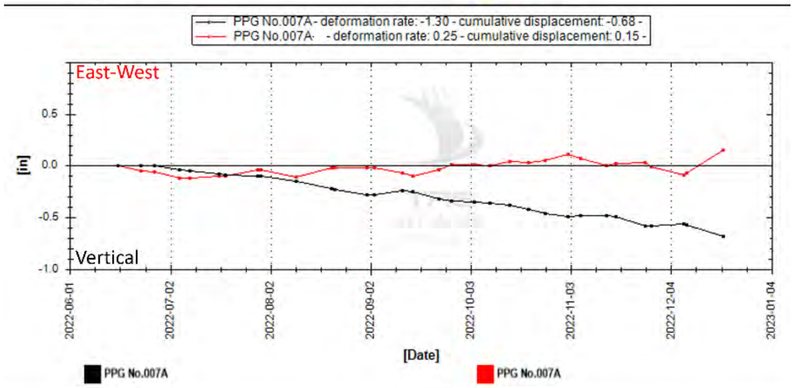
PPG No.007A - deformation rate: -1.30 - cumulative displacement: -0.68 -
PPG No.007A - deformation rate: 0.25 - cumulative displacement: 0.15 -
East-West
Vertical
[m]
0.5
0.0
-0.5
-1.0
2022-06-01
2022-07-02
2022-08-02
2022-09-02
2022-10-03
2022-11-03
2022-12-04
2023-01-04
[Date]
PPG No.007A
PPG No.007A

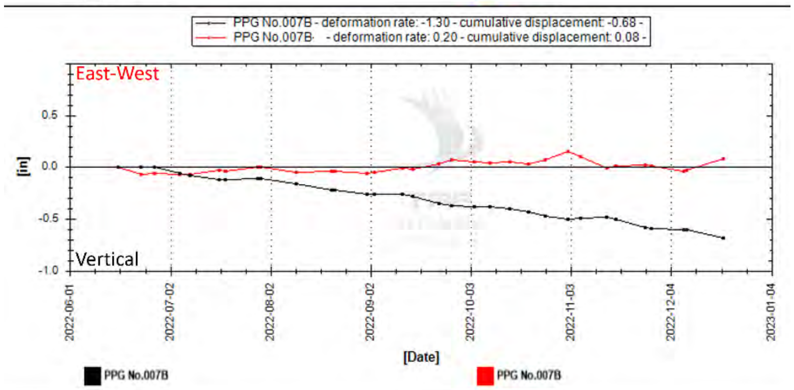
PPG No.007B - deformation rate: -1.30 - cumulative displacement: -0.68 -
PPG No.007B - deformation rate: 0.20 - cumulative displacement: 0.08 -
East-West
Vertical
[m]
0.5
0.0
-0.5
-1.0
2022-06-01
2022-07-02
2022-08-02
2022-09-02
2022-10-03
2022-11-03
2022-12-04
2023-01-04
[Date]
PPG No.007B
PPG No.007B

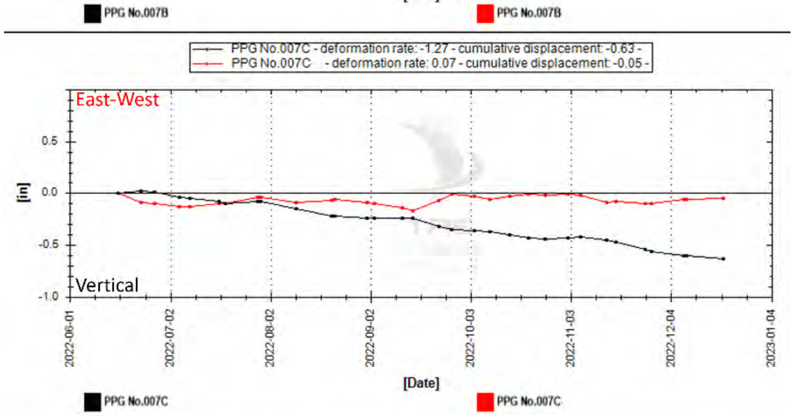
PPG No.007C - deformation rate: -1.27 - cumulative displacement: -0.63 -
PPG No.007C - deformation rate: 0.07 - cumulative displacement: -0.05 -
East-West
Vertical
[m]
0.5
0.0
-0.5
-1.0
2022-06-01
2022-07-02
2022-08-02
2022-09-02
2022-10-03
2022-11-03
2022-12-04
2023-01-04
[Date]
PPG No.007C
PPG No.007C

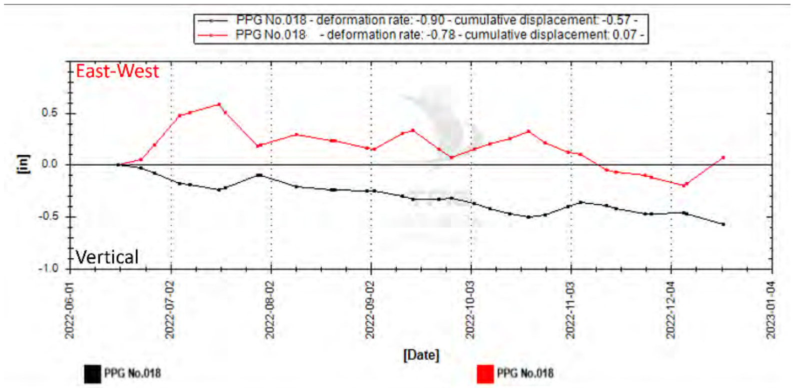
PPG No.018 - deformation rate: -0.90 - cumulative displacement: -0.57 -
PPG No.018 - deformation rate: -0.78 - cumulative displacement: 0.07 -
East-West
Vertical
[m]
0.5
0.0
-0.5
-1.0
2022-06-01
2022-07-02
2022-08-02
2022-09-02
2022-10-03
2022-11-03
2022-12-04
2023-01-04
[Date]
PPG No.018
PPG No.018

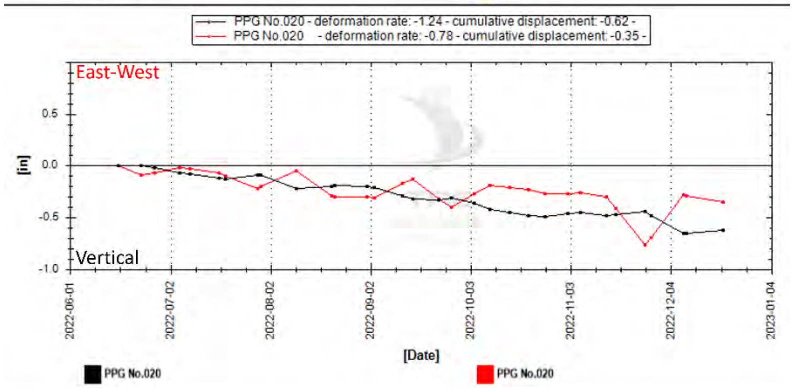
PPG No.020 - deformation rate: -1.24 - cumulative displacement: -0.62 -
PPG No.020 - deformation rate: -0.78 - cumulative displacement: -0.35 -
East-West
Vertical
[m]
0.5
0.0
-0.5
-1.0
2022-06-01
2022-07-02
2022-08-02
2022-09-02
2022-10-03
2022-11-03
2022-12-04
2023-01-04
[Date]
PPG No.020
PPG No.020

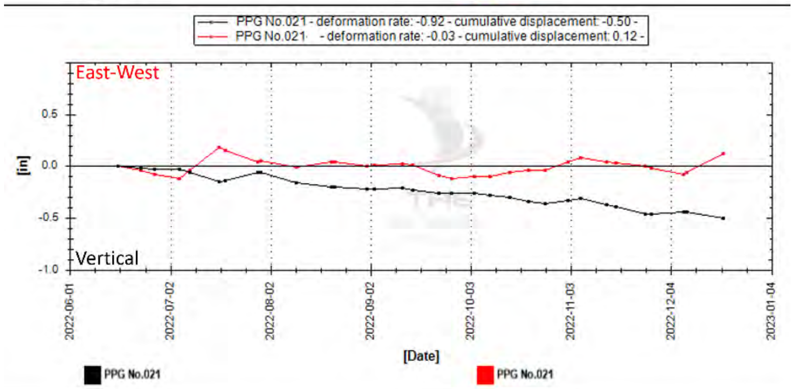
PPG No.021 - deformation rate: -0.92 - cumulative displacement: -0.50 -
PPG No.021 - deformation rate: -0.03 - cumulative displacement: 0.12 -
East-West
Vertical
[m]
0.5
0.0
-0.5
-1.0
2022-06-01
2022-07-02
2022-08-02
2022-09-02
2022-10-03
2022-11-03
2022-12-04
2023-01-04
[Date]
PPG No.021
PPG No.021

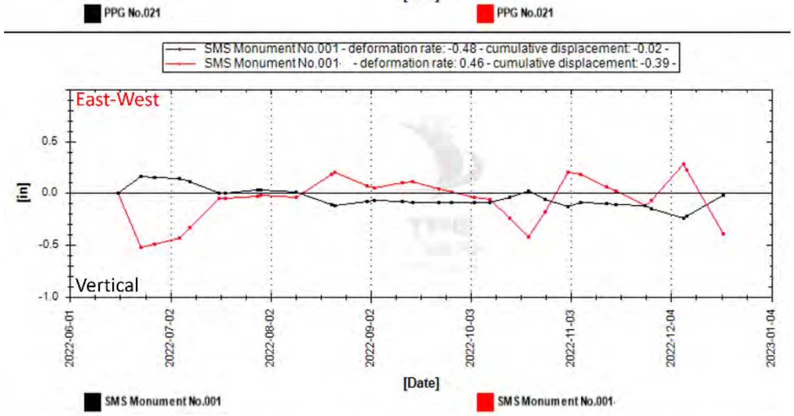
SMS Monument No.001 - deformation rate: -0.48 - cumulative displacement: -0.02 -
SMS Monument No.001 - deformation rate: 0.46 - cumulative displacement: -0.39 -
East-West
Vertical
[m]
0.5
0.0
-0.5
-1.0
2022-06-01
2022-07-02
2022-08-02
2022-09-02
2022-10-03
2022-11-03
2022-12-04
2023-01-04
[Date]
SMS Monument No.001
SMS Monument No.001

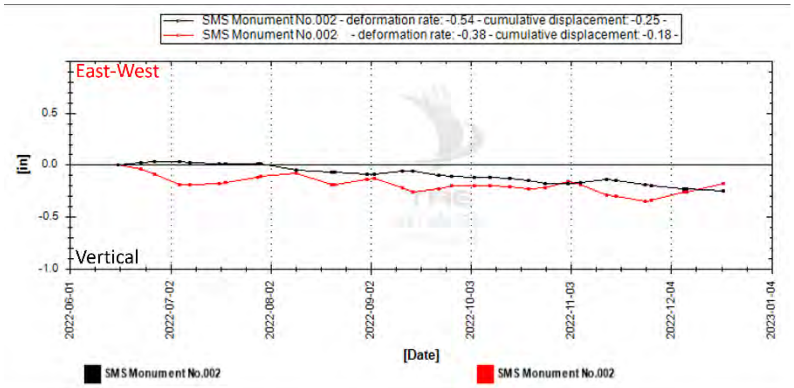
SMS Monument No.002 - deformation rate: -0.54 - cumulative displacement: -0.25 -
SMS Monument No.002 - deformation rate: -0.38 - cumulative displacement: -0.18 -
East-West
Vertical
[m]
0.5
0.0
-0.5
-1.0
2022-06-01
2022-07-02
2022-08-02
2022-09-02
2022-10-03
2022-11-03
2022-12-04
2023-01-04
[Date]
SMS Monument No.002
SMS Monument No.002

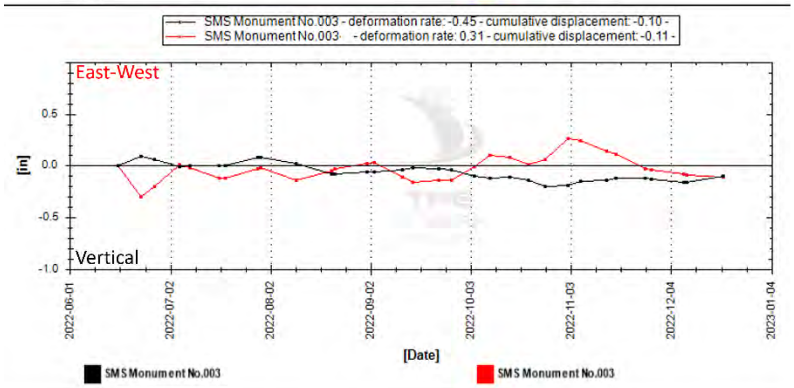
SMS Monument No.003 - deformation rate: -0.45 - cumulative displacement: -0.10 -
SMS Monument No.003 - deformation rate: 0.31 - cumulative displacement: -0.11 -
East-West
Vertical
[m]
0.5
0.0
-0.5
-1.0
2022-06-01
2022-07-02
2022-08-02
2022-09-02
2022-10-03
2022-11-03
2022-12-04
2023-01-04
[Date]
SMS Monument No.003
SMS Monument No.003

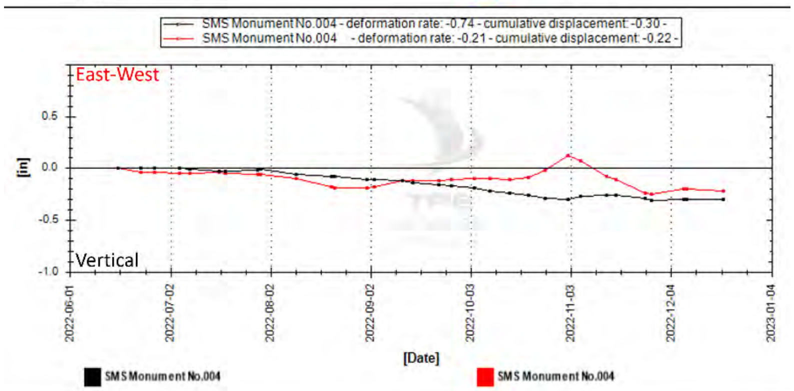
SMS Monument No.004 - deformation rate: -0.74 - cumulative displacement: -0.30 -
SMS Monument No.004 - deformation rate: -0.21 - cumulative displacement: -0.22 -
East-West
Vertical
[m]
0.5
0.0
-0.5
-1.0
2022-06-01
2022-07-02
2022-08-02
2022-09-02
2022-10-03
2022-11-03
2022-12-04
2023-01-04
[Date]
SMS Monument No.004
SMS Monument No.004

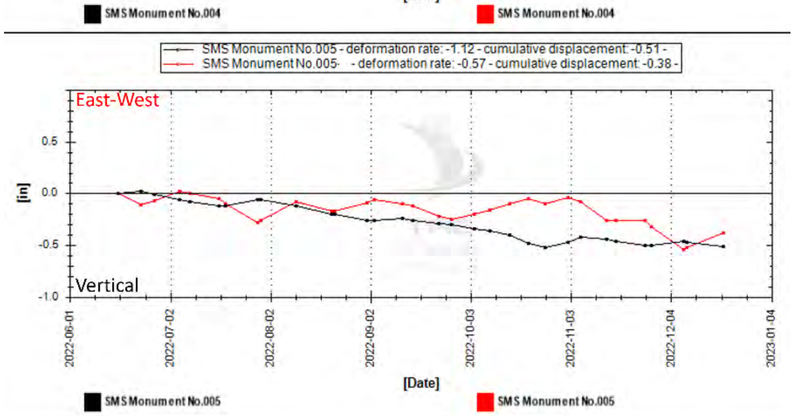
SMS Monument No.005 - deformation rate: -1.12 - cumulative displacement: -0.51 -
SMS Monument No.005 - deformation rate: -0.57 - cumulative displacement: -0.38 -
East-West
Vertical
[m]
0.5
0.0
-0.5
-1.0
2022-06-01
2022-07-02
2022-08-02
2022-09-02
2022-10-03
2022-11-03
2022-12-04
2023-01-04
[Date]
SMS Monument No.005
SMS Monument No.005

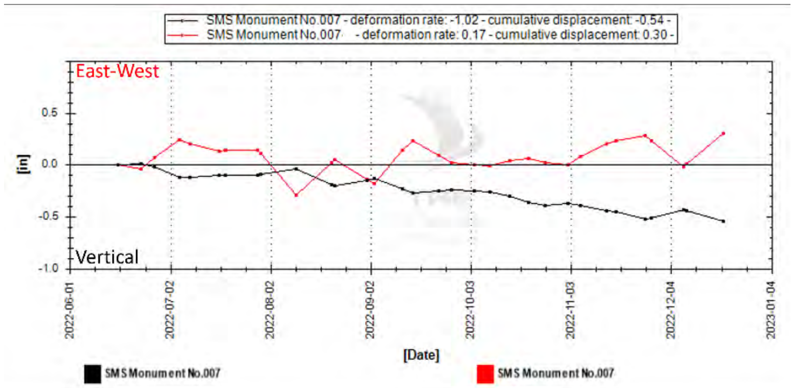
SMS Monument No.007 - deformation rate: -1.02 - cumulative displacement: -0.54 -
SMS Monument No.007 - deformation rate: 0.17 - cumulative displacement: 0.30 -
East-West
Vertical
[m]
[Date]
SMS Monument No.007
SMS Monument No.007

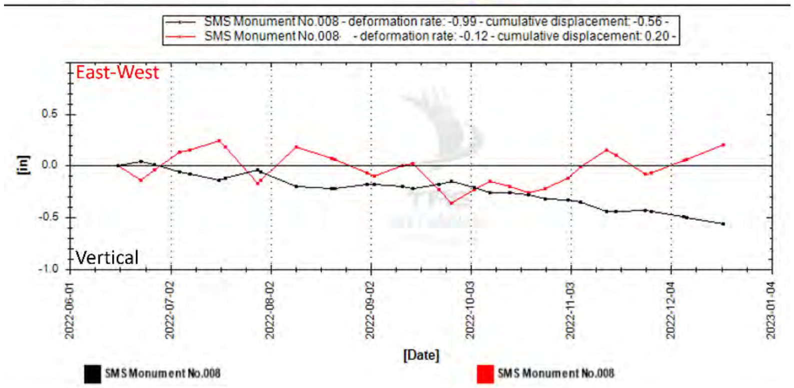
SMS Monument No.008 - deformation rate: -0.99 - cumulative displacement: -0.56 -
SMS Monument No.008 - deformation rate: -0.12 - cumulative displacement: 0.20 -
East-West
Vertical
[m]
[Date]
SMS Monument No.008
SMS Monument No.008

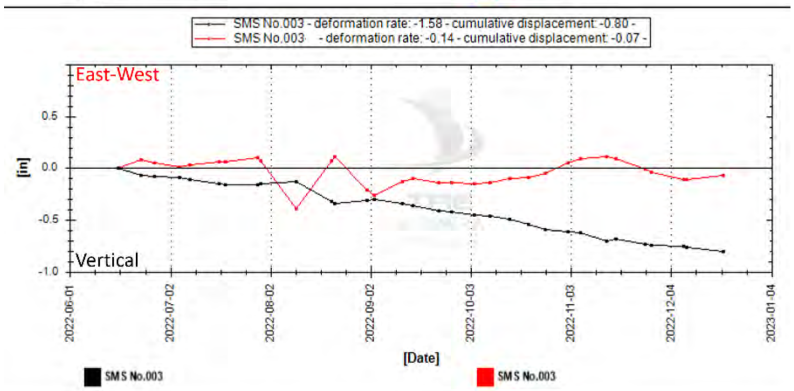
SMS No.003 - deformation rate: -1.58 - cumulative displacement: -0.80 -
SMS No.003 - deformation rate: -0.14 - cumulative displacement: -0.07 -
East-West
Vertical
[m]
[Date]
SMS No.003
SMS No.003

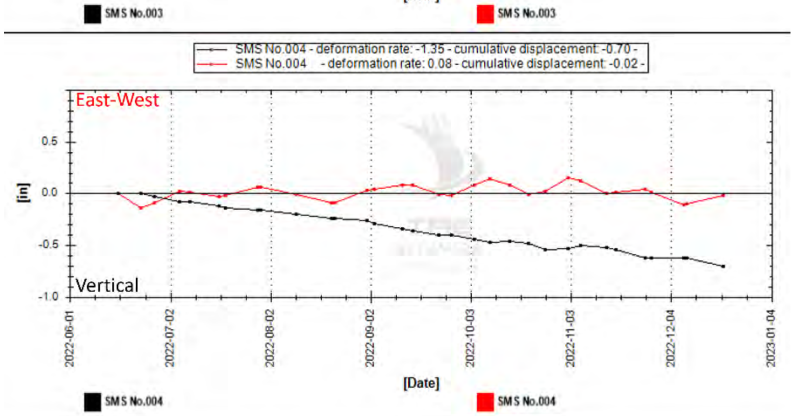
SMS No.004 - deformation rate: -1.35 - cumulative displacement: -0.70 -
SMS No.004 - deformation rate: 0.08 - cumulative displacement: -0.02 -
East-West
Vertical
[m]
[Date]
SMS No.004
SMS No.004

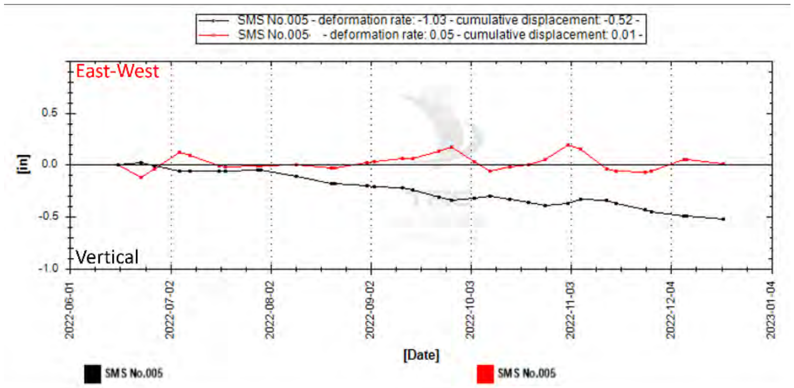
SMS No.005 - deformation rate: -1.03 - cumulative displacement: -0.52 -
SMS No.005 - deformation rate: 0.05 - cumulative displacement: 0.01 -
East-West
Vertical
[m]
0.5
0.0
-0.5
-1.0
2022-06-01
2022-07-02
2022-08-02
2022-09-02
2022-10-03
2022-11-03
2022-12-04
2023-01-04
[Date]
SMS No.005
SMS No.005

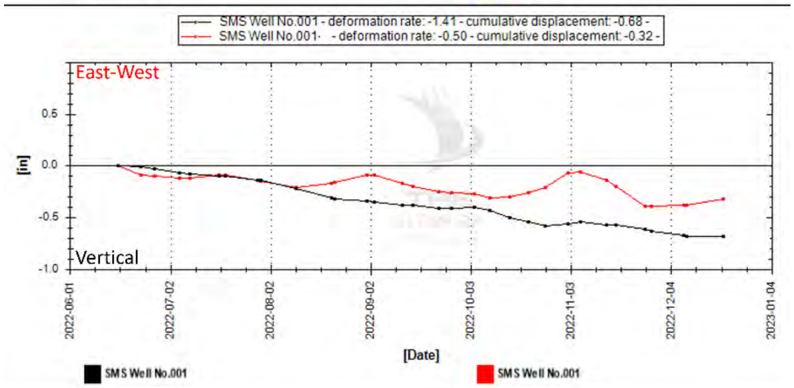
SMS Well No.001 - deformation rate: -1.41 - cumulative displacement: -0.68 -
SMS Well No.001 - deformation rate: -0.50 - cumulative displacement: -0.32 -
East-West
Vertical
[m]
0.5
0.0
-0.5
-1.0
2022-06-01
2022-07-02
2022-08-02
2022-09-02
2022-10-03
2022-11-03
2022-12-04
2023-01-04
[Date]
SMS Well No.001
SMS Well No.001

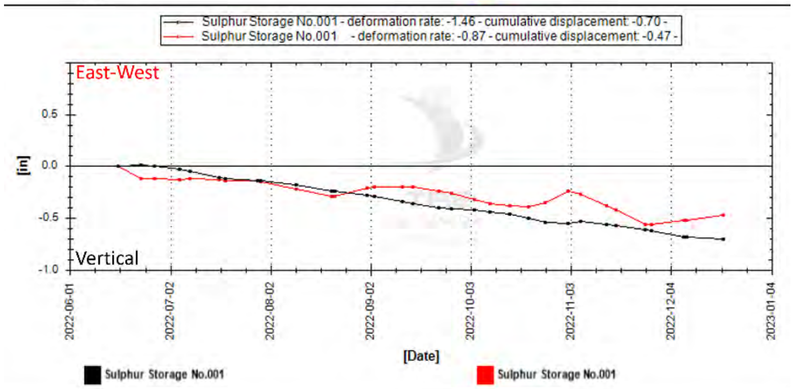
Sulphur Storage No.001 - deformation rate: -1.46 - cumulative displacement: -0.70 -
Sulphur Storage No.001 - deformation rate: -0.87 - cumulative displacement: -0.47 -
East-West
Vertical
[m]
0.5
0.0
-0.5
-1.0
2022-06-01
2022-07-02
2022-08-02
2022-09-02
2022-10-03
2022-11-03
2022-12-04
2023-01-04
[Date]
Sulphur Storage No.001
Sulphur Storage No.001

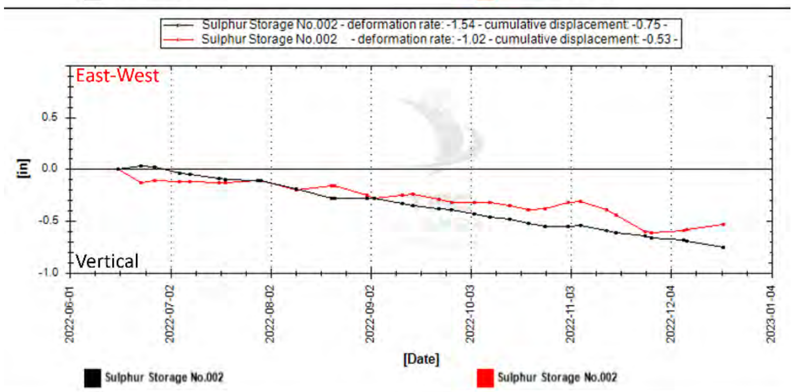
Sulphur Storage No.002 - deformation rate: -1.54 - cumulative displacement: -0.75 -
Sulphur Storage No.002 - deformation rate: -1.02 - cumulative displacement: -0.53 -
East-West
Vertical
[m]
0.5
0.0
-0.5
-1.0
2022-06-01
2022-07-02
2022-08-02
2022-09-02
2022-10-03
2022-11-03
2022-12-04
2023-01-04
[Date]
Sulphur Storage No.002
Sulphur Storage No.002

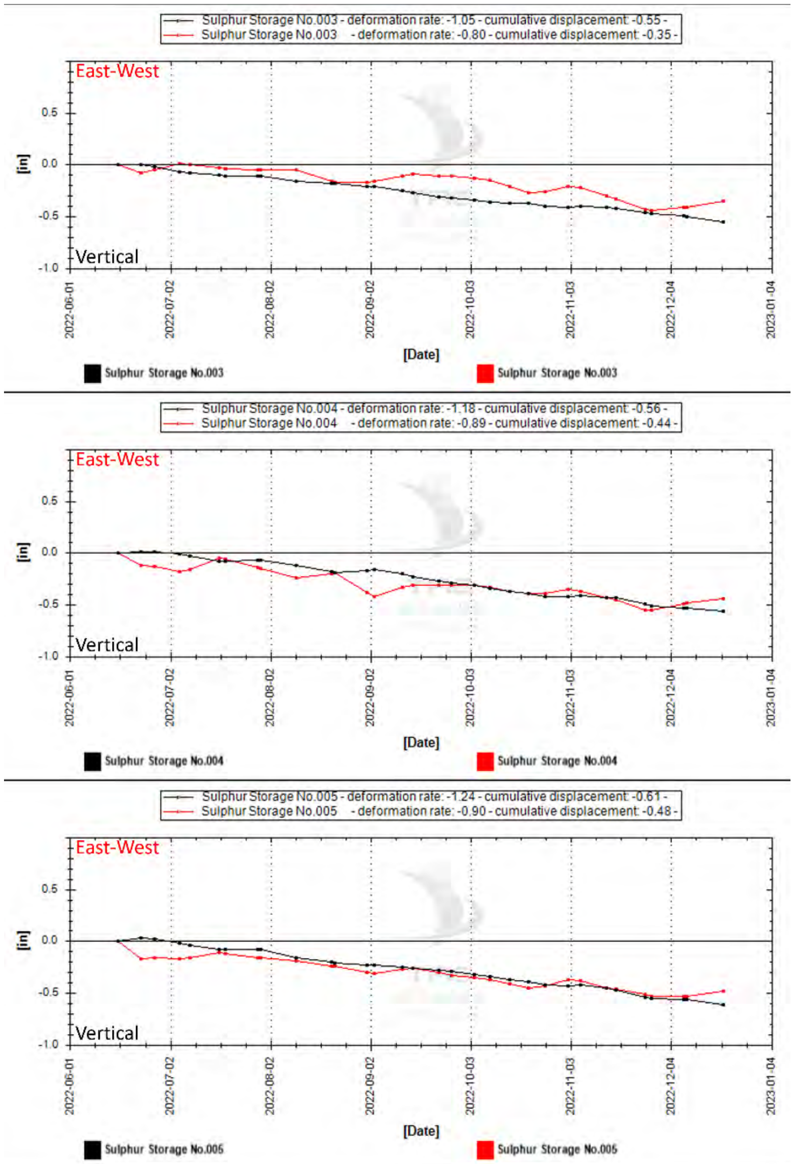

Figure 30. Average time series of the vertical and east-west displacement rates of all measurement points within 100- feet of each survey monument. Vertical displacement rates are shown in black and east-west displacement rates are shown in red. For east-west measurement, negative values indicate movement towards the west and positive values indicate movement towards the east.

TRE
ALTAMIRA
A CLS Group Company

TRE ALTAMIRA s.r.l.
Ripa di Porta Ticinese, 79
20143 Milan Italy
Tel: +39 02 4343 121

TRE ALTAMIRA S.L.U.
Carrer de Còrsega, 381-387
08037 Barcelona Spain
Tel.: +34 93 183 57 50

TRE ALTAMIRA Inc.
Suite 410, 475 West Georgia Street
Vancouver, BC V6B 4M9 Canada
Tel: +1 604 331 2512

tre-altamira.com